Anna de Wit

The Design and Analysis of a Reversible Solid Oxide Cell and Gas Turbine Integrated System

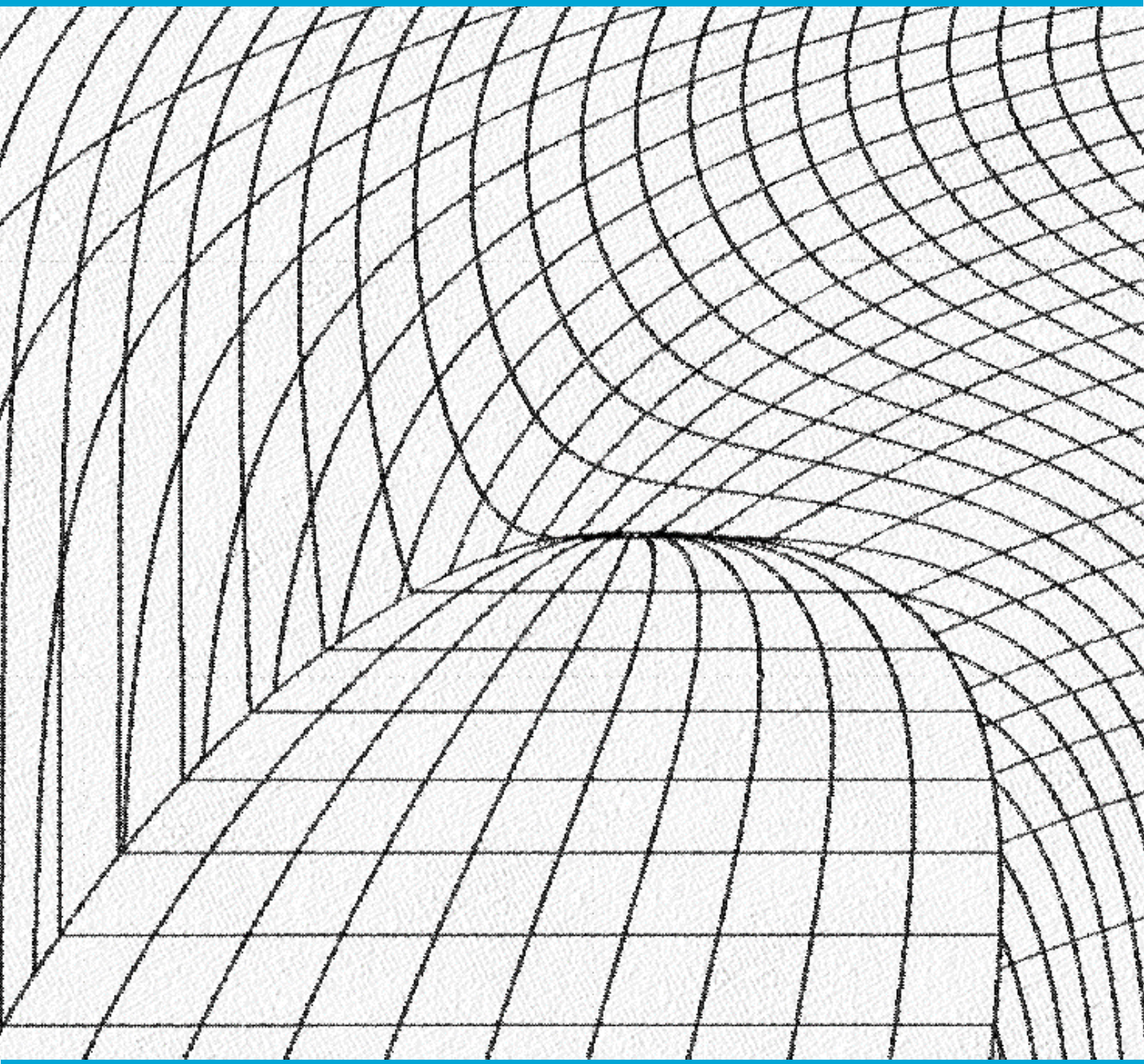

TU Delft

The Design and Analysis of a Reversible Solid Oxide Cell and Gas Turbine Integrated System

by

Anna de Wit

in partial fulfilment of the requirements for the degree of

Master of Science

at the Delft University of Technology,
to be defended publicly on Wednesday March 13, 2024 at 09:00.

Student number:	4463242		
Thesis committee:	Prof. dr. ir. S.A. Klein,	TU Delft	Supervisor
	Dr. ir. L. van Biert,	TU Delft	Supervisor
	Dr. ir. M. Ramdin,	TU Delft	Committee member

Abstract

The increase in the use of renewable energy sources, like wind and solar energy, results in fluctuating power production, which causes imbalances in the electricity grid. In balancing these fluctuations, a significant role can be played by energy storage systems. A relatively new energy storage technology is the reversible solid oxide cell. A reversible solid oxide cell is an electrochemical device that can operate as an electrolyser to produce a fuel from electricity, and as a fuel cell to produce electricity from the fuel. When storing the fuel that is produced during electrolyser mode and later using it to produce electricity during fuel cell mode, the reversible solid oxide system can function as an energy storage system.

At Delft University of Technology, a solid oxide fuel cell system has been designed that can produce electricity from pure hydrogen and oxygen. The fuel cell is coupled to a gas turbine system to increase the systems energy efficiency. In order to redesign this solid oxide fuel cell combined gas turbine system into a reversible solid oxide cell system, the design of a solid oxide electrolyser system is required. One of the main challenges when designing a solid oxide electrolyser system is the heat requirement of the system. However, little research on the design of solid oxide electrolyser systems has yet focussed on thermal optimization of the system. Therefore, three solid oxide electrolyser systems, displaying different heat integration layouts, were designed and examined on their energy and exergy performance. The first system, the basis electrolyser system, reuses heat from the electrolyser's hot outlet streams to heat up the electrolyser's cold inlet streams. The second system, the heat integration electrolyser system, evaporates the water in the system using heat exchangers instead of an electric heater. The third system, the oxygen cooled electrolyser system, has a configuration that is comparable to the solid oxide fuel cell and gas turbine integrated system and thus requires a minimal number of alterations when combining the solid oxide fuel cell and gas turbine integrated system with the solid oxide electrolyser system. The three systems were examined using a thermodynamic model and an electrochemical model, which was validated using a reversible solid oxide cell manufactured by Elcogen and optimized by the Technical University of Denmark and CEA-Liten.

The results show that the highest energy and exergy efficiencies, respectively 75.52% and 75.42%, are obtained by the heat integration electrolyser system. Furthermore, the parameter analysis indicates that the energy efficiency of the electrolyser system altered minimally for adjustments in the electrolyser's operating temperature and operating voltage. The results also show that the lowest energy and exergy efficiencies are obtained by the basis electrolyser system, therefore, the basis electrolyser system is not selected for redesigning the solid oxide fuel cell combined gas turbine system into a reversible solid oxide cell system. The heat integration electrolyser system requires more alterations compared to the oxygen-cooled electrolyser system when combining the electrolyser system with the solid oxide fuel cell and gas turbine integrated system. However, since the difference in efficiencies between the two systems is almost ten percentage points, the heat integration electrolyser system was selected for redesigning the solid oxide fuel cell and gas turbine integrated system into a reversible solid oxide cell system. A round-trip energy efficiency, based on the lower heating value of hydrogen, of 48.40% is reached by this new reversible solid oxide cell system.

Acknowledgements

First and foremost, I would like to express my gratitude to my supervisors, Prof. dr. ir. S.A. Klein and Dr. ir. L. van Biert, for their enthusiasm and guidance throughout this process. They challenged me to trust my capabilities and knowledge of the subject matter and in general. This enabled me to look critically at known research which helped me contrive innovative solutions for the problem. Furthermore, they were supportive and understanding of external circumstances influencing my thesis process, which allowed me to produce a better thesis than I could have imagined beforehand.

I am also grateful for the love and support from my boyfriend, friends and family members. The many cups of tea and talks functioned as a great sounding board and made my concerns feel more manageable. Furthermore, their encouraging words worked both motivating and inspiring.

Anna de Wit
Delft, February 2024

Contents

Nomenclature

Symbols and abbreviations

A	area [m^2]
c_p	specific heat at constant pressure [J/kg]
E	equilibrium voltage [V]
E^0	standard potential [V]
EER	energy efficiency ratio [-]
e_f	specific flow exergy [J/kg]
E_d	exergy destruction [J]
η	efficiency [-]
η_{conc}	concentration overpotential [V]
η_{ohm}	ohmic overpotential [V]
F	Faraday constant [C/mol]
ΔG	change in Gibbs free energy [J]
GT	gas turbine
h	enthalpy [J/kg]
ΔH	change in enthalpy [J]
H_2	hydrogen
H_2O	water
J	current density [A/m^2]
LHV	lower heating value
M	molar mass [g/mol]
m	mass [kg]
N_{cell}	number of cells [-]
O_2	oxygen
p	pressure [Pa]
P	power [J/s]
Q	heat [J]
R	universal gas constant [$J/(mol \cdot K)$]
R_c	cell resistance [Ωm^2]
R_p	pressure ratio [-]
rSOC	reversible solid oxide cell
s	entropy [$J/(kg \cdot K)$]
ΔS	change in entropy [J/K]
SOEC	solid oxide electrolyser cell
SOFC	solid oxide fuel cell
T	temperature [K]
TES	thermal energy storage
U_f	utilization factor [%]
V	cell voltage [V]
W	work [J]
x	Mole fraction [-]

Sub- and superscripts

0	standard state
cell	cell
chem	chemical
comp	compressor
cooler	cooler

en	energy
ex	exergy
heater	heater
HEX	heat exchanger
i	species i
in	inlet
is	isentropic
J	system boundary
L	limiting
loss	losses
mech	mechanical
min	minimum
mix	mixer
nernst	Nernst potential
o	environment
out	outlet
phys	physical
rt	round trip
stack	stack
sys	system
tn	thermo-neutral
turb	turbine

1. Introduction

To face the challenge of decreasing their carbon dioxide emissions to zero by 2050, many countries invest in renewable energy sources [2, 3]. However, renewable energy sources like wind and solar energy have a fluctuating power production as is visualized in Figure 1 [4]. These fluctuations cause imbalances in the electricity grid and might reduce power supply stability [5]. In balancing these fluctuations, a significant role can be played by energy storage systems [6].

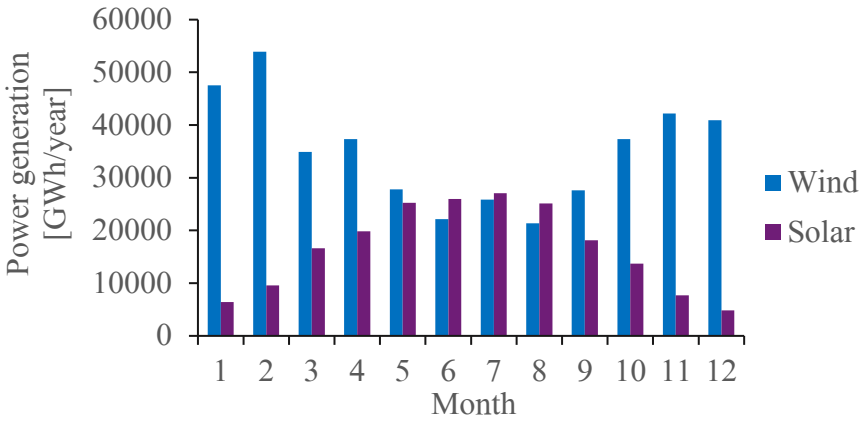

Figure 1 The monthly power production from wind and solar energy sources in the European Union in 2022, data retrieved from Eurostat [4].

Energy can be stored mechanically, thermally, electrically, electrochemically, and chemically, depending on the requirements of the system [7]. An overview of some generally considered storage options is given in Figure 2 [8], where the storage technologies are categorized by storage capacity and storage time. According to Figure 2 hydrogen and pumped hydro systems seem the best option for large storage capacity and storage time, however, it must be noted that there are many factors influencing the selection of a certain storage option. These factors include storage capacity and time, but also energy density, response time, system efficiency, life time, and system costs, among others [7]. Due to the growing demand for storage systems to balance the fluctuations in the electricity grid, research on the development of energy storage systems is increasing. Also relatively new technologies, like reversible fuel cells, are receiving increasing attention due to their promising potential.

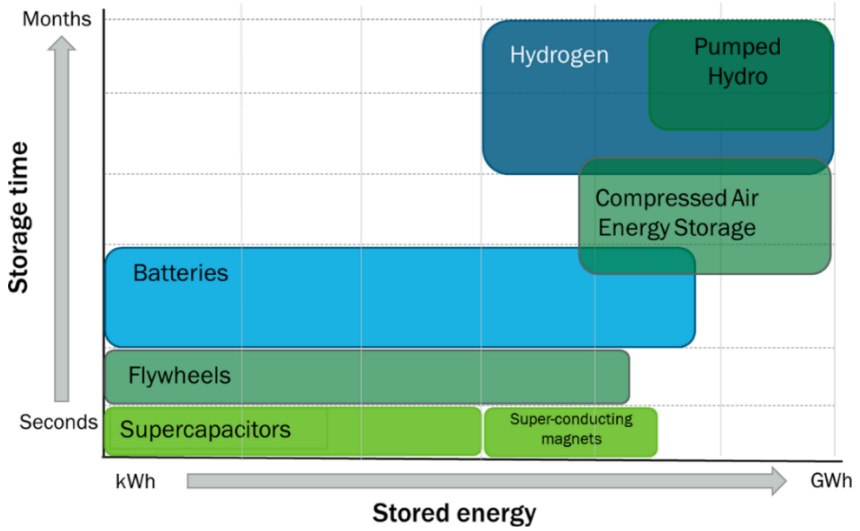

Figure 2 Energy storage technologies categorized by storage capacity and time, from [8].

A reversible fuel cell is an electrochemical device that can operate as an electrolyser to produce a fuel from electricity, and as a fuel cell to produce electricity from the fuel [7]. Reversible fuel cells are generally classified by their operating temperature: Low temperature cells, like alkaline and proton exchange membrane cells, operate at a temperature around 343 K and are already used for commercial hydrogen production; high temperature cells, like reversible solid oxide cells (rSOC), operate at a temperature around 1000 K and are still in the demonstration phase [9]. AlZahrani et al. [10] argue that the interest in high temperature cells, like the rSOC, compared to low temperature cells is mainly due to the fact that they do not require expensive catalysts for improved reaction rates, have the ability to cope with impurities in the fuel, and are expected to reach increased conversion efficiencies [10]. Furthermore, Venkataraman et al. [7] state that an rSOC has the possibility of using one unit as both electrolyser and fuel cell; it can operate as a solid oxide fuel cell (SOFC) to produce electricity and as a solid oxide electrolyser cell (SOEC) to produce fuel [7]. According to Wang et al. [11] chemicals such as methane, hydrogen, syngas, ammonia and methanol can all be used in an rSOC, however, a reformer is required for each of these fuels except for hydrogen [11].

Although reversible solid oxide cells are still in the demonstration phase, multiple projects aim to demonstrate the performance of rSOC systems in real environments. Two interesting examples are the GrInHy2.0 and the REFLEX project. In the GrInHy2.0 project, the steel-producing Salzgitter Group works together with Sunfire GmbH, Paul Wurth S.A., Tenova SpA, and CEA on the realization of a reversible solid oxide cell. The installation is currently operated as an electrolyser for the production of 200 Nm^3/h hydrogen at a nominal power input of 720 kWe [12]. In the future, the installation will also operate as a reversible solid oxide cell to increase stability of the company's power supply [13]. In the REFLEX project, a consortium of CEA, Sylfen, Technical University of Denmark, VTT, Elcogen, Engie, Envipark, GPTech, and University of Sevilla aims to develop an rSOC that can function as an energy storage system for the headquarter of Envipark. The installation is expected to produce 10 kWe during fuel cell mode and require 50 kWe during electrolysis mode [14]. Together with other projects worldwide, the results of these projects will show what role the rSOC technology will play in the transition towards the use of renewable energy sources.

1.1. Thesis objective and outline

At Delft University of Technology, a hydrogen SOFC system has been designed that can produce electricity from pure hydrogen and oxygen, leading to an improved energy efficiency and zero greenhouse gas emissions. The outlet streams of an SOFC often contain heat and unused fuel, therefore, the SOFC is coupled to a gas turbine (GT) system to increase the systems energy efficiency [15]. The system from Delft University of Technology was originally designed by Schouten, B. [15], who reached an energy efficiency, based on the lower heating value of hydrogen, of 83.8% [15]. In this system, three fuel cell units were coupled to an optimized hydrogen and oxygen fuelled Graz cycle [15]. The system designed by Schouten, B. [15] was later redesigned into a lab-scale test set-up by Malhotra, D. [16]. The SOFC+GT system by Malhotra, D. [16] reaches an energy efficiency, based on the lower heat value of hydrogen, of 64.09% [16]. This SOFC+GT system can potentially also be used as an energy storage system by redesigning it into an rSOC system. Therefore, this thesis will examine how the SOFC+GT system can be redesigned into a reversible SOC+GT system. The following research question plays a central role:

How can the SOFC+GT system designed by Malhotra, D. [16] be redesigned with minimal alterations to create an rSOC+GT system with optimal round-trip energy efficiency?

An rSOC system operates in two modes, namely as an SOFC system to produce electricity and as an SOEC system to produce fuel. Therefore, since the SOFC+GT system was already designed by Malhotra, D. [16], the design of an SOEC system is required to form an rSOC system. One of the main challenges when designing an SOEC system is the heat requirement of the system. A significant amount of heat is required for the evaporation of water in an SOEC system. Furthermore, unlike a fuel cell, an electrolyser does not always operate exothermally and thus often requires heat to maintain its high operating temperature. Little research on the design of SOEC systems has yet focussed on thermal optimization of the system. Therefore, in this thesis, three SOEC systems displaying different heat integration layouts are designed and examined on their energy and exergy performance.

The thesis process that was followed after completing the literature review is visualized in Figure 3. The first phase focussed on the rSOC. First, an electrochemical model was constructed to represent the electrochemical processes taking place inside the rSOC. Then, a reference rSOC was selected. Since the SOFC+GT system designed by Malhotra, D. [16] uses pure hydrogen and oxygen, the reference rSOC has to be able to operate using pure oxygen as well. In the final step of phase one, the electrochemical model was validated using the reference rSOC. The second phase focussed on the design and analysis of the SOEC systems. First, a thermodynamic model was constructed, that was used to design a basis SOEC system. The layout of this basis SOEC system was based on research on SOEC system design. After designing the basis SOEC system, the energy and exergy performances of the system were examined. Using the results from the basis SOEC system, a new system called the heat integration SOEC system was designed and analysed. This heat integration SOEC system aimed to improve the energy and exergy efficiency of the basis SOEC system. However, the layout of the heat integration SOEC system differed strongly from the SOFC+GT layout, and thus a large number of alterations would be required when combining the two systems into an rSOC system. Therefore, a third system, the oxygen-cooled SOEC system, was designed and analysed. This system has a configuration that is comparable to the SOFC+GT system and focussed on requiring a minimal number of alterations when combining the SOFC+GT and the SOEC systems. After analysing the results of each SOEC system, a parameter analysis was performed to examine the effect of three parameters on the energy efficiency of the heat integration system. These three parameters included the system's heat loss, the electrolyser's operating temperature, and the electrolyser cell's operating voltage. In the final phase, the results of the three SOEC systems were compared and the performance of the rSOC system was estimated.

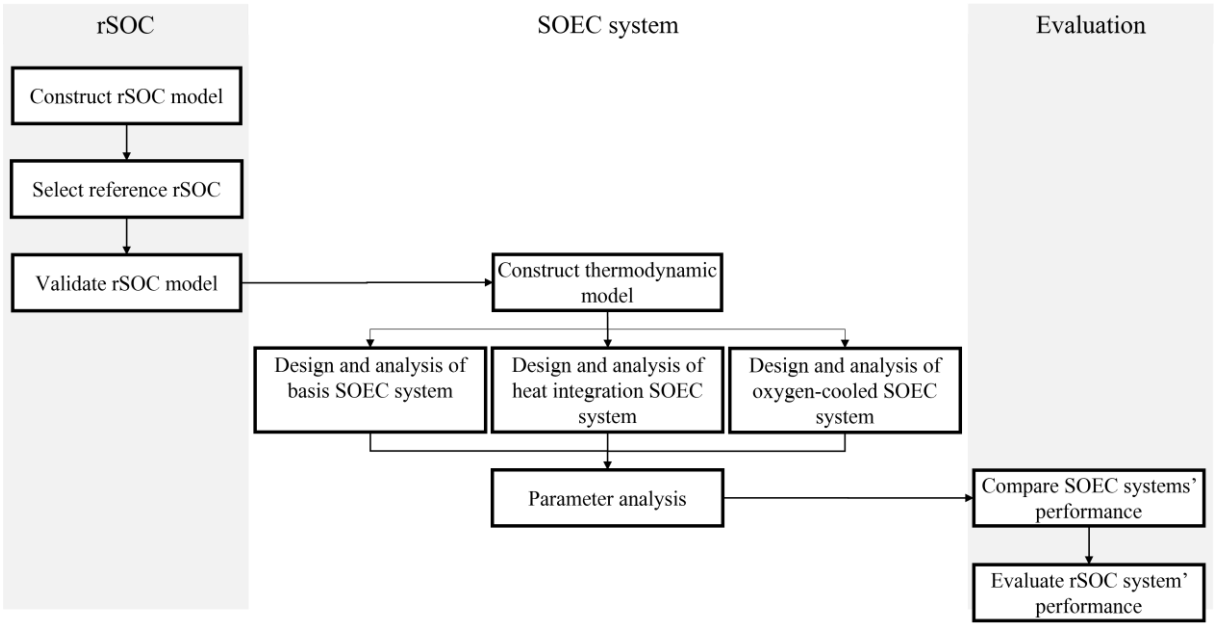

Figure 3 Flow chart of the thesis process.

2. Background information

A reversible solid oxide cell (rSOC) is an electrochemical device that can operate as an electrolyser to produce a fuel from electricity, and as a fuel cell to produce electricity from the fuel [7]. An rSOC system thus consists of two subsystems, namely a solid oxide fuel cell (SOFC) subsystem to produce electricity and a solid oxide electrolyser (SOEC) subsystem to produce fuel. The operating principles of a reversible solid oxide cell (rSOC) and its system are described in sections 2.1 and 2.2 respectively. But first, the rSOC technology is briefly introduced in comparison with two other electrolyser and fuel cell technologies.

In literature, the rSOC technology is often compared with two other electrolyser and fuel cell technologies: The alkaline electrolyser/fuel cell and the Proton Exchange Membrane (PEM) electrolyser/fuel cell. The main difference between the rSOC and the other two technologies is the operating temperature of the cells; an rSOC operates at a temperature around 1000 K and the Alkaline and PEM operate at a temperature around 343 K [9]. This means that the low-temperature alkaline and PEM cells work with liquid water, while the rSOC works with steam. Another difference between the three technologies is their electrolyte material and transported ions: In PEM cells, a solid polymer electrolyte transports hydrogen ions; in alkaline cells, a liquid alkaline electrolyte transports hydroxide ions; and in solid oxide cells, a ceramic electrolyte transports oxygen ions [17]. A third difference is that an rSOC can switch between operating as an electrolyser and a fuel cell, while low temperature cells like alkaline and PEM can only operate as either a fuel cell or an electrolyser, mainly due to water management issues [7]. Typical efficiencies of the three technologies when operated as either an electrolyser or a fuel cell are given in Table 1 [17, 18].

Table 1 Typical efficiencies for PEM, alkaline and rSOC technology, data from [17, 18].

	PEM technology	Alkaline technology	rSOC technology
Electrolyser	60-80% [17]	60-80% [17]	<110% [17]
Fuel cell	40-60% [18]	60-70% [18]	50-60% [18]

Table 1 shows that the efficiency during electrolyser mode for rSOC technology is much higher compared to PEM and alkaline technology. When only considering the cells and not the entire system, the rSOC electrolyser can even reach efficiencies over 100% [17]. A more detailed analysis of the differences in electrolyser efficiencies is given in section 2.2.

2.1. The rSOC

This section describes the operating principles of a reversible solid oxide cell (rSOC). An oxygen conducting rSOC is a high temperature reversible electrochemical device that can operate in fuel cell mode (SOFC) to produce electricity and water, and in electrolyser mode (SOEC) to produce oxygen and hydrogen. The operating principles of an rSOC are visualized in Figure 4.

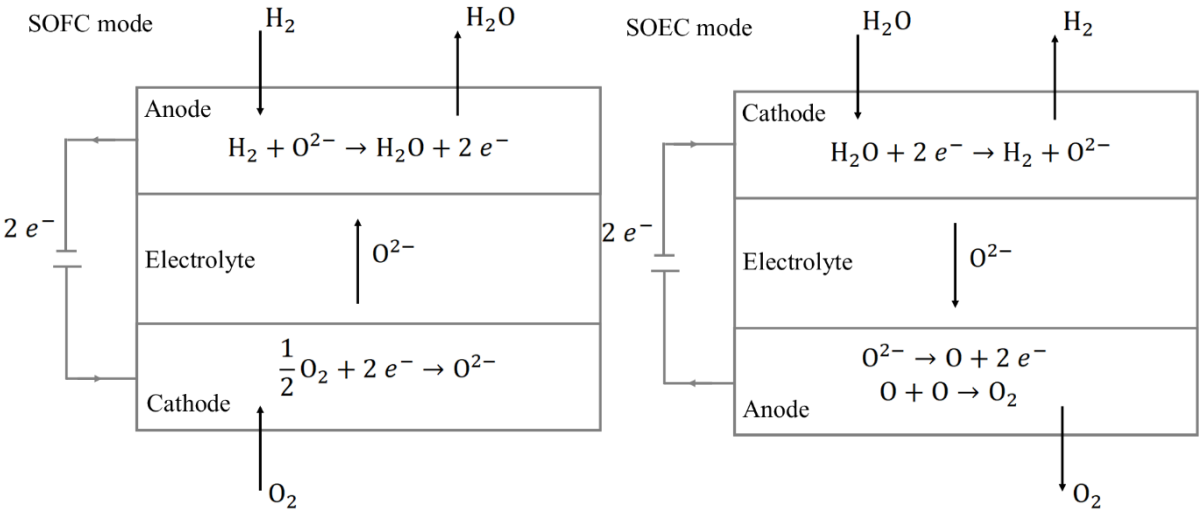

Figure 4 Operating principles of an rSOC, operating in SOFC mode (left) and SOEC mode (right). Image adapted from [19].

During SOFC mode, oxygen gas reacts under influence of electrons to form oxygen ions at the cathode. The oxygen ions transfer through the electrolyte to the anode, where they react with hydrogen gas to form steam and electrons. The electrons move through a load to the cathode and the steam leaves the cell to be stored, released to the environment, or used in a bottoming cycle. The net reaction taking place in the SOFC mode thus results in [9]

$$H_2 + \frac{1}{2}O_2 \rightarrow H_2O. \quad (1)$$

During SOEC mode, steam splits into oxygen ions and hydrogen gas at the cathode when a voltage is applied to the cell. The hydrogen gas and residual steam leave the cell and must be separated to obtain pure hydrogen gas. The oxygen ions are transferred through the electrolyte to the anode, where they combine and form oxygen gas, which leaves the cell and can be collected and stored. The net reaction taking place in the SOEC results in [20]

$$H_2O \rightarrow H_2 + \frac{1}{2}O_2. \quad (2)$$

The complex electrochemical processes taking place inside an rSOC can be represented via several different models. These models can differ in state (steady, transient), level (micro, macro, or system), or dimensions (zero, one, two, or three), amongst others. Often, steady-state macro-level models are used for SOFC, SOEC, and rSOC design, since they are less complex, and thus result in less computational costs, than transient models. Furthermore, they form a compromise between the detailed but complex micro-level models, and the simplified system-level models [21, 22]. In macro-level models, the cell's electrochemical losses are subtracted from an equilibrium voltage, which are both calculated using global-kinetic expressions [21]. Different modelling approaches have also been examined, for example by Bessler et al. [23], who created a model based on an elementary-kinetic approach of the electrochemistry taking place inside the cell instead of a global-kinetic approach [23]. Since this thesis focuses on the operating principles of a whole rSOC system, the complex processes taking place within the cell are represented by a global-kinetics model.

In this model, the voltage that is required for the SOEC mode or produced during the SOFC mode consists of the equilibrium voltage E and the voltage related to the losses in the cell η [24]

$$V = E \pm \eta. \quad (3)$$

A fuel cell (SOFC) produces a voltage that is lower than the equilibrium voltage due to the losses inside the cell. An electrolyser (SOEC) on the other hand requires a voltage that is higher than the equilibrium voltage due to the losses [24]. This situation is illustrated in Figure 5.

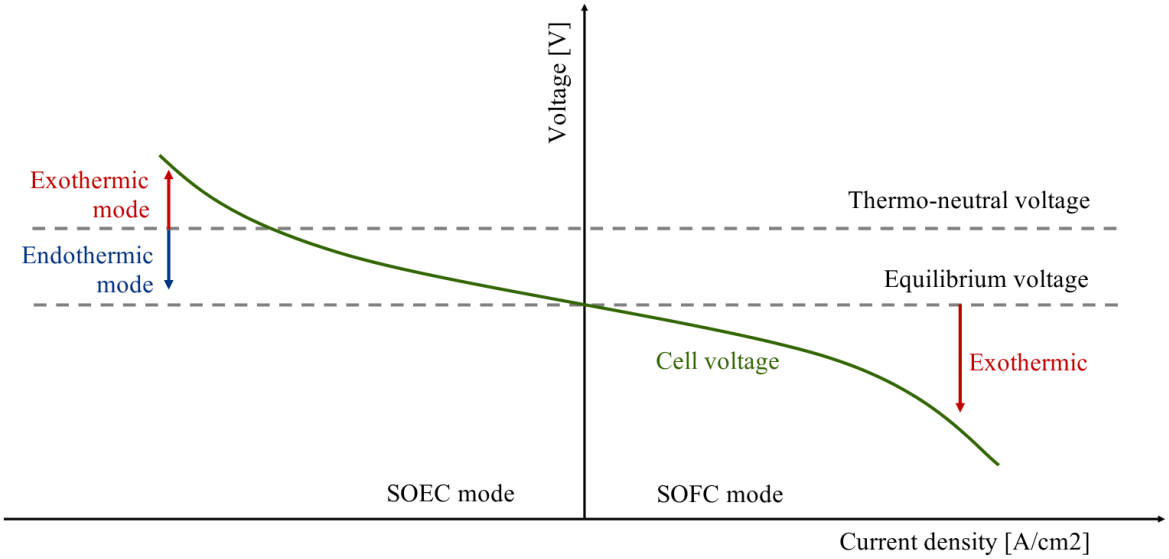

Figure 5 Illustration of a polarisation curve of an rSOC.

For SOECs, another voltage in addition to the equilibrium voltage is relevant; the thermo-neutral cell voltage. The thermo-neutral cell voltage represents the potential at which the heat required for electrolysis equals the heat produced by the losses inside the cell [25]. When the SOEC is operated at a voltage lower than the thermo-neutral cell voltage, the electrolyser operates endothermically; there is more heat required than is produced inside the cell itself. Often, this heat is supplied by increasing the temperature of the inlet streams of the SOEC [26]. When the SOEC is operated at a voltage higher than the thermo-neutral cell voltage, the electrolyser operates exothermically; there is more heat produced than required in the cell. Often, this heat is released via an increased temperature of the outlet streams of the SOEC [26]. The thermo-neutral cell voltage and its relation to the thermal operating mode of the SOEC is illustrated in Figure 5. For an SOEC, the thermo-neutral voltage generally varies between 1.287 V and 1.292 V, depending on the operating temperature of the electrolyser [27].

2.2. The rSOC system

A hydrogen reversible solid oxide cell (rSOC) system is a system that can operate as a fuel cell system to produce electricity and heat by the conversion of hydrogen and oxygen gas into steam, and as an electrolyser system to convert steam into pure hydrogen and oxygen gas by the application of electricity and heat. When storing the hydrogen that is produced during electrolyser mode and later using it to produce electricity during fuel cell mode, the rSOC system can function as an energy storage system. This situation is illustrated in Figure 6.

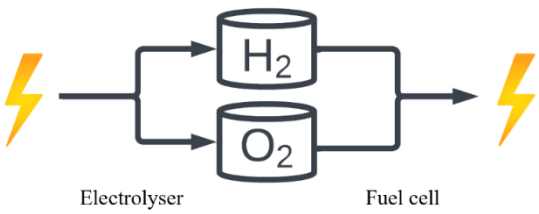

Figure 6 Illustration of a hydrogen reversible solid oxide cell system, consisting of an electrolyser and a fuel cell subsystem, functioning as an energy storage system.

An rSOC system thus consists of a combination of two systems: A solid oxide fuel cell (SOFC) system and a solid oxide electrolyser cell (SOEC) system. At Delft University of Technology, a hydrogen SOFC system was designed that can produce electricity from pure hydrogen and oxygen. When this SOFC system is redesigned into an rSOC system, an SOEC system is required to produce this pure hydrogen and oxygen from electricity. The

operating principles of the SOFC and SOEC systems are described in sections 2.2.1 and 2.2.2 respectively.

2.2.1. Operating principles of the SOFC system

At Delft University of Technology, an SOFC system was designed that can produce electricity from pure hydrogen and oxygen [16]. The use of pure oxygen leads to an improved system efficiency and zero greenhouse gas emissions [15, 28]. The outlet streams of an SOFC often contain heat and unused fuel, therefore, the SOFC is coupled to a gas turbine (GT) system to increase the systems energy efficiency [15]. The system from Delft University of Technology was originally designed by Schouten, B. [15], who reached an energy efficiency, based on the lower heating value of hydrogen, of 83.8% [15]. In this system, three fuel cell units are coupled to an optimized hydrogen and oxygen fuelled Graz cycle [15]. To the authors current knowledge, only one other SOFC+GT system has been designed that operates using pure hydrogen and oxygen. In this system, designed by Jericha et al. [29], an SOFC stack is coupled to the hydrogen and oxygen fuelled Graz cycle [29]. This system reaches an energy efficiency, based on the lower heating value of hydrogen, of 73.8% [29].

The system designed by Schouten, B. [15] is redesigned into a lab-scale test set-up by Malhotra, D. [16]. The SOFC+GT system by Malhotra, D. [16] reaches an energy efficiency, based on the lower heating value of hydrogen, of 64.09% [16]. An overview of the SOFC+GT system is given in Figure 7. An overview of the stream data of the system is given in Appendix A.

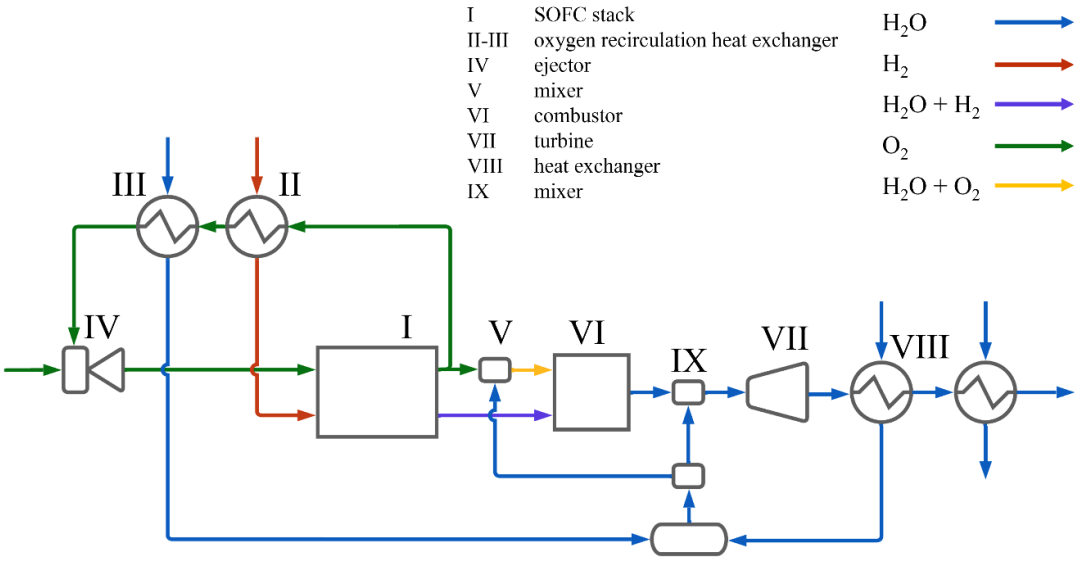

Figure 7 Layout of the SOFC+GT system designed by Malhotra, D. [16].

As described in section 2.1, an SOFC operates exothermally and therefore requires cooling. One way to do this is by using excess sweep air at the oxygen electrode [27]. Schouten, B. [15] examined the effect of three other cooling methods on the efficiency of the system; one that inserts extra oxygen at the oxygen electrode, one that inserts a mixture of steam and oxygen at the oxygen electrode, and one that inserts a mixture of steam and hydrogen at the fuel electrode [15]. It was found that the insertion of extra oxygen at the oxygen electrode resulted in the highest system efficiency and was easiest to integrate into the cycle [15]. Figure 7 shows that in the system designed by Malhotra, D. [16], the extra oxygen at the oxygen electrode is used for cooling of the SOFC stack [16]. In Figure 7, the excess oxygen exiting the SOFC (I) is partly used to heat up the SOFC inlet hydrogen (II) and to evaporate water (III), before

recirculating back into the SOFC. The oxygen recirculation is driven by an ejector (IV) instead of a compressor, to reduce the system's power requirement [16]. The residual oxygen exiting the SOFC is mixed with steam (V) and fed into a combustor (VI), together with the hydrogen and steam exiting the SOFC. After the combustor, the produced steam is sent to the turbine (VII) to generate electricity. Residual steam from the turbine is passed through the evaporator (VIII) for the production of more steam, which can be mixed (IX) with the combustor outlet steam for increased turbine power production [16].

2.2.2. Operating principles of the SOEC system

In order to redesign the SOFC+GT system described in the previous section into an rSOC system, an SOEC system design is required. Therefore, in this section, the operating principles of an SOEC system are examined.

The system components that are required in an electrolyser system often depend on the operating temperature of the electrolyser cells. Low temperature electrolysers, like alkaline and proton exchange membrane cells, operate at a temperature around 343 K and high temperature electrolysers, like solid oxide electrolysers (SOEC), operate at a temperature around 1000 K [9]. High temperature electrolysers are recently gaining attention due to the claim that they would require less energy compared to low temperature electrolysers. However, this is not necessarily true.

The total amount of energy required for an electrolysis process can be represented by the change in enthalpy between the electrolysis products and reactants ΔH. This total amount of energy consists of both the electrical and thermal energy required for electrolysis, which are represented by the Gibbs free energy change and entropy change respectively [30]

$$\Delta H = \Delta G + T\Delta S. \quad (4)$$

The total, electrical and thermal energy for low and high temperature hydrogen electrolysers are visualized in Figure 8.

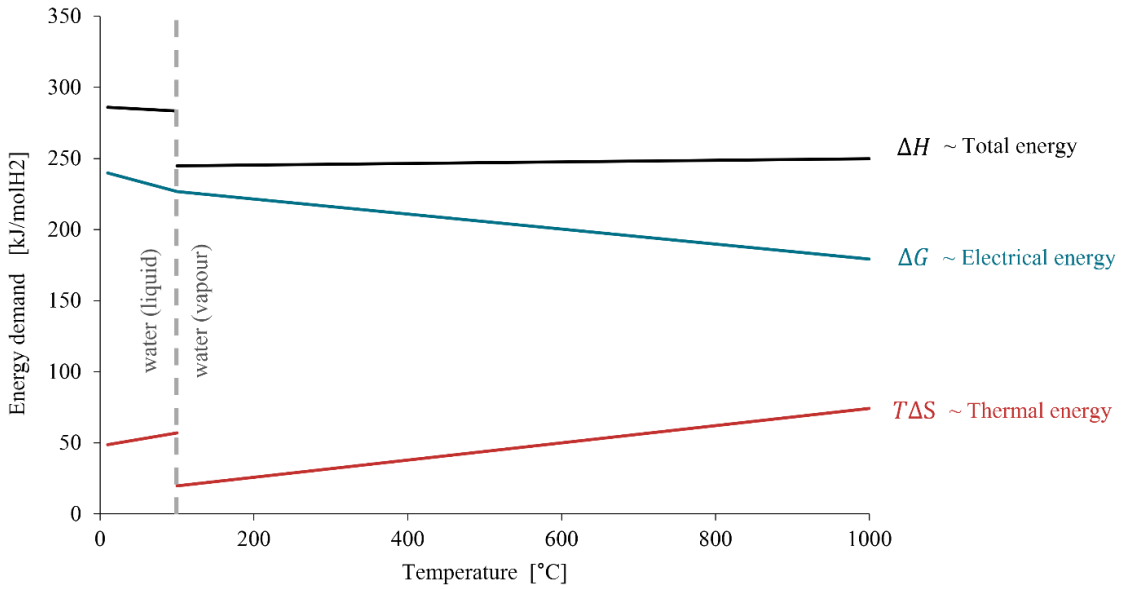

Figure 8 Illustration of the total, electrical and thermal energy required for low and high temperature hydrogen electrolysers. Adapted from [27].

Figure 8 shows that low temperature electrolysers require more energy than high temperature electrolysers. However, the main difference in energy requirement is caused by the use of steam instead of liquid water in high temperature electrolysers. The electrolyser itself thus requires less energy at high temperatures, because the liquid water is already turned into steam. However, since the high temperature cells require steam, the water must be evaporated elsewhere in the system.

To cover the thermal energy demand for the water evaporation in SOEC systems, research has focussed on using either an external (waste) heat source or an electric heater. In most research, the external heat source or electric heater is combined with heat exchangers that use the electrolyser's hot outlet streams to heat up the cold inlet streams. A schematic representation of this heat addition method is given in Figure 9. In Figure 9, the cold inlet stream is heated up in a heat exchanger (I) using the hot SOEC outlet stream. Since the hot outlet stream cannot cover the entire heat demand of the cold inlet stream, heat addition Q is required (II).

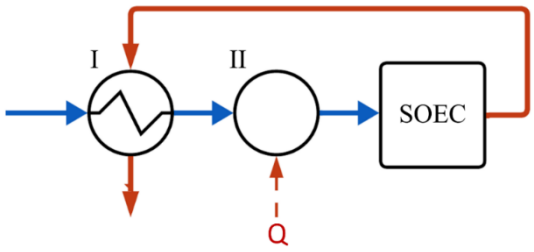

Figure 9 A schematic representation of heat addition in SOEC systems.

The amount of heat that can be exchanged between a hot and a cold stream is determined by the change in enthalpy in which they overlap and the temperature difference between the two streams [31]. At the oxygen electrode of an electrolyser, the hot outlet stream often has a temperature that is high enough and an enthalpy change that is large enough to fully heat up the cold inlet stream. However, at the fuel electrode, the hot outlet stream cannot cover the entire heat demand of the cold inlet stream. Figure 10 illustrates a temperature-enthalpy diagram of the fuel electrode inlet and outlet streams of an SOEC operated in thermo-neutral mode. The figure shows that the hot outlet stream does not have enough enthalpy change to fully heat up the cold stream and that the lines for the hot and cold streams intersect. The intersection of the streams is caused by their different saturation points. The fuel electrode inlet stream contains water combined with a small amount of hydrogen and the outlet stream contains hydrogen with a small amount of water. Due to this change in water and hydrogen composition before and after the electrolyser, the partial pressure of the water in the outlet stream is lower than in the inlet stream. As a result, the saturation temperature of the water in the hot outlet stream is lower than the evaporation temperature of the cold inlet stream. Furthermore, this results in a smaller enthalpy change for the outlet stream compared to the inlet stream. Additional heat is required to cover the residual heat demand.

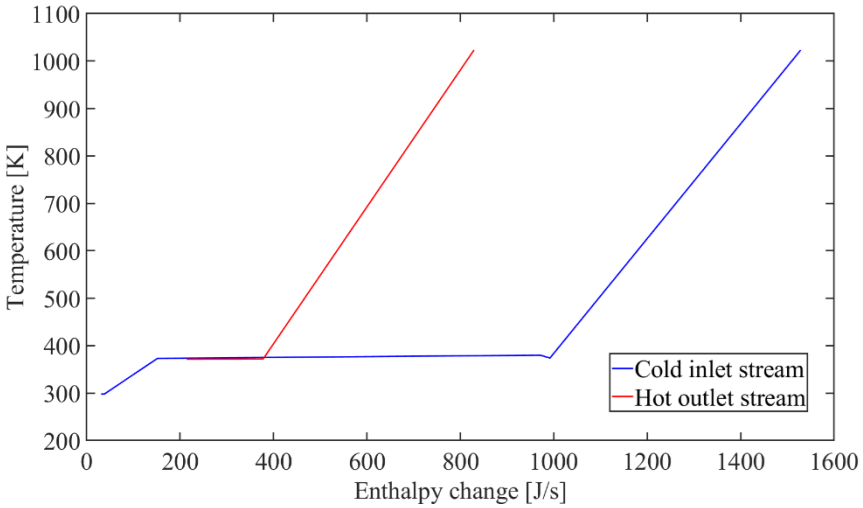

Figure 10 A temperature-enthalpy diagram of the fuel electrode inlet (cold) and outlet (hot) streams of an SOEC operated in thermo-neutral mode.

As stated earlier, the heat addition methods used in literature can be subdivided into two categories: One category that uses an external (waste) heat source and one that uses an electric heater. In the first category, heat for evaporating, preheating, or superheating the water is supplied by an external (waste) heat source. To examine how these SOEC systems use the external (waste) heat source to cover the thermal energy demand of the system, several researches were selected. Research on external (waste) heat integrated SOEC system design was selected based on the following criteria: The paper uses only steam (if necessary mixed with hydrogen) as SOEC cathode inlet; the paper focusses on optimizing both electrical and thermal performance of the entire system; the paper uses only an external (waste) heat source and heat exchangers (and if necessary an electric heater) for heating the SOEC inlet streams; and in case comparable system designs are examined in several papers, the paper that focusses most on the heat integration of the system and its operating results was chosen for this review. Table 2 gives an overview of the selected papers on SOEC system design using an external (waste) heat source. For each reference is stated whether the external (waste) heat source is used for preheating, evaporating, or superheating the SOEC inlet streams.

Table 2 Research on SOEC systems design using an external (waste) heat source. For each reference is stated whether the external (waste) heat source is used for preheating, evaporating, or superheating the SOEC inlet streams.

Reference	Year	SOEC operating mode	Heat purpose		
			Preheat	Evaporate	Superheat
Mohammadpour et al. [32]	2022	Exothermal		x	
Mohammadpour et al. [33]	2022	Exothermal		x	
Restrepo et al. [34]	2022	Thermo-neutral		x	x
Westover et al. [35]	2022	Thermo-neutral	x	x	
Wang et al. [36]	2021	Endothermal	x	x	
Zhao et al. [37]	2021	Thermo-neutral		x	
Mastropasqua et al. [38]	2020	Thermo-neutral			x
Yilmaz et al. [39]	2020	Exothermal	x	x	x
Jelodar et al. [40]	2019	Exothermal	x	x	
Schiller et al. [41]	2019	Exothermal	x	x	x
Yuksel et al. [42]	2019	Thermo-neutral		x	x
Balta et al. [43]	2016	Exothermal	x	x	
Manage et al. [44]	2014	Exothermal	x	x	
McKellar et al. [45]	2007	Thermo-neutral			x
Sigurvinsson et al. [46]	2007	Exothermal		x	

Most research uses the external (waste) heat source for the evaporation of the electrolyser's inlet water, because the evaporation accounts for most of the heat requirement of the electrolyser's inlet streams [37]. When the temperature of the external (waste) heat source was high enough, for example nuclear (waste) heat and solar heat, it was also used to superheat the water [34, 38, 39, 42, 45]. Otherwise, either an electric heater was used to bring the inlet streams to the required temperature or the electrolyser was operated in exothermal mode to recover the high-temperature heat from the electrolyser's outlet streams [32, 33, 35-37, 40, 43, 44, 46]. As described in section 2.1, the electrolyser's thermal operating mode, which can be endothermal, thermo-neutral, or exothermal, dictates whether heat has to be added to or removed from the cells. In literature on external (waste) heat integrated SOEC system design, the effect of the electrolyser's thermal operating mode on the system's efficiency is disputed. Table 2 shows that most systems use an electrolyser operating in exothermal mode. These researchers state that operating in exothermal mode delivers higher hydrogen production per stack area and allows for more heat recovery from the electrolyser's outlet streams [32, 33, 39-41, 43, 44, 46]. Other researchers use an electrolyser operating around thermo-neutral mode, because they argue that this results in the least thermal stresses for the electrolyser and is the best compromise between electrolyser losses and hydrogen production [34, 35, 37, 38, 42, 45]. Only Wang et al. [36] uses an electrolyser operating in endothermal mode [36]. Although they do not state their reasoning behind this decision, it is assumed that they operate in endothermal mode because their electrochemical model is based on a paper that argues that operating in endothermal mode results in optimal electrolyser efficiency [10, 36]. In the rSOC system that is designed in this thesis, no external (waste) heat source is available. Some researches on rSOC system design use a thermal energy storage system to store the excess heat that is released during SOFC mode, to cover the heat demand during SOEC mode [47, 48]. However, in the SOFC+GT system designed by Malhotra, D. [16] the excess SOFC heat is already used in a gas turbine system. Additional research altering the SOFC+GT system would be required to evaluate the effects of adding a thermal energy storage system. Therefore, the external (waste) heat category is not implemented in the SOEC system designs in this thesis.

In the second category of heat addition methods, heat for evaporating, preheating, or superheating the water is supplied by an electric heater. To examine how these SOEC systems use the electric heater to cover the thermal energy demand of the system, several researches were selected. Research on SOEC system design using an electric heater was selected based on the following criteria: The paper uses only steam (if necessary mixed with hydrogen) as SOEC cathode inlet; the paper focusses on optimizing both electrical and thermal performance of the entire system; the paper uses only an electric heater and heat exchangers for heating the SOEC inlet streams; and the designed system is independent, i.e., not depending on an external process for heat and/or electricity demand without incorporating it in the efficiency calculations. It was found that the researches on SOEC systems using an electric heater present large variations in the energy efficiency of their systems. One explanation for these large variations can be the chosen operating parameters. Literature on SOEC system design is yet in disagreement on the effect of several operating parameters on the efficiency of the system. Especially the effect of the electrolyser's thermal operating mode on the system's efficiency is disputed. As described in section 2.1, the electrolyser's thermal operating mode, which can be endothermal, thermo-neutral, or exothermal, dictates whether heat has to be added to or removed from the cells. Proponents of endothermal operating mode state that an SOEC is more likely to operate in endothermal mode at high temperatures and that at high temperatures the electrolyser achieves a higher efficiency [10, 49]. According to these researches, the increased electrolyser efficiency would result in a higher system efficiency. However, Hauch et al. [50] state that the efficiency of the electrolyser does not necessarily increase with increasing operating temperatures [50]. Furthermore, Choi et al. [51] argue that their system's efficiency remains almost constant with varying operating temperature [51]. Proponents of operating in exothermal mode state that the decrease in thermal energy requirement for heating up the inlet streams due to heat recovery would outweigh the increase in electric energy requirement for the

electrolyser [46, 52, 53]. Other research states that the difference in system performance between endothermal and exothermal SOEC operation is negligible [37, 54]. Literature on SOEC systems using an electric heater is in disagreement on the effect of operating parameters on the efficiency of the system, therefore, the operating parameters used in the selected researches were compared. Table 3 gives an overview of the selected researches and their operating parameters. References that compare multiple system configurations are shown separately in the table. Some references have included the compression of hydrogen into the efficiency calculations, for these studies the pressure up to which the hydrogen is compressed is given.

Table 3 Research on SOEC system design using an electric heater. All system efficiencies are based on the lower heating value of hydrogen. A question mark is used where the parameter was not given by the reference.

Reference	Year	Hydrogen compression [MPa]	SOEC current density [A/m^2]	SOEC operating voltage [V]	SOEC operating temperature [K]	SOEC operating mode	SOEC steam utilization	System energy efficiency
Model								
AlZahrani et al. [10]	2018	No	10 000	? [a]	1073	Endothermal	85%	85%
		15	10 000	?	1073	Endothermal	85%	79%
Botta et al. [55]	2015	No	8 204	1.14	1073	Endothermal	75%	75%
Peters et al. [56]	2015	7	3 950	1.15	1123	Endothermal	58%	69%
		7	6 730	1.29	1123	Thermo-neutral	58%	76%
		7	7 770	1.35	1123	Exothermal	58%	77%
Model + experiment								
Kupecki et al. [57]	2019	No	?	1.15	1073	? [b]	70%	74%
		No	?	1.35	1073	? [c]	90%	74%
Saarinen et al. [53]	2021	No	10 000	1.34	1023	Exothermal	80%	60%
Experiment								
AVL [58]	2018	No	?	? [d]	1053	?	?	79%
FuelCell Energy [59]	2020	2	10 000	1.29	1023	? [e]	60%	78%
Peters et al. [60]	2021	No	8 900	1.26	1034	Endothermal	85%	70%

a Assuming an operating voltage of 1.27 V, given the specifications from [10].
b Assuming endothermal operating mode, see section 2.1 for more information.
c Assuming exothermal operating mode, see section 2.1 for more information.
d Assuming an operating voltage of 1.23 V, given the specifications from [58].
e Assuming thermo-neutral operating mode, see section 2.1 for more information.

The efficiencies in Table 3 were all calculated using the same equation, therefore, the systems' efficiencies can be compared. However, Figure 11 visualises that no correlation between the systems' efficiencies and either year of publication, cell current density, operating voltage, steam utilization, cell temperature or research method was found.

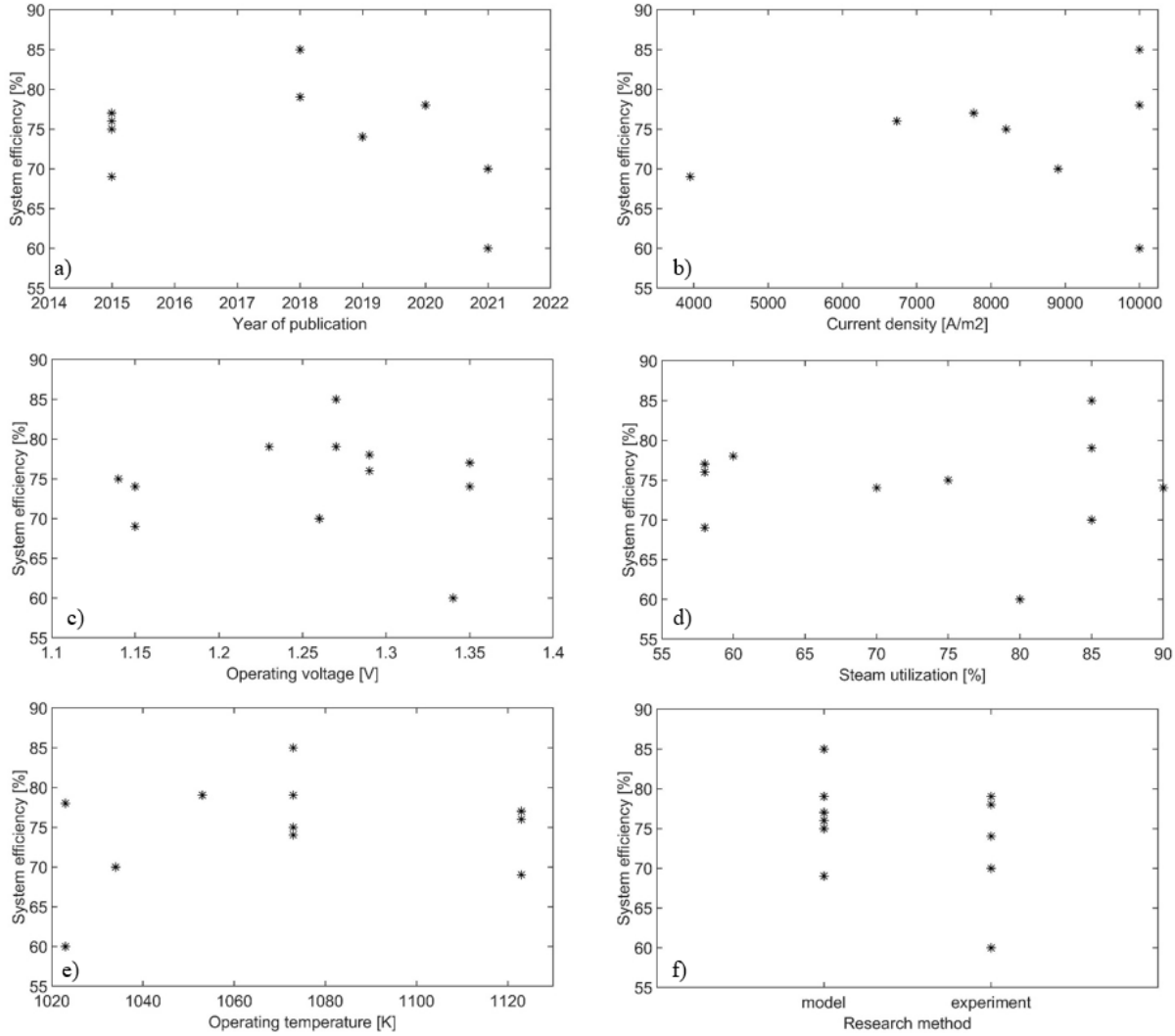

Figure 11 Graphs showing the SOEC systems' efficiencies, based on the lower heating value of hydrogen, and a) year of publication, b) current density, c) operating voltage, d) steam utilization, e) operating temperature, and f) research method.

Another explanation for the large efficiency variations might be the extend of heat integration in the system. Some references reuse only part of the heat that is available in the electrolyser's hot outlet streams to heat up the electrolyser's cold inlet stream, while others focus on reusing as much of this available heat as possible. The relation between the SOEC system's heat integration and efficiency was examined by Peters et al. [56]. They found that the efficiency of an SOEC system using only electric heaters reached a value of 63%, while an SOEC system using both electric heaters and optimal heat integration reached a value of 76% [56]. The extend of heat recovery can thus have a substantial effect on the systems efficiency and should be considered when designing SOEC systems.

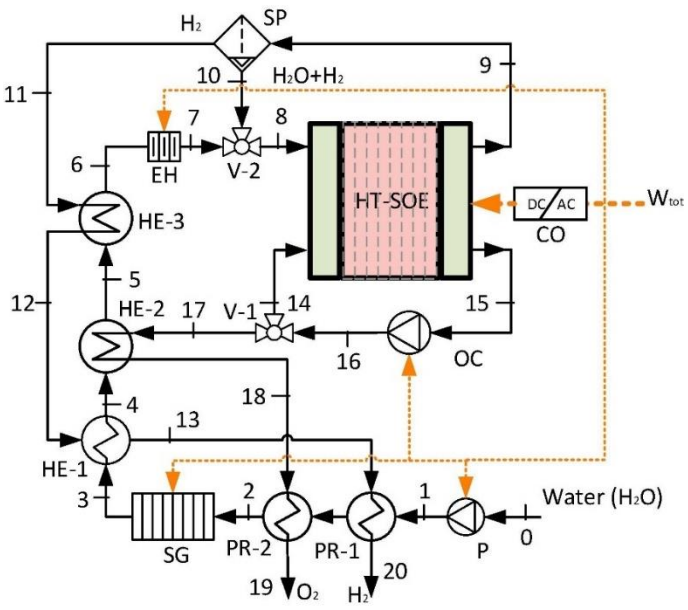

Figure 12 Layout of the SOEC system designed by AlZahrani et al. [10], image from [10].

The effect of heat integration on the system's efficiency can be one of the reasons why AlZahrani et al. [10] obtained the highest system efficiency in Table 3. An overview of their SOEC system is given in Figure 12 [10]. Figure 12 shows that AlZahrani et al. [10] use not only the electrolyser's hot hydrogen and steam outlet stream (stream 9) for preheating (PR-1) and superheating (HE-1 and HE-3) the electrolyser's inlet water and hydrogen, but also the electrolyser's hot oxygen outlet stream (stream 15: PR-2, HE-2) [10]. Electric heaters are used for the evaporation (EH) and additional superheating (SG) of the inlet water and hydrogen [10]. Other references in Table 3 that use this heat exchanger layout are Botta et al. [55], AVL [58], and FuelCell Energy [59]. However, AlZahrani et al. [10] is the only reference that uses an oxygen recirculation loop for the supply of inlet oxygen (stream 14) [10]. Furthermore, it is the only reference that separates the electrolyser's hydrogen and steam outlet stream (stream 9) directly after the electrolyser. A more detailed description of the differences in heat integration between the researches in Table 3 and how they are used to construct the SOEC systems in this thesis is given in section 3.1.

Apart from covering the thermal energy demand of the system, another requirement of SOEC systems is the hydrogen separation. The hydrogen and steam leaving the electrolyser's fuel electrode require separation in order to obtain pure hydrogen. The hydrogen and steam are often separated via either partial condensation or membrane separation [27]. Since hydrogen gas and steam differ in condensation temperature, partial condensation separation is a relatively easy technique for separating the two components [61]. The disadvantage of separation via condensation is that it can only occur at temperatures below 373 K, the condensation temperature of water, and re-using the excess water as electrolyser fuel would require heating it up again. Membrane separation offers the possibility of separating the steam and hydrogen at higher temperature, allowing the steam to be recirculated back into the system at a higher temperature. Although membrane separation is a promising technique, there still are some issues concerning material stability [62]. Therefore, condensation is chosen as the separating technique for the SOEC systems in this thesis.

3. System description

In this thesis, three solid oxide electrolyser (SOEC) systems were designed and examined in order to redesign the solid oxide fuel cell combined gas turbine (SOFC+GT) system described in section 2.2.1 into a reversible solid oxide cell (rSOC) system. First, a basis SOEC system was designed that reuses heat from the SOEC's hot outlet streams to heat up the SOEC's cold inlet streams. Secondly, the heat integration SOEC system was designed in which water is evaporated using heat exchangers instead of an electric heater. Thirdly, the oxygen-cooled SOEC system was designed which has a configuration that is comparable to the SOFC+GT system and thus requires a minimal number of alterations when combining the SOFC+GT and the SOEC systems. The differences between the three designed SOEC systems are briefly summarized in Table 4.

Table 4 Overview of the main differences between the three designed SOEC systems.

	The basis SOEC system	The heat integration SOEC system	The oxygen-cooled SOEC system
Water evaporation	Electric heater	Heat exchangers	Heat exchangers
H_2 and O_2 cooling	Electric coolers	Heat exchangers and electric coolers	Heat exchangers and electric coolers
Oxygen recirculation	• Minimal O_2 mass flow rate • Compressor • No additional O_2 from storage	• Minimal O_2 mass flow rate • Compressor • No additional O_2 from storage	• High O_2 mass flow rate • Ejector • Additional O_2 from storage

3.1. The basis SOEC system

The layout of the basis SOEC system is shown in Figure 13. Water from the storage tank (I) is mixed with recirculating water (II) and preheated (III), evaporated (IV, XIII), and superheated (VI, VII) to the required stack temperature. The water is also mixed with hydrogen (V) to improve the stack's durability [63]. The hot hydrogen and steam leaving the stack (VIII) are used to preheat (III) and partially superheat (VI) the cold inlet stream and are separated using partial condensation (IX). While the water and part of the hydrogen are recirculated back into the cycle, the remaining hydrogen is compressed for storage (X). The hydrogen gas is cooled down in between the compressor stages (XI). At the oxygen electrode inlet of the stack (VIII), oxygen is inserted to minimize performance degradation due to leakages [27]. For this, part of the produced oxygen is recirculated back into the stack (XII). The remaining produced oxygen is used to evaporate part of the inlet water (XIII) and is subsequently compressed for storage (XIV). The oxygen gas is cooled down in between the compressor stages (XV).

I	water storage
II	water mixer
III	preheating heat exchanger
IV	evaporating electric heater
V	water and hydrogen mixer
VI	superheating heat exchanger
VII	superheating electric heater
VIII	rSOC stack
IX	fuel electrode electric cooler
X	hydrogen storage compressor
XI	hydrogen storage compressor cooler
XII	oxygen recirculation compressor
XIII	evaporating heat exchanger
XIV	oxygen storage compressor
XV	oxygen storage compressor cooler

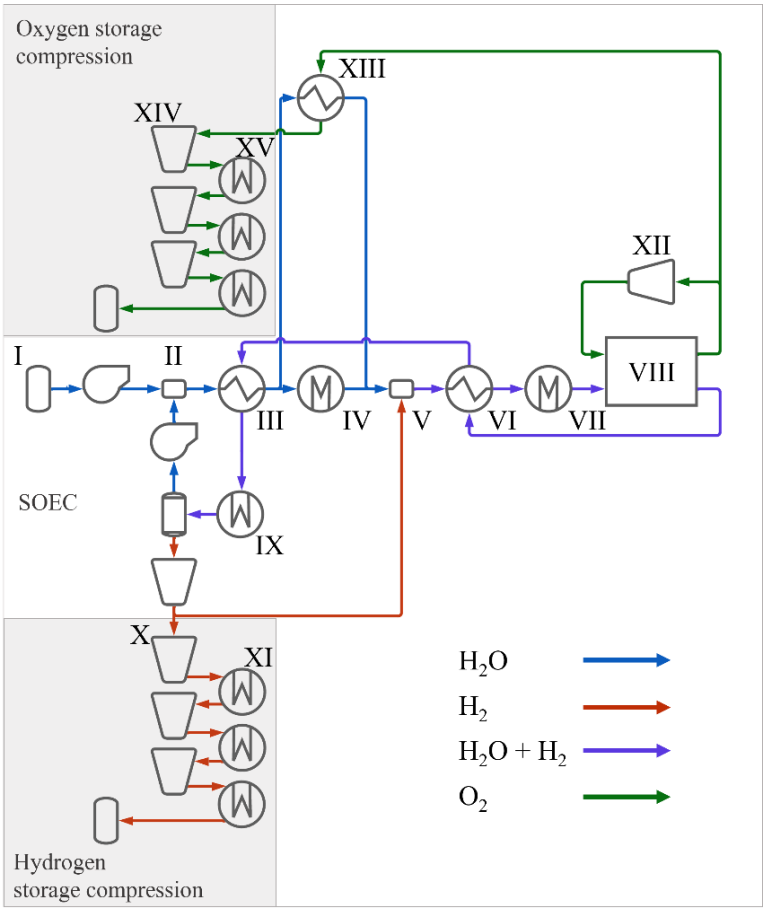

Figure 13 Layout of the basis SOEC system.

The literature on SOEC system design summarized in Table 2 and Table 3 was used to construct this basis SOEC system. Since the literature review in section 2.2.2 showed that the extend of heat integration in an SOEC system can have a substantial effect on the system's efficiency, the heat exchanger layout in basis SOEC system was based on a combination of researches. For example, to heat up the inlet water and hydrogen (III-VII) most researches use only the electrolyser's hot hydrogen and steam outlet streams. However, Botta et al. [55], Kupecki et al. [57], AVL [58], FuelCell Energy [59], and AlZahrani et al. [10] use not only the electrolyser's hot hydrogen and steam outlet stream to heat up the inlet water and hydrogen (III-VII), but also the electrolyser's hot oxygen outlet stream. Botta et al. [55], AVL [58], FuelCell Energy [59], and AlZahrani et al. [10] use this hot oxygen outlet stream for part of the preheating and superheating of the inlet water and hydrogen, thereby reducing the electric power requirement for preheating and superheating. This heat exchanger layout was shown in section 2.2.2 Figure 12. Kupecki et al. [57] use the hot oxygen outlet stream for part of the water evaporation, thereby reducing the electric power requirement for evaporation. In the basis SOEC system constructed in this thesis, the electrolyser's hot oxygen outlet stream is used to evaporate (XIII) part of the inlet water. The inlet water and hydrogen is preheated (III) and superheated (VI) using the electrolyser's hot hydrogen and steam outlet stream. The remaining heat required for evaporating and superheating the inlet water and hydrogen stream is supplied by electric heaters (IV and VII).

The separator (IX) used in the basis SOEC system is based on the partial condensation units from Zhao et al. [37], Mastropasqua et al. [38] and Kupecki et al. [57]. In these partial condensation units, the electrolyser's hydrogen and steam outlet stream is cooled down to ambient temperature before separation [37, 38, 57]. After separation, the water is recirculated back into the system to be heated up again (II). Also part of the hydrogen is recirculated back into the system after separation (V). The hydrogen recirculation occurs after the water evaporation due to both practical and safety reasons. Other

systems with hydrogen recirculation, such as Peters et al. [56], AVL [58], and FuelCell Energy [59], recirculate the hydrogen before the water condensation. Their recirculated hydrogen stream thus contains more steam [56, 58, 59]. AlZahrani et al. [10] separate the hydrogen and steam directly when it leaves the electrolyser using membrane separation. As described in section 2.2.2, membrane separation offers the possibility of separating the steam and hydrogen at a high temperature, allowing both steam and hydrogen to be recirculated back into the system at this higher temperature. However, there still are some issues concerning material stability in membrane separators and therefore condensation is chosen as the separation technique in the basis SOEC systems [62].

Literature on SOEC system design is in disagreement on the effect of the electrolyser's thermal operating point on the system's efficiency, as was described in section 2.2.2. Since operating the electrolyser in the thermo-neutral mode results in the least thermal stresses in the electrolyser, the electrolyser in the basis SOEC system is operated at this thermo-neutral point [38]. Another advantage of operating the electrolyser in the thermal-neutral mode, is that the electrolyser does not require additional heating or cooling. This means that at the electrolyser's oxygen electrode, no additional gas is required for this heating or cooling. All researches in Table 2 and Table 3 do however insert additional gas at the oxygen electrode. O'Brien et al. [27] state that inserting gas at the oxygen electrode, the gas being either air or pure oxygen, will minimize performance degradation in the electrolyser [27]. Furthermore, they argue that inserting air at the oxygen electrode can decrease the required cell voltage, and thus increase the cell's efficiency, due to a reduction in oxygen partial pressure [27]. Most of the researches in Table 2 and Table 3 therefore insert air at the electrolyser's oxygen electrode. AlZahrani et al [10] is the only reference in Table 2 and Table 3 that inserts pure oxygen instead of air at the oxygen electrode. In this thesis, pure oxygen is required when redesigning the SOFC+GT system into an rSOC system. Therefore, the basis SOEC system inserts pure oxygen at the electrolyser's oxygen electrode instead of air. This inlet oxygen could be supplied by the oxygen storage tank in Figure 13, however, then the oxygen would have to be heated up from the ambient storage temperature to the required electrolyser temperature. In the SOFC+GT system designed by Malhotra, D. [16], the inlet oxygen is supplied by recirculating oxygen from the fuel cell's outlet stream to the fuel cell's inlet [16]. Also AlZahrani et al. [10] use an oxygen recirculation loop for the inlet oxygen [10]. Since the oxygen recirculation reduces the heat requirement of the system, the inlet oxygen in the basis SOEC system is supplied via a recirculation loop as well (XII).

3.2. The heat integration SOEC system

In the heat integration SOEC system, water is evaporated using heat exchangers instead of an electric heater. The layout of the heat integration SOEC system is shown in Figure 14. The configuration of this system is comparable to the basis SOEC system, however, the hydrogen and oxygen gas are cooled down between the compressor stages via heat exchangers (XIIIa-g) instead of via coolers. In the heat exchangers, the hydrogen and oxygen gas give off their heat in order to evaporate the inlet water. Therefore, the coolers between the storage compressors and the electric heater for the water evaporation are no longer required. To cool the hydrogen and oxygen streams to the required storage temperature, coolers XI and XV are required.

I	water storage
II	water mixer
III	preheating heat exchanger
V	water and hydrogen mixer
VI	superheating heat exchanger
VII	superheating electric heater
VIII	rSOC stack
IX	fuel electrode electric cooler
X	hydrogen storage compressor
XI	hydrogen storage compressor cooler
XII	oxygen recirculation compressor
XIIIa-g	evaporating heat exchanger
XIV	oxygen storage compressor
XV	oxygen storage compressor cooler

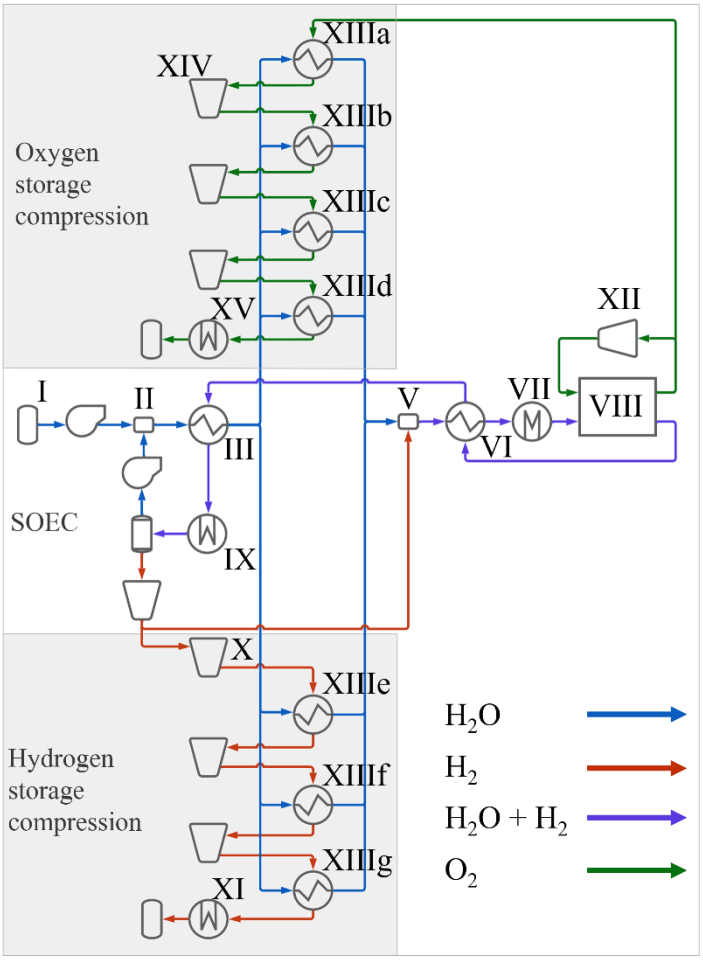

Figure 14 Layout of the heat integration SOEC system. The roman numerals in the figure represent the components in the heat integration SOEC system that are equal to the corresponding components in the basis SOEC system. In case a roman letters is added to the roman numeral, the component is altered compared to the basis SOEC system.

3.3. The oxygen-cooled SOEC system

The oxygen-cooled SOEC system focusses on a configuration that is comparable to the SOFC+GT system and on minimizing the number of required alterations when combining the SOFC+GT and the SOEC systems. In the SOFC+GT system, a high oxygen recirculation flow is used for cooling of the SOFC stack. As described in section 2.2.1, oxygen from a storage tank is mixed with this recirculated oxygen in an ejector, to obtain the required oxygen mass flow rate. In order to minimize the alterations required when combining the SOFC+GT and SOEC systems, the oxygen-cooled SOEC system also uses this high oxygen recirculation mass flow rate and ejector. The ejector in the SOFC+GT system is designed for specific operating conditions, therefore, these conditions are also met in the oxygen-cooled SOEC system. In the SOFC+GT system designed by Malhotra, D. [16], oxygen enters the ejector at a temperature of 288 K and a pressure of 0.6 MPa [16]. However, in the rSOC system, the oxygen will be stored at atmospheric temperature and a pressure of 16 MPa. The oxygen will thus have to be expanded in the SOFC+GT system using turbines before entering the ejector. Since the oxygen-cooled SOEC system focusses on minimizing the number of required alterations when combining the SOFC+GT and the SOEC systems, the oxygen-cooled SOEC system will also used these turbines for expansion of the oxygen gas.

The layout of oxygen-cooled SOEC system is comparable to that of the basis SOEC system, except for the oxygen recirculation and water evaporation. The layout of the oxygen-cooled SOEC system is shown

in Figure 15. In Figure 15, oxygen from the storage tank (XVI) is first heated up in a heat exchanger (XVa) and then expanded in two turbines (XIIa) before entering the ejector (XIIb). In the SOFC+GT system, the other ejector inlet uses recirculated oxygen. The SOEC stack in the oxygen-cooled SOEC system (VIII) produces oxygen, therefore, only part of the oxygen is recirculated back into the ejector and the remaining oxygen is compressed (XIV) for storage (XVI). Comparable to the heat integration SOEC system, heat exchangers are used for evaporation of the inlet water (XIIIa-d). Due to the increase in oxygen mass flow rate, less heat exchangers are required for this evaporation. The hydrogen and oxygen gas are therefore cooled down between the remaining compressor stages via coolers (XV, XI).

I	water storage
III	preheating heat exchanger
V	water and hydrogen mixer
VI	superheating heat exchanger
VII	superheating electric heater
VIII	rSOC stack
IX	fuel electrode electric cooler
X	hydrogen storage compressor
XI	hydrogen storage compressor cooler
XIIa	oxygen recirculation turbine
XIIb	oxygen recirculation ejector
XIIIa-d	evaporating heat exchanger
XIV	oxygen storage compressor
XV	oxygen storage compressor cooler
XVa	oxygen storage heat exchanger
XVI	oxygen storage

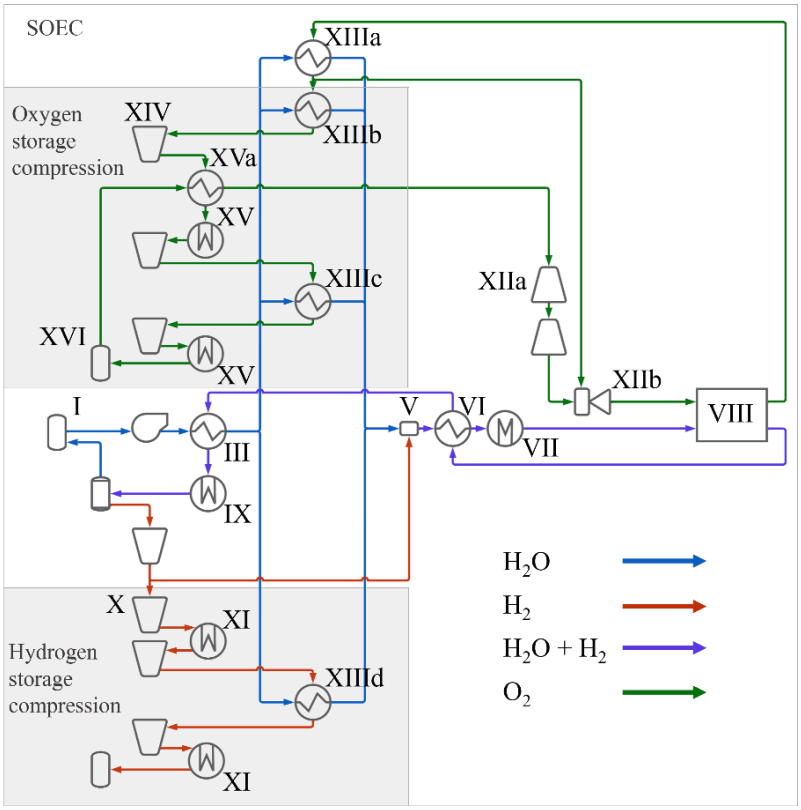

Figure 15 Layout of the oxygen-cooled SOEC system. The roman numerals in the figure represent the components in the heat integration SOEC system that are equal to the corresponding components in the basis SOEC system. In case a roman letters is added to the roman numeral, the component is altered compared to the basis SOEC system.

4. Methods

The three solid oxide electrolyser (SOEC) systems described in the previous section were examined using the electrochemical and thermodynamic models described in section 4.1 and the simulation parameters described in section 4.2.

4.1. Modelling of the SOEC systems

This section describes the electrochemical model, thermodynamic model and efficiency definitions that were used to examine the performance of the SOEC systems. The model equations were computed using MATLAB software version 9.11.0 (R2021b) [64]. The COOLPROP database version 6.4.3 was used to determine the properties of the fluids [65].

4.1.1. Electrochemical model

In the electrochemical model that was used to examine the SOEC systems, the voltage required for the electrolysis cells consists of the equilibrium voltage E and the voltage related to the losses in the cell η, as described in section 2.1 [24]. The electrolysis cells were assumed to operate at steady-state conditions. Furthermore, it was assumed that the losses, also called the overpotentials, of an electrolysis cell could be determined using the same equations as the overpotentials of a solid oxide fuel cell (SOFC) [66]. The formulas that have been used to describe the SOEC overpotentials were therefore based on the SOFC models from Chan et al. [67, 68].

The equilibrium voltage, or Nernst potential, was determined as [37]

$$E = E^0 + \frac{RT}{2F} \ln\left(\frac{\frac{p_{\mathrm{H_2}}}{P^0}\left(\frac{p_{\mathrm{O_2}}}{P^0}\right)^{1/2}}{\frac{p_{\mathrm{H_2O}}}{P^0}} \right), \quad (5)$$

with T representing the cell operating temperature and $p_{\mathrm{H_2}}$, $p_{\mathrm{O_2}}$ and $p_{\mathrm{H_2O}}$ the partial pressures of the hydrogen, oxygen, and water, respectively. The term E^0 represents the standard potential and depends on the change in Gibbs free energy of the reaction. For hydrogen SOECs, the standard potential results in [19]

$$E^0 = {\Delta G^0}/{2F} \approx 1.253 - 2.4516 \cdot 10^{-4} T. \quad (6)$$

The losses or overpotentials of a cell can be classified in three categories: Activation overpotential, which is the voltage that is required to overcome the activation energy of the chemical reactions [20]; ohmic overpotential, which is the voltage that is required to overcome the ohmic resistance [68]; and concentration overpotential, which is the voltage that is required to overcome any resistances related to mass transport [20]. Research suggests that for high temperature electrochemical cells, the activation and concentration overpotentials are small compared to the ohmic overpotential [19, 68]. However, since the electrolysis cells were operated close to their limiting current density, the concentration overpotential was included in the electrochemical model. The electrolysis cell voltage was thus determined as [24]

$$V = E + \eta_{\mathrm{ohm}} + \eta_{\mathrm{conc}}. \quad (7)$$

The ohmic overpotential was determined as a function of the current density J and the sum of the electronic and ionic resistances of the cell R_c [68]

$$\eta_{ohm} = J \cdot R_c. \quad (8)$$

The concentration overpotential was determined as a function of the temperature, current density and limiting current density of the cell [67]

$$\eta_{conc} = \frac{RT}{2F} \ln\left[1 - \frac{J}{J_L}\right]. \quad (9)$$

For electrolysers, another voltage in addition to the equilibrium voltage is relevant; the thermo-neutral cell voltage. As described in section 2.1, the thermo-neutral cell voltage represents the potential at which the heat required for electrolysis equals the heat produced by the losses inside the cell [25]. The thermo-neutral cell voltage was determined as [26]

$$V_{tn} = \frac{\Delta H}{2F}. \quad (10)$$

The change in enthalpy between the electrolysis products and reactants ΔH represents the total amount of energy required for the electrolysis process. This total amount of energy consists of both the electrical and thermal energy required for electrolysis, which are represented by the Gibbs free energy change and entropy change respectively [30]

$$\Delta H = \Delta G + T\Delta S. \quad (11)$$

Equation (6) showed that the equilibrium voltage is related to the Gibbs free energy change. Thus, when the cell is operated at a voltage below or above the thermo-neutral voltage, thermal energy shall have to be respectively added to or removed from the cell. This was also illustrated in section 2.1 Figure 5.

4.1.2. Thermodynamic model

The electrochemical model described in the previous section was used to examine the performance of the SOEC stack. The thermodynamic model described in this section was used to examine the performance of the other components in the SOEC system. It was assumed that all fluids in the system behaved as ideal fluids and that there was negligible loss of mass and energy in the pipes between the components. Each component was examined using the mass and energy balances for a control volume with one-dimensional flow [69]. It was assumed that all system components operated at steady state and that the influence of potential and kinetic energy changes were negligible.

The mass and energy balances of the system thus simplified to

$$\sum \dot{m}_{in} = \sum \dot{m}_{out}, \quad (12)$$

$$0 = \dot{Q} - \dot{W} + \sum [\dot{m} \cdot h]_{in} - \sum [\dot{m} \cdot h]_{out}. \quad (13)$$

The enthalpy of a mixture containing components i was defined as [69]

$$\dot{m}_{tot} \cdot h_{tot} = \sum [\dot{m} \cdot h]_i. \quad (14)$$

Several components in the system were examined using these equations. Heat transfer with the environment was assumed to be negligible in all components except the SOEC stack. Exchange of work

with the environment was assumed to be negligible in the heat exchangers, heaters, mixers, and separators.

The enthalpy of the compressor outlet stream $h_{\mathrm{comp,out}}$ was determined using the definition of the isentropic compressor efficiency [69]

$$\eta_{\mathrm{comp,is}} = \frac{h_{\mathrm{comp,out,s}} - h_{\mathrm{comp,in}}}{h_{\mathrm{comp,out}} - h_{\mathrm{comp,in}}}. \quad (15)$$

The power required for compression was calculated as [69]

$$P_{\mathrm{comp}} = \frac{\dot{W}_{\mathrm{comp}}}{\eta_{\mathrm{comp,mech}}}, \quad (16)$$

with $\eta_{\mathrm{comp,mech}}$ the mechanical compressor efficiency. For pumps, the same equations were used as for compressors.

The enthalpy of the turbine outlet stream $h_{\mathrm{turb,out}}$ was determined using the definition of the isentropic turbine efficiency [69]

$$\eta_{\mathrm{turb,is}} = \frac{h_{\mathrm{turb,in}} - h_{\mathrm{turb,out}}}{h_{\mathrm{turb,in}} - h_{\mathrm{turb,out,s}}}. \quad (17)$$

The power required for the turbines was calculated as [69]

$$P_{\mathrm{turb}} = \dot{W}_{\mathrm{turb}} \cdot \eta_{\mathrm{turb,mech}}, \quad (18)$$

with $\eta_{\mathrm{turb,mech}}$ the mechanical turbine efficiency.

For the mixers, it was assumed that the pressure and specific heat of the fluids remained constant inside the mixer. The temperature of the mixer outlet stream was then determined as [69]

$$T_{\mathrm{mix,out}} = \frac{n_{\mathrm{mix,in1}} c_{p,\mathrm{mix,in1}} T_{\mathrm{mix,in1}} + n_{\mathrm{mix,in2}} c_{p,\mathrm{mix,in2}} T_{\mathrm{mix,in2}}}{n_{\mathrm{mix,in1}} c_{p,\mathrm{mix,in1}} + n_{\mathrm{mix,in2}} c_{p,\mathrm{mix,in2}}}. \quad (19)$$

For the separators, it was assumed that the temperature of the fluids in the separator remained constant.

In addition to the energy analysis, the SOEC systems were examined using an exergy analysis. Exergy represents the maximum amount of work that can be obtained when bringing a system in equilibrium with the environment [70]. This environment, or reference state, was defined at a temperature of 298.15 K and a pressure of $1.01 \cdot 10^5$ Pa. Irreversibilities within a system lead to the destruction of exergy, therefore, the exergy destruction in a system represents how effectively the energy resources are used [70]. The rate of exergy destruction of each component was determined as [70]

$$\dot{\mathrm{E}}_{\mathrm{d}} = \sum \left[\left(1 - \frac{T_0}{T}\right) \dot{Q} \right]_{\mathrm{j}} - \dot{W} + \sum \left[\dot{m} \cdot \mathrm{e}_{\mathrm{f}}\right]_{\mathrm{in}} - \sum \left[\dot{m} \cdot \mathrm{e}_{\mathrm{f}}\right]_{\mathrm{out}}, \quad (20)$$

with T_{o} the temperature of the reference environment. The term $\sum \left[\frac{\dot{Q}}{T}\right]_{\mathrm{j}}$, representing the heat transfer into or out of the system, was assumed to be negligible for all components except the stack. The term $\dot{W}$, representing the work transfer into or out of the system, was assumed to be negligible in the heat exchangers, heaters, mixers, and separators. The term e_{f} represents the specific flow exergy, consisting of both the physical and chemical exergy, which was determined as [70]

$$\mathrm{e}_{\mathrm{f}} = \mathrm{e}_{\mathrm{f}}^{\mathrm{phys}} + \mathrm{e}_{\mathrm{f}}^{\mathrm{chem}} = (h - h_{\mathrm{o}}) - T_{\mathrm{o}}(s - s_{\mathrm{o}}) + \mathrm{e}_{\mathrm{f}}^{\mathrm{chem}}. \quad (21)$$

The standard chemical exergies of hydrogen, oxygen, and water were retrieved from Bakshi et al. [71].

4.1.3. Efficiency definitions

The results from the electrochemical and thermodynamic models were used to evaluate the performance of the SOEC systems via the energy and exergy efficiencies.

The energy efficiency of an SOEC system was expressed as the ratio of the chemical energy, based on the lower heating value (LHV), of the produced hydrogen by the energy required for the stack and other system components [60]

$$\eta_{\text{en,SOEC}} = \frac{\text{LHV}_{\text{H}_2}\dot{m}_{\text{H}_2,\text{out}}}{P_{\text{stack}}+\dot{Q}_{\text{stack}}+P_{\text{sys}}+\dot{Q}_{\text{sys}}} \cdot 100\%. \quad (22)$$

The power required for the stack was determined by the multiplication of its operating voltage and current density [15]

$$P_{\text{stack}} = J_{\text{stack}} \cdot V_{\text{stack}}. \quad (23)$$

The heat required for the stack was determined as [52]

$$\dot{Q}_{\text{stack}} = J_{\text{stack}} \cdot (V_{\text{tn}} - V_{\text{stack}}). \quad (24)$$

The power and heat required for the other system components were determined using the equations from the thermodynamic model.

The exergy efficiency of the SOEC system was expressed as the ratio of the exergy content of the produced hydrogen by the amount of exergy required by the system [70]

$$\eta_{\text{ex,SOEC}} = \frac{e_{\text{f}_{\text{H}_2}}\dot{m}_{\text{H}_2,\text{out}}}{P_{\text{stack}}+\dot{Q}_{\text{stack}}+P_{\text{sys}}+\dot{Q}_{\text{sys}}+\left(e_{\text{f}_{\text{H}_2\text{O}}} \cdot \dot{m}_{\text{H}_2\text{O,in}}\right)} \cdot 100\%. \quad (25)$$

The specific flow exergies of the hydrogen and water were determined using Equation (21).

When combining the SOEC system and the SOFC+GT system to form an rSOC system, the round-trip energy efficiency can be determined by multiplication of the SOEC and the SOFC+GT systems' energy efficiencies [72]

$$\eta_{\text{en,rSOC,rt}} = \left(\eta_{\text{en,SOEC}} \cdot \eta_{\text{en,SOFC+GT}}\right) \cdot \frac{1}{100}. \quad (26)$$

4.2. Simulation parameters

This section describes the simulation parameters that were used to examine the SOEC systems.

The simulation parameters of the rSOC stack, operated in SOEC mode, were based on an rSOC that was manufactured by Elcogen and optimized by the Technical University of Denmark and CEA-Liten [50]. The simulation parameters are summarized in Table 5. Initially, an average stack temperature of 1023.15 K was chosen, which is in the middle of the suggested operating range of 973.15-1073.15 K. At this temperature, the stack operated in a thermo-neutral mode at a cell voltage of 1.29 V and current density of -12400 A/m^2. The heat loss in the stack was assumed to be 5% of the stack's input power.

Table 5 RSOC simulation parameters. Based on the parameters from Hauch et al. [50].

Parameter	Value	
rSOC effective cell area, $A_{\mathrm{rSOCcell,eff}}$	0.01	m^2
rSOC number of cells, N_{rSOCcell}	25	-
SOEC mode hydrogen fraction, $x_{\mathrm{H_2,Nernst,SOEC}}$	0.1	-
SOEC mode steam fraction, $x_{\mathrm{H_2O,Nernst,SOEC}}$	0.9	-
SOEC mode oxygen fraction, $x_{\mathrm{O_2,Nernst,SOEC}}$	1	-
SOEC mode cell resistance, $R_{\mathrm{c,SOEC}}$	$2.8 \cdot 10^{-5}$	$\Omega\mathrm{m}^2$
SOEC mode limiting current density, $J_{\mathrm{L,SOEC}}$	-13500	$\mathrm{A/m}^2$
SOEC mode average stack temperature, T_{SOEC}	1023.15	K
SOEC mode average stack pressure, p_{SOEC}	$1 \cdot 10^5$	Pa
SOEC mode pressure loss, $p_{\mathrm{SOEC,loss}}$	2	%
SOEC mode thermo-neutral cell voltage, $V_{\mathrm{SOEC,cell}}$	1.29	V
SOEC mode thermo-neutral current density, $J_{\mathrm{SOEC,cell}}$	-12400	$\mathrm{A/m}^2$
SOEC mode utilization factor, $U_{\mathrm{f,rSOC}}$	80	%

The simulation parameters of the other system components are summarized in Table 6. In addition to the component parameters listed in Table 6, the water was assumed to be stored at atmospheric temperature and pressure, and the hydrogen and oxygen were stored at atmospheric temperature and a pressure of 16 MPa. The fuel electrode inlet stream was assumed to contain 90% steam and 10% hydrogen.

Table 6 Simulation parameters of the other system components.

Parameter	Value		
Individual compressor isentropic efficiency, $\eta_{\mathrm{comp,is}}$	70	%	[56]
Individual compressor mechanical efficiency, $\eta_{\mathrm{comp,mech}}$	90	%	[56]
Individual H_2 and O_2 compressor pressure ratio, $\mathrm{R_{p,comp}}$	5.5	-	[73]
Individual turbine isentropic efficiency, $\eta_{\mathrm{turb,is}}$	70	%	[69]
Individual turbine mechanical efficiency, $\eta_{\mathrm{turb,mech}}$	90	%	[69]
Individual turbine pressure ratio, $\mathrm{R_{p,turb}}$	5	-	[16]
Heat exchanger pressure loss, $p_{\mathrm{HEX,loss}}$	1	%	[67]
Heat exchanger minimum temperature difference, $\Delta T_{\mathrm{HEX,min}}$	15	K	[31]
Electric heater efficiency, η_{heater}	99	%	[69]
Cooler energy efficiency ratio, $\mathrm{EER_{cooler}}$	5	-	[74]

5. Results and discussion

The SOEC systems were examined using the models and parameters described in the previous section. In this section, the electrochemical model is validated in section 5.1. Then, the energy and exergy performance of the three SOEC systems are discussed in sections 5.2 and 5.3 respectively. Lastly, the results of the parameter analysis are discussed in section 5.4.

5.1. Electrochemical model validation

In order to examine whether the assumptions in the electrochemical model were valid, the results from the electrochemical model were compared to research by Hauch et al. [50]. In their research, Hauch et al. [50] examined the performance of an rSOC manufactured by Elcogen and optimized by the Technical University of Denmark and CEA-Liten [50]. The electrochemical model was assumed to be accurate enough when the calculated SOEC voltage deviated with a maximum of 3% from the SOEC voltage of Hauch et al. [50]. The equations used in the electrochemical model were described in section 4.1.1 and the parameters used for validation are equal to the parameters used by Hauch et al. [50]. These parameters are summarized in Table 7 [50].

Table 7 rSOC model parameters for the electrochemical model validation, from Hauch et al. [32].

Parameter	Value
T_{SOEC}	973 K
$p_{\mathrm{H_2,SOEC}}$	0.01 MPa
$p_{\mathrm{H_2O,SOEC}}$	0.09 MPa
$p_{\mathrm{O_2,SOEC}}$	0.02 MPa
J_{SOEC}	-13500 : 0 $\mathrm{A/m^2}$
$R_{\mathrm{c,SOEC}}$	0.000028 $\Omega\mathrm{m^2}$
$J_{\mathrm{L,SOEC}}$	-13500 $\mathrm{A/m^2}$

The cell's IV-curve during electrolyser mode that followed from filling in the parameters in the electrochemical model, is shown in Figure 16. This figure shows both the IV-curve that follows from the electrochemical model of this thesis and the results from the reference experiment conducted by Hauch et al. [50].

The figure shows that the equations used in the electrochemical model resembled the reference rSOC results from Hauch et al. [50] during SOEC mode. The figure shows that the concentration overpotential in Equation (9) slightly deviated from the actual rSOC voltage from Hauch et al. [50]. However, since this deviation was within the 3% deviation, the electrochemical model approximates the electrolysis cell voltage accurately enough.

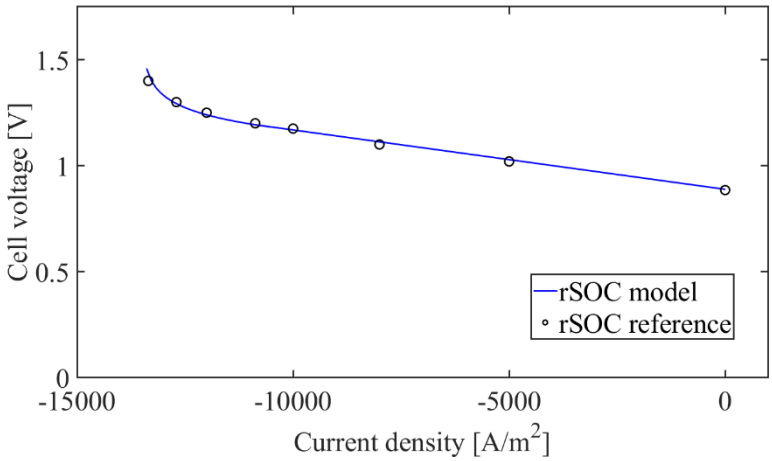

Figure 16 The cell's IV-curve during electrolyser mode using the electrochemical model of this thesis (solid line) and the experimental results from Hauch et al. [50] (dots).

5.2. Energy analysis

The three SOEC systems described in section 3 were examined using the energy equations and simulation parameters described in section 4. An overview of the stream data of the different systems is given in Appendix B, C, and D.

5.2.1. The basis SOEC system

In the basis SOEC system, the heat from the hot electrolyser's outlet streams is used to heat up the cold electrolyser's inlet streams. An illustration of the temperature-enthalpy diagram of the basis SOEC system is given in the top graph of Figure 20. It should be noted that this is not the actual temperature-enthalpy diagram of the basis SOEC system, because the water evaporation heat exchanger and electric heater are placed in parallel, as was shown in Figure 13, and not in series, as is visualized in Figure 20. However, by visualising the water evaporation in series, the figure gives a more comprehensive overview of how the heat requirement of the basis SOEC system is met. Figure 20 shows at the left side of the graph that the cold water stream is preheated by a heat exchanger. In this heat exchanger (III), the water is heated up to a temperature of 372 K, which is slightly below the water's evaporation temperature. The hot stream, which consists of a mixture of hydrogen and steam, cools down to the steam's condensation temperature and thus the steam starts to condensate. After the heat exchanger, the hot stream still contains some heat. However, since the amount of heat is relatively small and of a low temperature, this heat is not reused in the system. An electric cooler therefore cools down the hot stream to the required separation temperature. After the preheater, the water is evaporated by both a heat exchanger and an electric heater. A more detailed examination of the evaporation's heat requirement is described below. After evaporation, the steam is mixed with hydrogen. The hydrogen has a lower temperature than the steam and thus mixing results in a slight temperature drop in the graph. The temperature of the steam before the mixing has to be high enough to ensure that the temperature drop does not result in steam condensation. Finally, the steam and hydrogen inlet stream is superheated using both a heat exchanger and an electric heater. A more detailed examination of the superheater's heat requirement is described below.

The distribution of the power that is required for the electrolyser and other system components in the basis SOEC system is shown in Figure 17. The total power requirement of the basis SOEC system is 49.20 kWh/kgH_2. The minimal power requirement of water electrolysis, as was visualized in Figure 8, is 34.40 kWh/kgH_2.

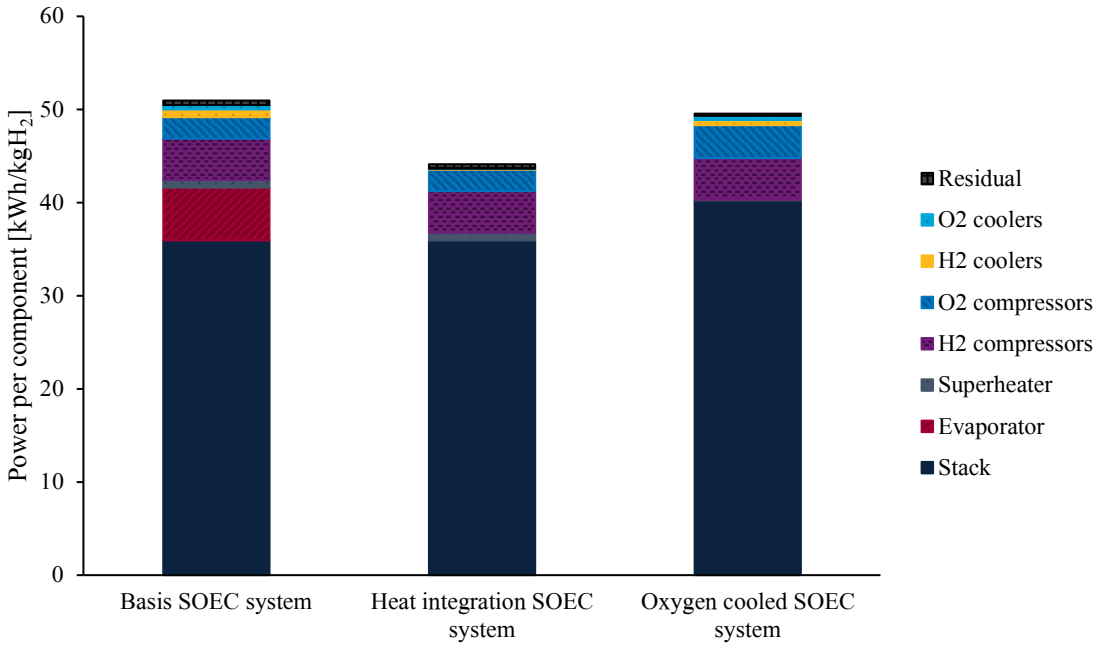

Figure 17 Distribution of the power required for the three SOEC systems.

Figure 17 shows that the stack requires significantly more power than the other system components, namely 35.94 kWh/kgH_2. This stack power requirement is comparable to the minimum power requirement of water electrolysis, since the stack is operated at the thermo-neutral voltage. In sections 2.1 and 4.1.1, it was explained that the thermo-neutral voltage represents the voltage at which the electric power supply to the electrolyser equals the amount of energy required for water electrolysis. However, the stack's power requirement in the basis SOEC system is slightly higher than the minimum power requirement for water electrolysis due to the heat losses considered at the stack. After the stack, most power in the basis SOEC system is required by the electric heater that evaporates the water, which is component IV in Figure 13. This relatively high fraction of power required for the evaporation of the inlet water is a problem common to SOEC systems [10, 37, 75]. The evaporation power requirement in Figure 17 does not represent the entire heat demand for water evaporation, because twenty percent of the inlet water is evaporated in heat exchanger XIII instead of the electric heater. In heat exchanger XIII, the water is evaporated using the electrolyser's hot oxygen outlet stream. The temperature-enthalpy diagram for this heat exchanger is given in Figure 18. The remaining water is evaporated using electric heater IV.

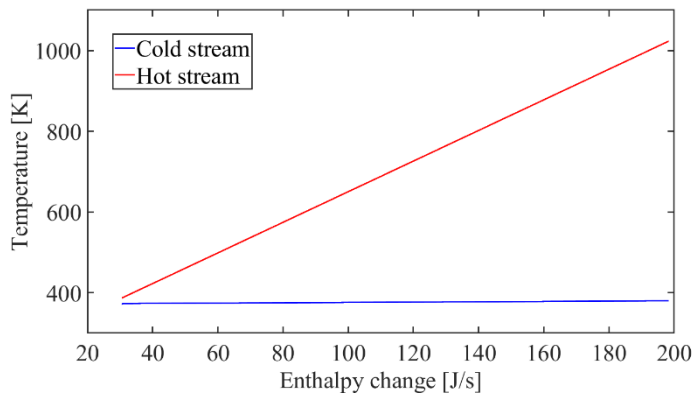

Figure 18 The temperature-enthalpy diagram of water evaporation in heat exchanger XII of the basis SOEC system. The cold stream represents the water stream and the hot stream represents the electrolyser's oxygen outlet stream.

Figure 17 shows that the basis system also requires power for superheating the inlet steam and hydrogen to the required stack temperature. The total amount of heat that is required for superheating the cold steam and hydrogen inlet stream is visualized in Figure 19. Figure 19 shows that most of the heat required for superheating the cold inlet stream can be covered by the hot outlet stream in heat exchanger VI (Q_{HEX}). However, due to the different stream compositions of the

electrolyser's inlet and outlet streams and the minimum temperature difference required for the heat exchanger, the hot outlet stream cannot superheat the cold inlet stream to the required stack temperature and therefore electric superheater VII is required (Q_{heater}).

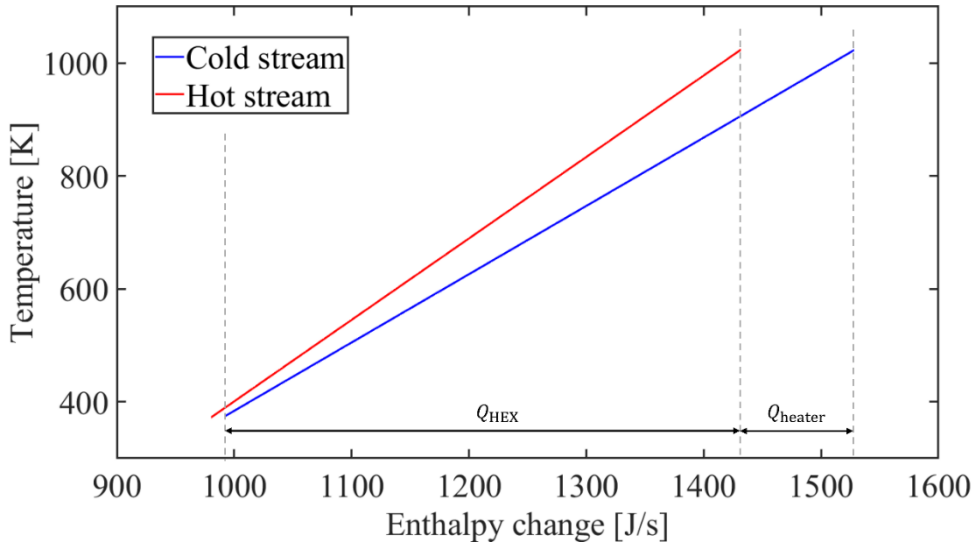

Figure 19 The temperature-enthalpy diagram of superheating the cold steam and hydrogen inlet stream in heat exchanger VI and electric heater VII of the basis SOEC system. The hot stream represents the electrolyser's hydrogen and steam outlet stream.

Additional power in the basis system is required for the hydrogen and oxygen storage compressors and the coolers in between these compressors. Little power is required for the other system components, like the water pumps and recirculation compressors.

It was found that the basis SOEC system reaches an energy efficiency, based on the lower heating value of hydrogen, of 65.40%. The efficiency of the basis SOEC system can be compared to SOEC system efficiencies found in literature, which were summarized in Table 3. Compared to these reference systems, the efficiency of the basis SOEC system is relatively low. However, most references did not include the hydrogen compression in their efficiency calculation. To enable comparison with the basis SOEC system, the references' SOEC system efficiencies including hydrogen compression were estimated. Figure 17 shows that approximately 5.26 kWh/kgH_2 is required for the compression of hydrogen to 16 MPa including the cooling in between the compression stages. For each reference, the hydrogen production rate was determined using the cells' current density and area given in the reference and the equation [19]

$$\dot{m}_{\text{H}_2,\text{prod}} = \left(J \cdot A \cdot M_{\text{H}_2}\right) \Big/ (2 \cdot 1000 \cdot F) \cdot \qquad (27)$$

The hydrogen production rate was then multiplied with the compression power requirement of 5.26 kWh/kgH_2 and incorporated in the efficiency calculation. For the references that already compressed their hydrogen to a lower storage pressure, which were Peters et al. [56] and FuelCell Energy [59], the power requirement was adjusted accordingly. Table 8 shows the efficiencies of the reference systems and the estimated efficiencies which include hydrogen compression. Two reference systems, by Kupecki et al. [57] and AVL [58], are not included in this table since these references did not publish the data that was required for recalculation. When comparing the efficiency of the basis SOEC system to the estimated efficiencies including hydrogen compression of the reference systems, the basis SOEC system's efficiency has a more median value. The basis SOEC system's efficiency still is not high

compared to the other systems, however, none of the references compressed their oxygen product for storage.

Table 8 Three efficiencies of SOEC systems in literature: The first efficiency is given by the reference, the second includes hydrogen compression to a storage pressure of 16 MPa, and the third includes hydrogen and oxygen compression to a storage pressure of 16 MPa.

Reference	Efficiency in reference	Efficiency including H_2 compression to 16 MPa	Efficiency including H_2 and O_2 compression to 16 MPa
AlZahrani et al. [10]	85%	75%	71%
Botta et al. [55]	75%	67%	62%
Peters et al. [56]	76%	75%	71%
Saarinen et al. [53]	60%	55%	51%
FuelCell Energy [59]	78%	75%	70%
Peters et al. [60]	70%	63%	60%

To enable a more equal comparison of the basis SOEC system to the reference systems, the references' SOEC system efficiencies were estimated including both hydrogen and oxygen compression to 16 MPa. Figure 17 shows that approximately 8.04 kWh/kgH_2 is required for the compression of both hydrogen and oxygen to 16 MPa including the cooling in between the compression stages. For each reference, this power requirement was added to the efficiency calculation. Compared to the procedure described above of including only hydrogen compression in the efficiency calculations, the procedure of including both hydrogen and oxygen compression requires extra steps. In section 3.1, it was described that most SOEC references use air instead of pure oxygen at the oxygen electrode. The reference systems' oxygen outlet streams therefore contain both air and oxygen. According to O'Brien et al. [27] air at the oxygen electrode is not only used as a sweep gas, but it also results in a decreased cell voltage, as was described in section 3.1 [27]. This means that when operating the cell at a certain voltage, more hydrogen and oxygen can be produced when using air compared to pure oxygen. Thus, the power required for hydrogen and oxygen compression changes. The references did not publish enough information to recalculate their cell's operating point for pure oxygen and therefore, the effect of using pure oxygen on the hydrogen production was estimated using the basis SOEC system. In the basis SOEC system, the use of pure oxygen instead of air at the oxygen electrode results in a decrease in current density of 330 A/m^2 when the cells are operated at the thermo-neutral voltage. For each reference, this current density was included in the estimation of the hydrogen production rate using Equation (27). The hydrogen production rate was then multiplied with the compression power requirement of 8.04 kWh/kgH_2 and incorporated in the efficiency calculation. AlZahrani et al. [10] is the only reference that uses pure oxygen instead of air, and thus did not require the current density correction. Table 8 shows the estimated efficiencies when including hydrogen and oxygen compression to 16 MPa. The table indicates that when including both hydrogen and oxygen compression into the efficiency calculations, the efficiency of the basis SOEC system is slightly higher than the systems designed by Botta et al. [55], Saarinen et al. [53], and Peters et al. [60]. However, the systems designed by AlZahrani et al. [10], Peter et al. [56], and FuelCell Energy [59] still reach higher efficiency values. This means that the basis SOEC system can be optimized to improve its energy efficiency.

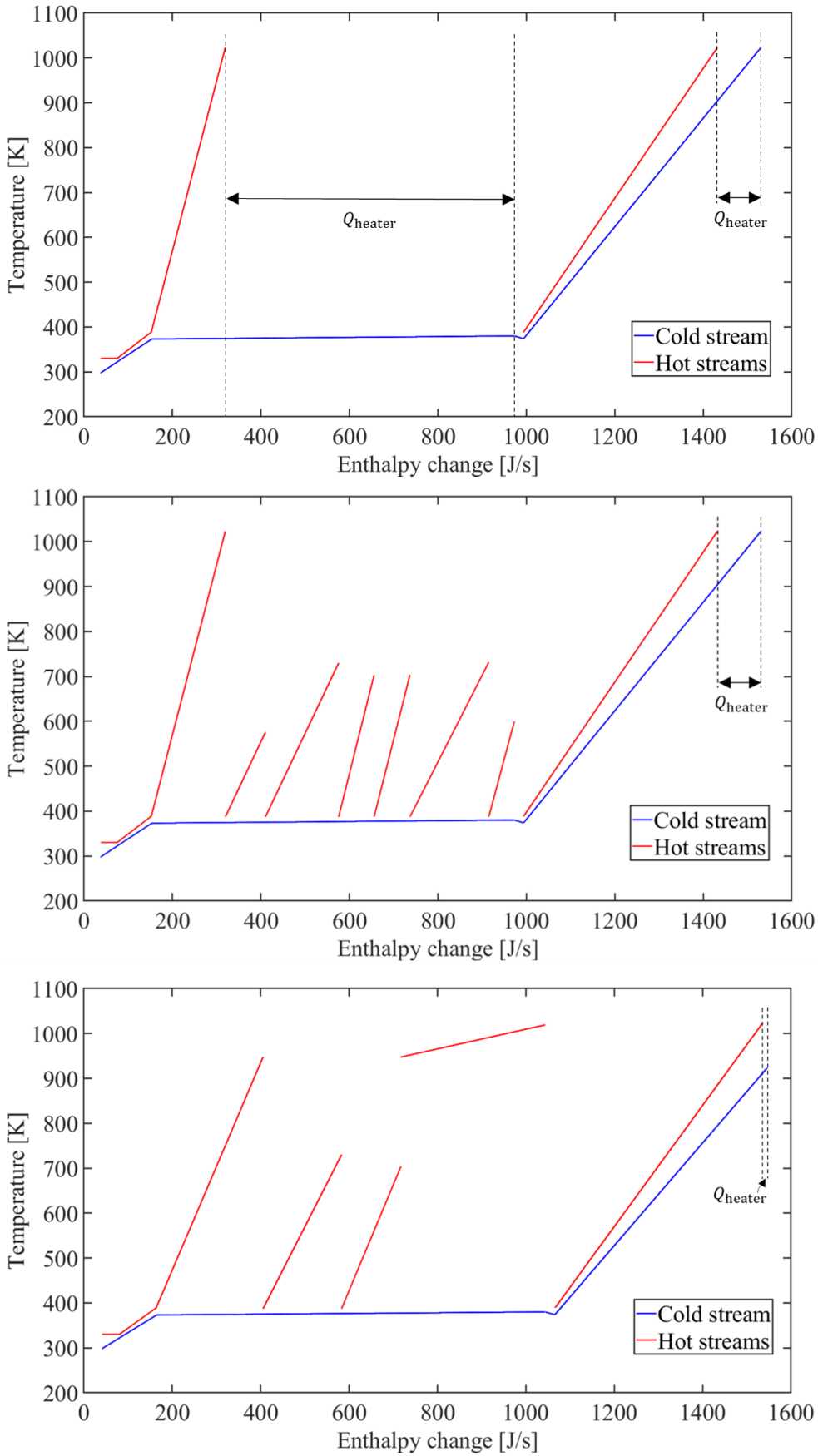

Figure 20 Illustrations of the temperature-enthalpy diagrams of the basis SOEC system (top), the heat integration SOEC system (middle), and the oxygen-cooled SOEC system (bottom). The cold stream represents the fuel electrode inlet stream, the hot streams represent the fuel electrode and oxygen electrode outlet streams.

5.2.2. The heat integration SOEC system

In the basis SOEC system, a large amount of power is required for the evaporation of water. A solution for this high power requirement is proposed in the heat integration SOEC system. In the heat integration SOEC system, the water is evaporated using heat exchangers instead of an electric heater. These heat exchangers evaporate the water using the heat that would otherwise be released in the hydrogen and oxygen coolers. Figure 17 shows that in this new system, the electric heater that aided the evaporation is no longer required. Furthermore, the electric coolers for the hydrogen and oxygen cooling in between the storage compressors are no longer required.

An illustration of the temperature-enthalpy diagram of the heat integration SOEC system is given in the middle graph of Figure 20. It should be noted that this is not the actual temperature-enthalpy diagram of the heat integration SOEC system, because the water evaporation heat exchangers are placed in parallel, as was shown in Figure 14, and not in series, as is visualized in Figure 20. However, by visualising the water evaporation in series, the diagram gives a more comprehensive overview of how the heat requirement of the heat integration SOEC system is met. Figure 20 shows that the preheating and superheating of the cold fuel electrode inlet stream in the heat integration SOEC system is equal to that of the basis SOEC system. The systems' diagrams differ however for the evaporation of the cold fuel electrode inlet stream. In the heat integration SOEC system the water is evaporated using only heat exchangers, and no electric heater is required. These heat exchangers, which are numbered XIIIa-XIIIg in Figure 14, evaporate the water using the electrolyser's hot oxygen outlet stream (XIIIa) and the hot compressor streams (XIIIb-XIIIg). The heat exchanger on the left side of the evaporation line in Figure 20, which is heat exchanger XIIIa, is equal to that of the basis SOEC system. The detailed temperature-enthalpy diagram of this heat exchanger is thus equal to that of the basis SOEC system in Figure 18. The detailed temperature-enthalpy diagrams of heat exchangers XIIIb-XIIIg, in which the water is evaporated using the hot compressor streams, are given in Figure 21.

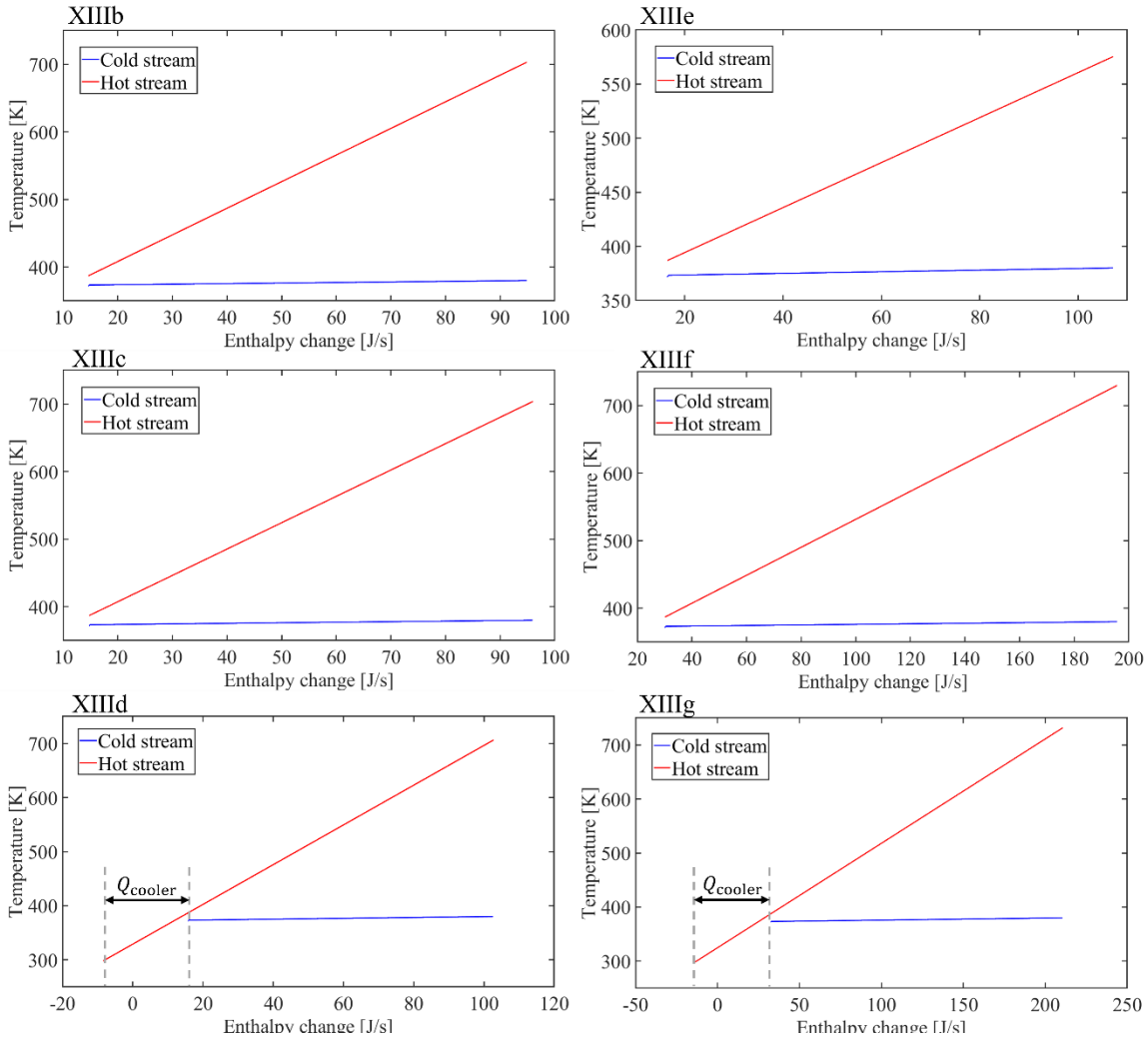

Figure 21 The temperature-enthalpy diagrams of water evaporation in heat exchangers XIIIb-g of the heat integration SOEC system. The red lines in diagrams XIIIb, XIIIc, and XIIId represent the hot oxygen streams in between the storage compressors. The red lines in diagrams XIIIe, XIIIf, and XIIIg represent the hot hydrogen streams in between the storage compressors.

Figure 21 shows that the hot hydrogen and oxygen streams in between the storage compressors, which are represented by the red lines in temperature-enthalpy diagrams XIIIb, XIIIc, XIIIe, and XIIIf, are cooled down to 387 K, which is the lowest temperature possible considering the required minimum temperature difference in the heat exchangers. The hot hydrogen and oxygen streams after the storage compressors, which are represented by the red lines in temperature-enthalpy diagrams XIIId and XIIIg, have to be cooled down to the storage temperature of 298.15 K. Since in the heat exchangers the hot streams cannot be cooled down below 387 K, additional coolers XI and XV are required to cool the hot hydrogen and oxygen streams to the storage temperature (Q_{cooler}). Nevertheless, Figure 17 shows that the power requirement of these coolers, 0.12 kWh/kgH_2, is small in comparison with the system's total power requirement of 44.13 kWh/kgH_2.

Just like in the basis SOEC system, the electrolyser is operated at the thermo-neutral voltage in the heat integration SOEC system. As a result, the amount of power required for the stack, superheater, and residual components in the heat integration SOEC system are equal to that of the basis SOEC system. Furthermore, since the temperature to which the hydrogen and oxygen streams in the heat integration SOEC system are cooled down in between the storage compressors is equal to that in the basis SOEC system, the amount of power required for the hydrogen and oxygen compressors remains equal to the basis SOEC system as well.

The heat integration SOEC system reaches an energy efficiency, based on the lower heating value of hydrogen, of 75.52%. Due to the use of heat exchangers for the water evaporation, the heat integration SOEC system requires less power per kilogram produced hydrogen compared to the basis SOEC system, leading to an increase in the energy efficiency. The efficiency of the heat integration SOEC system can be compared to the reference efficiencies in Table 8. Compared to the efficiencies as given by the references, the heat integration SOEC system efficiency is lower than the efficiencies of AlZahrani et al. [10], Peters et al. [56], and FuelCell Energy [59], and higher than the efficiencies of Botta et al. [55], Saarinen et al. [53], and Peters et al. [60]. More importantly, compared to the efficiencies including hydrogen and oxygen compression, the heat integration SOEC system efficiency is higher than all the reference systems' efficiencies. This indicates that the alteration of using compression heat for the water evaporation is worthwhile with regard to the SOEC system's energy efficiency.

5.2.3. The oxygen-cooled SOEC system

In the third SOEC system, the oxygen-cooled SOEC system, the number of required alterations when combining the SOFC+GT and the SOEC system is minimized. Therefore, the oxygen-cooled SOEC system contains a high oxygen recirculation mass flow rate and the ejector. Figure 17 shows that the oxygen-cooled SOEC system requires more stack power than the other two systems. This is caused by a change in the stack's operating point due to the increased oxygen recirculation mass flow rate. The increased oxygen recirculation mass flow rate in the SOFC+GT system is used for cooling of the stack. The ejector in the SOFC+GT system that is used for this oxygen recirculation is designed for specific operating conditions. Since this ejector is also used in the oxygen-cooled SOEC system, both systems have the same oxygen recirculation mass flow rate and oxygen recirculation temperature. In the oxygen-cooled SOEC system, the oxygen recirculation therefore also leads to cooling of the stack. However, unlike an SOFC, an SOEC does not always operate exothermally and thus does not always require cooling. In order to compensate for the cooling caused by the increased oxygen mass flow rate, the SOEC stack has to operate above the thermo-neutral point to maintain the required operating temperature. However, when operated close to the limiting current density, the stack can become less efficient and require more power per kilogram produced hydrogen. This is also the case for the oxygen-cooled SOEC system. Figure 22 shows the IV-curve of an SOEC in which the left dot represents the exothermal operating point in the oxygen-cooled SOEC system, and the right dot represents the thermo-neutral operating point in the basis SOEC system and heat integration SOEC system. The figure also shows that there is a steep increase in the cell voltage at current densities above the thermo-neutral point. This increase in cell voltage is mainly caused by the concentration overpotential, which was described in section 4.1.1. The increase in cell voltage means that at the exothermal operating point, there is more power required for electrolysis per kilogram produced hydrogen compared to the thermo-neutral operating point. This is also visible in Figure 17, which shows that the oxygen-cooled SOEC system requires more stack power than the other two SOEC systems.

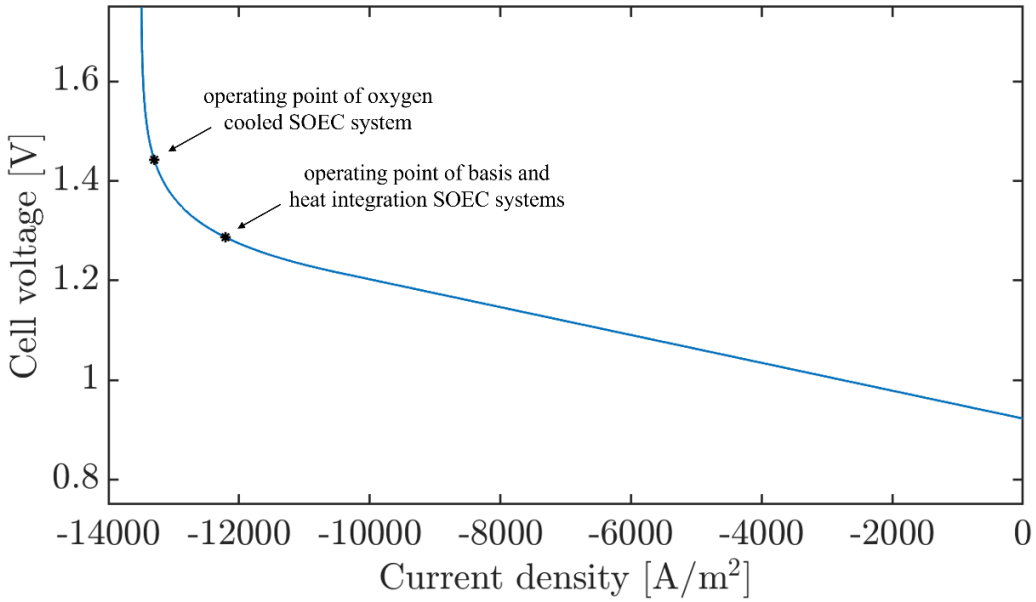

Figure 22 IV-curve of the SOEC. The left dot represents the exothermal operating point in the oxygen-cooled SOEC system and the right dot represents the thermo-neutral operating point in the basis and heat integration SOEC systems.

An advantage of the electrolyser's exothermal operating point in the oxygen-cooled SOEC system is that it requires less power for superheating the water and hydrogen compared to the basis and heat integration SOEC systems; only 0.07 kWh/kgH2 instead of 0.84 kWh/kgH2. This reduction in power requirement is also visible in the temperature-enthalpy diagram of the oxygen-cooled SOEC system, of which an illustration is given in the bottom graph of Figure 20. It should be noted that this is not the actual temperature-enthalpy diagram of the oxygen-cooled SOEC system, because the water evaporation heat exchangers are placed in parallel, as was shown in Figure 15, and not in series, as is visualized in Figure 20. However, by visualising the water evaporation in series, the diagram gives a more comprehensive overview of how the heat requirement of the oxygen-cooled SOEC system is met. Figure 20 shows that the oxygen-cooled SOEC system does not require an electric heater for the water evaporation. Furthermore, the heat requirement of the electric superheater in the oxygen-cooled SOEC system is less than that in the basis and heat integration SOEC systems. The detailed temperature-enthalpy diagram of superheating the fuel electrode inlet stream in the oxygen-cooled SOEC system is given in Figure 23. Figure 23 shows that most of the heat required for superheating the cold fuel electrode inlet steam can be covered by the hot fuel electrode outlet stream in the heat exchanger (Q_{HEX}). However, due to the different stream compositions of the electrolyser's inlet and outlet streams and the minimum temperature difference required for the heat exchanger, the hot outlet stream cannot superheat the cold inlet stream to the required stack temperature and therefore the electric superheater is required (Q_{heater}). When comparing Figure 23 with the superheating temperature-enthalpy diagram of the basis and heat integration SOEC systems in Figure 19, it becomes visible that the amount of heat that can be exchanged in the heat exchanger Q_{HEX} is larger in the oxygen-cooled SOEC system compared to the basis and heat integration SOEC systems. In section 2.1 it was explained that the extra heat that is produced when operating the electrolyser in exothermal mode is released via the electrolyser's outlet streams. Since the electrolyser's outlet stream is the hot stream in the superheater, the amount of heat that can be exchanged in the heat exchanger Q_{HEX} is larger when the electrolyser is operated in exothermal mode than in thermo-neutral mode. As a result, the electric superheater energy requirement Q_{heater} in Figure 23 is smaller than the electric superheater energy requirement in Figure 19. Therefore, the superheater's power requirement in the oxygen-cooled SOEC system is smaller than the superheater's power requirement in the basis and heat integration SOEC systems.

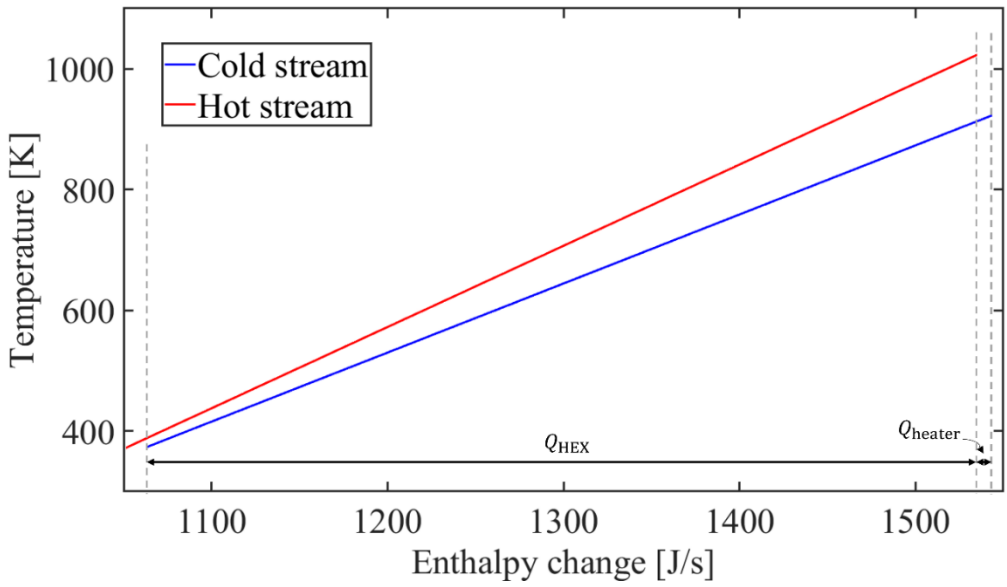

Figure 23 The temperature-enthalpy diagram of superheating the cold water and hydrogen inlet stream in the heat exchanger (VI) and electric heater (VII) of the oxygen-cooled SOEC system. The hot stream represents the electrolyser's hydrogen and steam outlet stream.

Equal to the heat integration SOEC system, the oxygen-cooled SOEC system uses heat exchangers instead of an electric heater for the evaporation of water. In the heat integration SOEC system, the water is evaporated using the heat from the electrolyser's hot oxygen outlet stream and the heat that is released in between the hydrogen and oxygen storage compressors. In the oxygen-cooled SOEC system, the increased oxygen mass flow rate results in an increase in heat recuperation in heat exchangers XIIIa, XIIIb, and XIIIc, where the water is evaporated using the oxygen stream. As a result, only four heat exchangers are required for evaporation of the water. The detailed temperature-enthalpy diagrams of the water evaporation heat exchangers XIIIa-d are given in Figure 24.

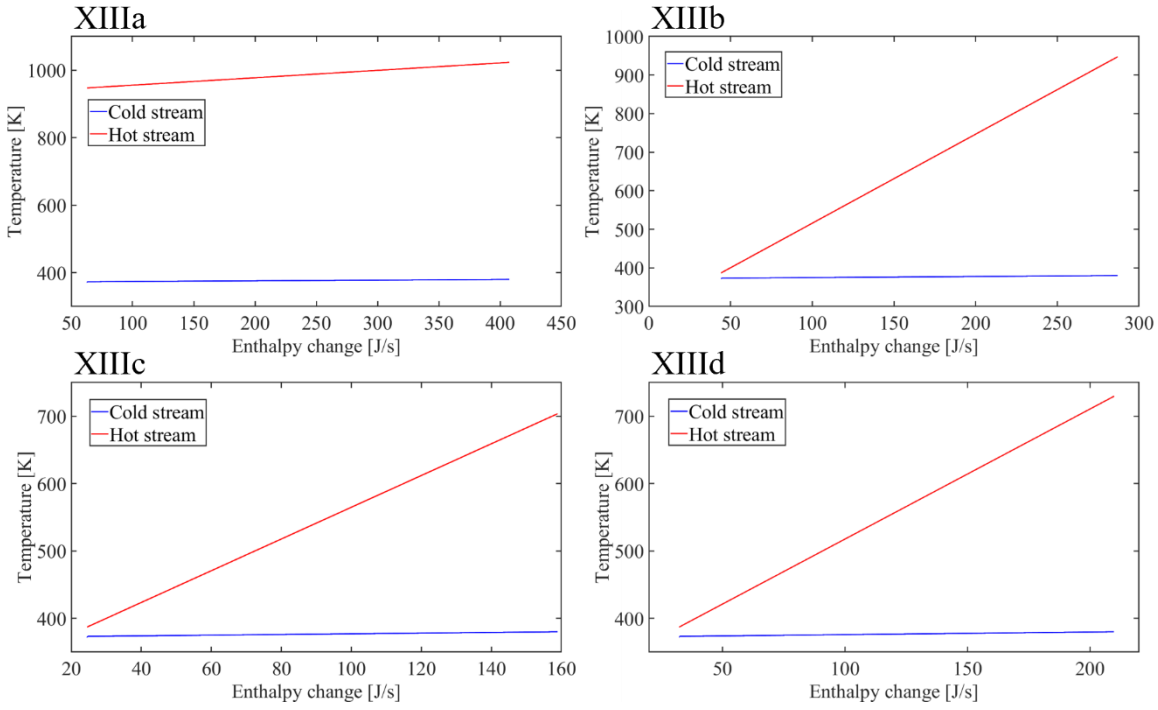

Figure 24 The temperature-enthalpy diagrams of water evaporation in heat exchangers XIIIa-d of the oxygen-cooled SOEC system. The red lines in diagrams XIIIa, XIIIb, and XIIIc represent the hot oxygen streams in between the storage compressors. The red line in diagram XIIId represents the hot hydrogen stream in between the storage compressors.

Figure 24 shows that the hot hydrogen and oxygen streams connected to the storage compressors, which are represented by the red lines in temperature-enthalpy diagrams XIIIb, XIIIc, and XIIId, are cooled down to 387 K, which is the lowest temperature possible considering the required minimum temperature difference in the heat exchangers. The hot oxygen stream connected to the oxygen recirculation loop, which is represented by the red line in diagram XIIIa, is cooled down to 947 K. This is the required inlet temperature of the ejector as designed by Malhotra, D. [16].

The oxygen-cooled SOEC system requires only four heat exchangers for the water evaporation, which is less than the seven heat exchangers in the heat integration SOEC system. Therefore, the oxygen-cooled SOEC system requires coolers (XI, XV) in between some of the hydrogen and oxygen storage compressors. This results in a slight increase in the hydrogen and oxygen cooler's power requirement compared to the heat integration system, as is visible in Figure 17. Another result of the increased oxygen mass flow rate in the oxygen-cooled SOEC system is an increase in the oxygen storage compressors' power requirement. Figure 17 shows that this power requirement in the oxygen-cooled SOEC system is 3.56 kWh/kgH_2, while the oxygen storage compressors' power requirement in the basis and heat integration SOEC systems is 2.31 kWh/kgH_2

The oxygen-cooled SOEC system reaches an energy efficiency, based on the lower heating value of hydrogen, of 67.26%. This efficiency is lower than the efficiency of the heat integration SOEC system, since the increase in stack, coolers, and oxygen storage compressor power is larger than the decrease in superheater power. However, the efficiency is still higher than the efficiency of the basis SOEC system, since no power is required for the water evaporation and less power is required for the storage cooling. When comparing the oxygen-cooled SOEC system's efficiency to the references' efficiencies given in Table 8, the efficiency of the oxygen-cooled SOEC system is relatively low. However, when comparing the oxygen-cooled SOEC system's efficiency to the references' efficiencies including both hydrogen and oxygen compression, the efficiency of the oxygen-cooled SOEC system is slightly higher than the systems designed by Botta et al. [55], Saarinen et al. [53], and Peters et al. [60]. Nevertheless, the systems designed by AlZahrani et al. [10], Peter et al. [56], and FuelCell Energy [59] still reach higher efficiency values.

Overall, the energy analysis shows that the heat integration SOEC system reaches the highest energy efficiency. This is mainly due to the use of heat exchangers for the water evaporation and the hydrogen and oxygen cooling. Furthermore, the stack's thermo-neutral operating point and decreased oxygen recirculation mass flow rate results in less stack, coolers, and oxygen storage compressor power required per kilogram of produced hydrogen compared to the oxygen-cooled SOEC system. When comparing the heat integration SOEC system's efficiency to the references' efficiencies including both hydrogen and oxygen compression in Table 8, the efficiency of the heat integration SOEC system efficiency is higher than the reference systems' efficiencies. This indicates that the use of compression heat for the water evaporation is a worthwhile alteration with regard to the SOEC system's energy efficiency.

5.3. Exergy analysis

The three SOEC systems described in section 3 were examined using the exergy equations and simulation parameters described in section 4.

In the basis SOEC system, the heat from the hot stack's outlet streams is used to heat up the cold stack's inlet streams. Figure 25 illustrates the exergy output rate and exergy destruction rate of the basis SOEC system in relation to the exergy input rate. The left-hand side of the figure shows that the system has an exergy efficiency of 65.56% and an exergy destruction rate of 30.14% of the total exergy input rate. The

right-hand side shows the distribution of the exergy destruction over the system components. The exergy destruction is mainly caused by the evaporation of the water, which is 9.63% of total exergy input rate; the SOEC stack, which is 8.05% of total exergy input rate; and the cooling of hydrogen and oxygen in between their compression stages, which is 7.47% of total exergy input rate. This exergy efficiency and distribution of exergy destruction is comparable to literature values [10, 76].

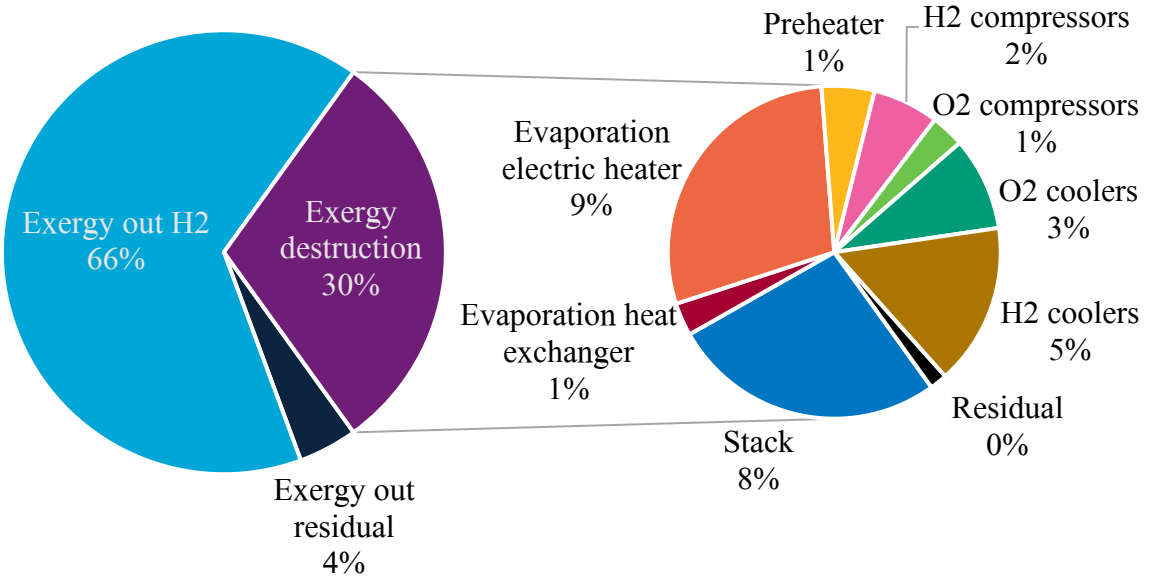

Figure 25 The exergy output and destruction rates in relation to the exergy input rate (left) and the distribution of the exergy destruction rate over the system components (right) of the basis SOEC system.

In the heat integration SOEC system, the water is evaporated using heat exchangers instead of an electric heater. The heat integration SOEC system was found to have an exergy efficiency of 75.42% and an exergy destruction rate of 19.64% of the total exergy input rate, as is shown in Figure 26. The exergy destruction is mainly caused by the SOEC stack, which is 9.30% of total exergy input rate, and the evaporation of the water, which is 4.11% of total exergy input rate. Compared to the basis SOEC system, there is no exergy destruction in the coolers in between the hydrogen and oxygen storage compressors since these coolers are not required. The exergy destruction of the other system components, like the hydrogen and oxygen compressors, water preheater, and pumps, is comparable to that of the basis SOEC system.

Compared to the basis SOEC system, the heat integration SOEC system has less exergy destruction in the water evaporation components. Although in the heat integration SOEC system no electric heater is required for the water evaporation, the heat exchangers still cause exergy destruction. The exergy destruction in the heat exchangers is mainly caused by the high temperature difference between the water evaporation temperature and the heat exchanger's hot inlet streams, which is visible in Figure 18. A reduction in this exergy destruction can be achieved by lowering the inlet temperature of the hot streams, however, this would require alterations in the storage compressors configuration that poses a trade-off between the complexity of the system and the efficiency of the components.

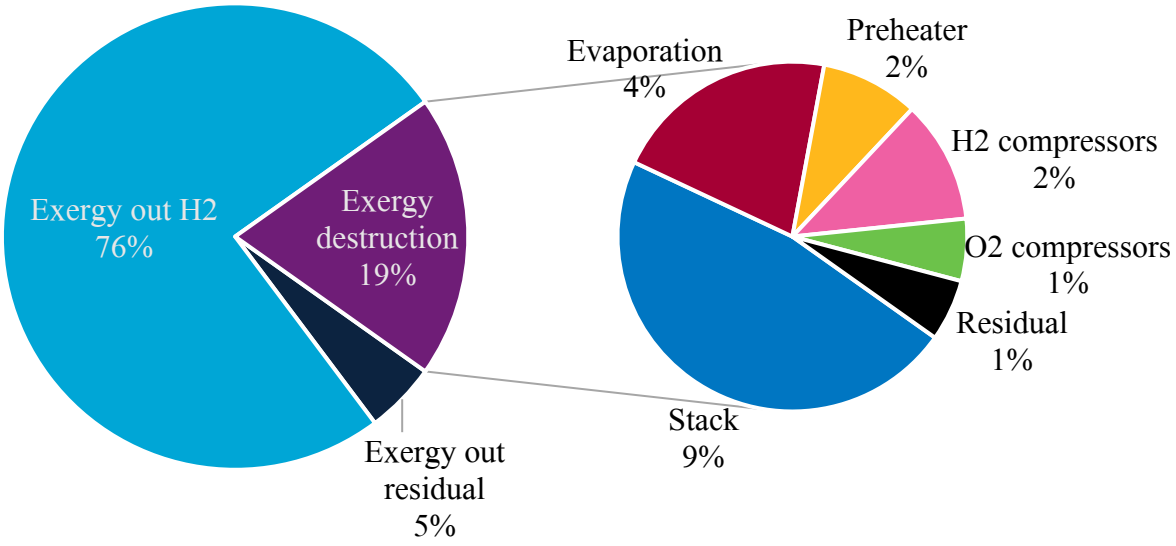

Figure 26 The exergy output and destruction rates in relation to the exergy input rate (left) and the distribution of the exergy destruction rate over the system components (right) of the heat integration SOEC system.

In the oxygen-cooled SOEC system, the number of required alterations when combining the SOFC+GT and the SOEC system is minimized by utilizing a high oxygen recirculation mass flow rate and an ejector. The oxygen-cooled SOEC system was found to have an exergy efficiency of 66.75% and an exergy destruction rate of 27.20% of the total exergy input rate, as is shown in Figure 27. The exergy destruction is mainly caused by the SOEC stack, which is 10.30% of total exergy input rate, and the evaporation of the water, which is 5.16% of total exergy input rate. The residual system components have a slightly higher exergy destruction compared to the basis and heat integration SOEC systems. This is mainly caused by the higher inlet temperature of the fuel electrode condensation cooler due to the exothermal operating point of the stack. The addition of turbines to the system also leads to some extra exergy destruction.

Compared to the other two SOEC systems, the exergy destruction in the stack is higher in the oxygen-cooled SOEC system. This is due to the less efficient stack operating point, as was described in section 5.2. Although the oxygen-cooled SOEC system, like the heat integration SOEC system, uses only heat exchangers for the evaporation of the water, the exergy destruction in these components is slightly higher for the oxygen-cooled SOEC system. Due to the increased oxygen mass flow rate, a higher fraction of the water is evaporated using the stack outlet stream in the oxygen-cooled SOEC system. The stack outlet stream has a higher temperature than the storage compressors outlet streams, causing a larger temperature difference and thus a larger exergy destruction in the heat exchanger.

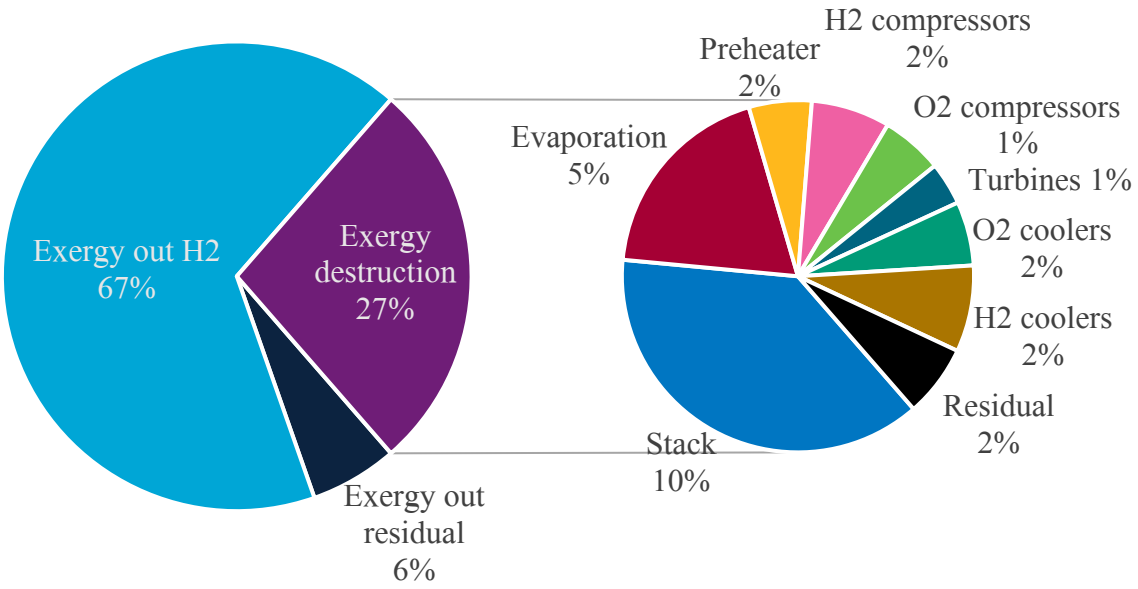

Figure 27 The exergy output and destruction rates in relation to the exergy input rate (left) and the distribution of the exergy destruction rate over the system components (right) of the oxygen-cooled SOEC system.

Overall, the exergy analysis shows that the heat integration SOEC system reaches the highest exergy efficiency. This is mainly due to the use of heat exchangers for the water evaporation and hydrogen and oxygen cooling. Furthermore, the stack's thermo-neutral operating point and decreased oxygen recirculation mass flow rate results in less exergy destruction in the stack, coolers, and oxygen storage compressors compared to the oxygen-cooled SOEC system.

5.4. Parameter analysis

This section describes the three parameters that were altered to examine their effect on the efficiency of the heat integration SOEC system: The amount of heat loss in the system, the average operating temperature of the electrolyser, and the average operating voltage of the electrolysis cells. The effects of these three parameters on the efficiency are disputed in literature, and therefore examined in this thesis.

5.4.1. Effect of heat loss

Literature on the design of SOEC systems using computer models often do not include the system's heat loss into their efficiency calculations. However, experiments suggest that the heat loss of an SOEC system can vary between 3.1%-11% of the stack's input power [53, 75]. The actual heat loss will depend on the characteristics of the system components and the extend of thermal insulation [53, 75]. To examine the effect of heat loss on the heat integration SOEC system's efficiency, the heat loss in the SOEC system was altered from 5% to 0% and 10% of the stack's input power.

In section 5.2, it was observed that the energy efficiency of the heat integration SOEC system using 5% heat loss was 75.52%. Figure 28 shows that the efficiency of the system decreased with approximately

three percentage points, from 75.52% to 72.68%, when the heat loss was increased to 10%. Alternatively, the efficiency increased with approximately three percentage points, from 75.52% to 78.60%, when the heat loss was reduced to 0%. Since the heat loss has a noteworthy effect on the energy efficiency of the heat integration SOEC system, further research is required to examine the actual heat loss of the system, which includes the equipment specification and thermal insulation placement.

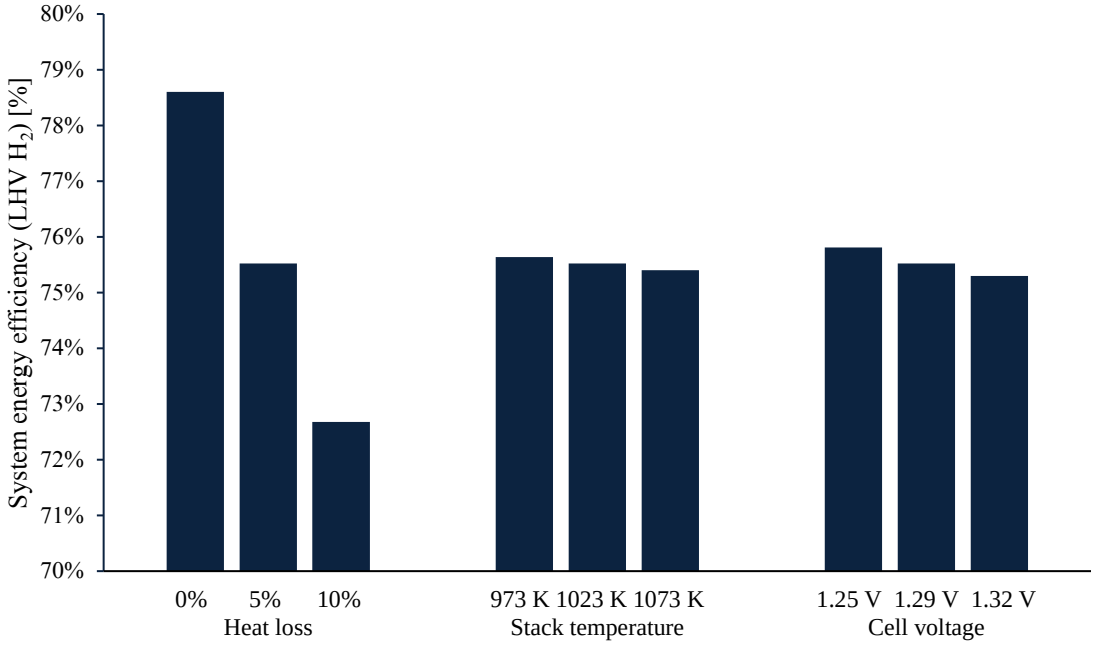

Figure 28 The effect of alterations in heat loss, stack temperature and cell voltage on the efficiency of the heat integration SOEC system.

5.4.2. Effect of operating temperature

In section 2.2.2, literature statements on the effect of the SOEC's operating temperature on the system's efficiency were discussed. In order to examine the effect of the SOEC stack's operating temperature on the efficiency of the heat integration SOEC system, the operating temperature of the stack was varied. The stack's average operating temperature was altered from 1023.15 K to 973.15 K and 1073.15 K.

In section 5.2, it was found that the energy efficiency of the heat integration SOEC system using a stack operating temperature of 1023.15K was 75.52%. Figure 28 shows that the effect of altering the temperature is minimal, with a slight increase to 75.64% for the lower operating temperature and a slight decrease to 75.40% for the higher operating temperature. The minimal deviation in energy efficiency can be explained by the power required for the electric superheater, which is given in Figure 29.

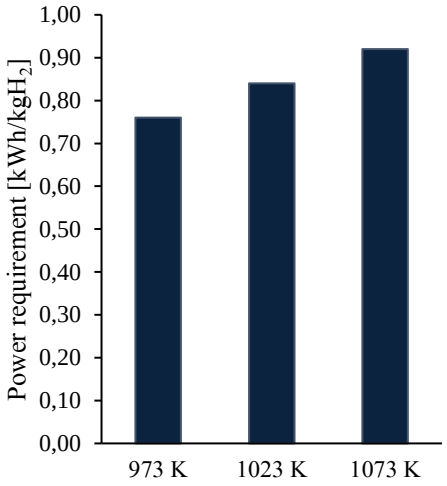

Figure 29 The power requirement of the electric superheater in the heat integration SOEC system for the three considered temperatures.

The figure shows that the superheater power requirement increases for an increase in stack operating temperature. The power requirements per kilogram of produced hydrogen of the other system components are comparable for all three considered operating temperatures. The increase in superheater power for increasing temperature is caused by a change in the operating point of the stack. For the higher and lower temperatures, the operating voltage of the electrolysis cells slightly changes due to different thermo-neutral voltage values. Furthermore, the corresponding current density also changes due to different IV-curves for the different operating temperatures. When operating the cells at the lower or higher temperature, the cells have a respectively lower or higher current density compared to the 1023 K heat integration SOEC system. This effect is also found in literature on the used rSOC [50]. The change in current density causes a change in the stack's mass balance, and thus in the amount of heat required for superheating the inlet water and hydrogen. However, in relation to the total amount of power required by the system, which has a value around 42 kWh/kgH_2, the deviation in superheater power has a minimal effect on the system's energy efficiency.

5.4.3. Effect of operating voltage

As was described in section 2.2.2, literature on SOEC system design is in disagreement on the optimal operating voltage of the electrolysis cells. Therefore, the heat integration SOEC system was examined at three different voltages. The selected voltages are below, at, and above the thermo-neutral voltage, and are indicated in Figure 30. Since operation above or below the thermo-neutral voltage requires respectively heat removal from or heat addition to the cells, the temperatures of the in- and outlet streams were altered to allow for this heat removal or addition. An anode-supported cell with a cell length of 10 cm, such as the reference cell used in this thesis, can handle a temperature difference around 100 K [77]. This temperature difference resulted in corresponding exothermal and endothermal operating voltages. An overview of the three operating modes, their inlet and outlet temperatures, and resulting operating voltages are given in Table 9. Operating above or below these voltages is possible, however, since this would require extra heating or cooling of the cells, this was not examined.

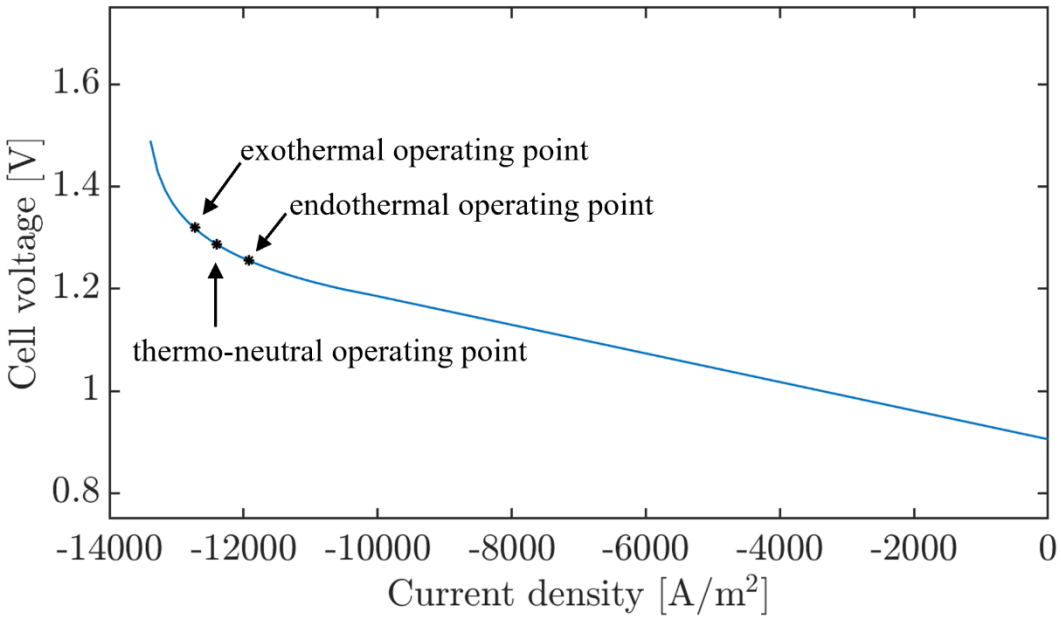

Figure 30 IV-curve of the electrolysis cells, indicating the three considered operating voltages in the heat integration SOEC system's parameter analysis.

Table 9 Simulation parameters for the evaluation of different operating voltages in the heat integration SOEC system's parameter analysis.

Operating mode	Stack inlet temperature [K]	Stack outlet temperature [K]	Cell voltage [V]
Endothermal	800	700	1.25
Thermo-neutral	750	750	1.29
Exothermal	700	800	1.32

In section 5.2, it was found that the energy efficiency of the heat integration SOEC system operated at the thermo-neutral voltage was 75.52%. Figure 28 shows that the effect of altering the voltage is minimal, with a slight increase for the lower operating voltage (75.81%) and a slight decrease for the higher operating voltage (75.30%). The decrease in efficiency for increasing operating voltage can be explained by the power requirement of the stack. When the stack is operated in exothermal mode, it requires more power than when operated in thermo-neutral or endothermal mode due to higher cell voltage and current density. In Figure 31, this effect is visualized for the three considered operating voltages.

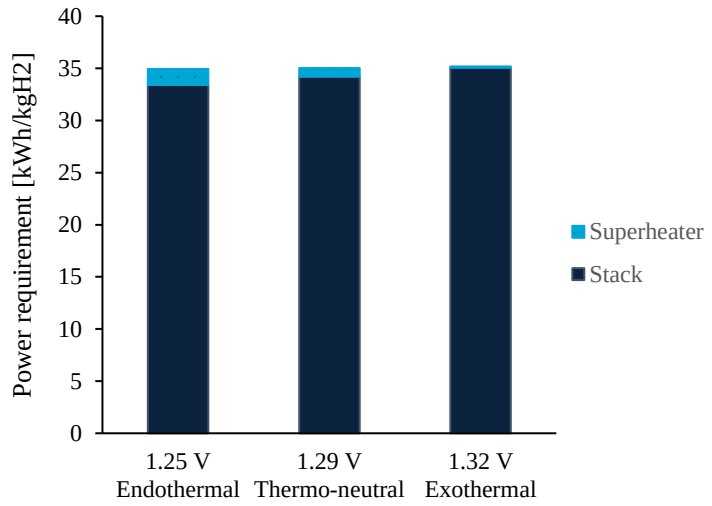

Figure 31 The power requirement of the stack and superheater in the heat integration SOEC system for the three considered cell voltages.

The figure shows that the SOEC system requires most stack power when operated in exothermal mode, and least stack power when operated in endothermal mode. The figure also shows that for the superheater power, the opposite effect occurs. This decrease in superheater power for increasing operating voltage is caused by the change in stack operating point, similar to the effect of the operating temperature as described in section 5.4.2. The power requirements of the other system components are comparable for all three considered operating voltages. Since the increase in stack power requirement is larger than the decrease in superheater power requirement, the energy efficiency decreases for increasing operating voltage. For decreasing operating voltage, the opposite effect occurs. However, in relation to the total amount of power required by the system, which has a value around 42 kWh/kgH_2, the net deviation in power requirement has a minimal effect on the system's energy efficiency.

Overall, the parameter analysis indicates that the heat loss in the system has a noteworthy effect on the energy efficiency of the heat integration SOEC system and should thus be included in future research on this system. The parameter analysis also indicates that the effects of operating temperature and voltage have a minimal effect on the efficiency of the heat integration SOEC system. In the analysis, the energy efficiency of the heat integration SOEC system slightly increased from 75.52% to 75.64% for decreased stack operating temperature and to 75.81% for decreased cell operating voltage. This increase in efficiency is mainly caused by a change in the power requirements of the stack and superheater. The minor effect of operating temperature and voltage on the efficiency indicates that from an efficiency perspective there is little preference for a certain temperature or voltage value. In future research on the heat integration SOEC system, one of the three temperatures and voltages can therefore be chosen based on other criteria than the system's efficiency, like component durability. However, further research evaluating more temperature and voltage values is required before general conclusions on the effect of operating temperature and voltage on the system's efficiency can be drawn.

5.5. The rSOC system

In this thesis, three solid oxide electrolyser (SOEC) systems were designed and examined in order to redesign the solid oxide fuel cell and gas turbine integrated (SOFC+GT) system described in section 2.2.1 into a reversible solid oxide cell (rSOC) system. The results that are described in the previous sections indicate that the lowest energy and exergy efficiencies are obtained by the basis SOEC system. Therefore, this basis SOEC system is not selected for redesigning the SOFC+GT system into an rSOC system. The results also indicate that the highest energy and exergy efficiencies are obtained by the heat integration SOEC system. However, compared to the oxygen-cooled SOEC system , the heat integration SOEC system requires more alterations when combining the SOFC+GT system with the SOEC system.

This poses a tradeoff between the complexity and the efficiency of the rSOC system. However, since the difference in efficiencies between the heat integration SOEC system and the oxygen-cooled SOEC system is almost ten percentage points, the heat integration SOEC system is recommended for redesigning the SOFC+GT system into an rSOC system.

A layout of the rSOC+GT system that is formed when combining the SOFC+GT system and the heat integration SOEC system is given in Figure 32. When the rSOC system is operated in SOFC mode, it produces electricity and heat by the conversion of hydrogen and oxygen gas into steam (green lines). When the rSOC system is operated in SOEC mode, it converts steam into pure hydrogen and oxygen gas by the application of electricity and heat (blue lines). The stream data of the rSOC+GT system is equal to the SOFC+GT stream data in Appendix A and the SOEC stream data in Appendix C. As described in section 3.3, oxygen enters the ejector in the SOFC+GT system designed by Malhotra, D. [16] at a temperature of 288 K and a pressure of 0.6 MPa [16]. In the rSOC system the oxygen is stored at atmospheric temperature and a pressure of 16 MPa, therefore, the oxygen will have to be brought to the right temperature and pressure using turbines and an electric heater before entering the ejector. The addition of these components is assumed not to affect the efficiency of the SOFC+GT system, due to the small difference between the energy requirement of the heater and energy released by the turbines.

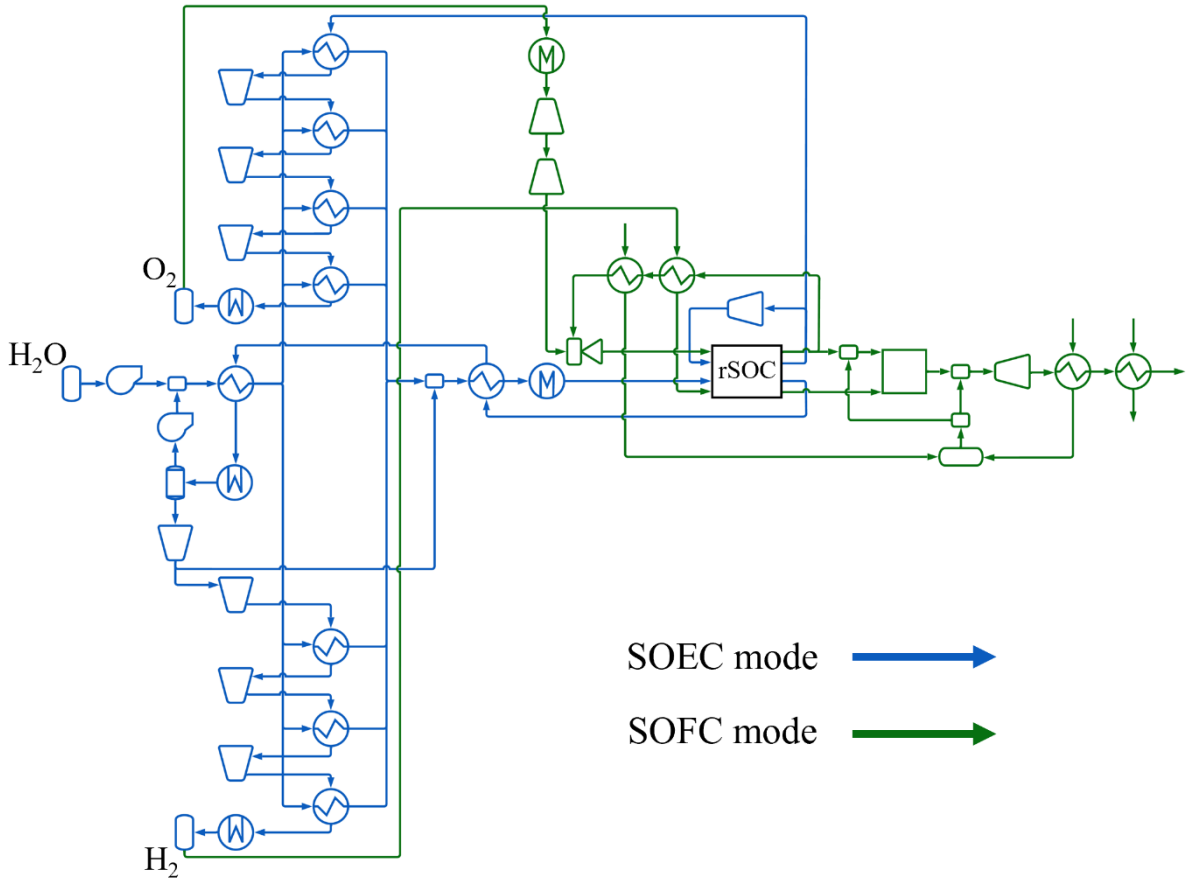

Figure 32 Layout of the rSOC system. The blue lines represent operation in electrolyser mode and the green lines represent operation in fuel cell mode.

The round-trip energy efficiency of this rSOC system, based on the lower heating value of hydrogen, reaches a value of 48.40%. In Table 10, this value is compared to the round-trip energy efficiency, also based on the lower heating value of hydrogen, of four researches on rSOC systems in literature. These researches use pure hydrogen as both SOEC product and SOFC reactant and determined their energy efficiencies in the same way as described in section 4.1.3.

Table 10 The round-trip energy efficiencies, based on the lower heating value of hydrogen, of the rSOC system in this thesis and four rSOC systems in literature.

	Round-trip efficiency as given in the reference	Efficiency including H_2 compression to 16 MPa	Efficiency including H_2 and O_2 compression to 16 MPa
rSOC in this thesis	48 %	48 %	48 %
Peters et al. [60]	44 %	40 %	38%
Ficili et al. [47]	35 %	31 %	29%
Giap et al. [78]	38 %	34 %	33%
Botta et al. [55]	30 %	27 %	25%

Table 10 shows that the energy efficiency of the rSOC system in this thesis is higher than the reference rSOC systems' efficiencies. From the reference rSOC systems, the highest round-trip energy efficiency is achieved by Peters et al. [60]. Peters et al. [60] argue that their relatively high round-trip efficiency is caused by the use of fuel electrode recirculation during fuel cell mode and a high stack temperature of 1103 K and steam utilization of 85% during electrolyser mode [60]. The energy efficiencies of their rSOC system during fuel cell and electrolyser mode are respectively 63% and 70% [60]. Both these values are lower than the fuel cell and electrolyser mode energy efficiencies of the rSOC system in this thesis, which are respectively 64% and 76%. This indicates that the fuel cell and electrolyser subsystems of the rSOC system in this thesis perform better. The difference in efficiency between the rSOC system in this thesis and the reference rSOC systems are even larger when including the compression of hydrogen and oxygen in the references' efficiency calculation. In the rSOC system in this thesis, the hydrogen and oxygen gases that are produced during electrolyser mode are compressed to 16 MPa for storage. In the reference systems, Giap et al. [78] compress their hydrogen to 2.2 MPa during electrolyser mode, and Peters et al. [60], Botta et al. [55], and Ficili et al. [47] do not compress the hydrogen in their systems. None of the reference systems compress the oxygen in their systems. To enable a more equal comparison between the reference rSOC systems and the rSOC system designed in this thesis, the references' rSOC system efficiencies including hydrogen and oxygen compression were estimated. The procedure for this estimation was described in section 5.2.1, and the results are given in Table 10. The table shows that when including the compression of hydrogen and oxygen into the efficiency calculation, the round-trip efficiency of the rSOC in this thesis is more than ten percentage points higher than the round-trip efficiencies of the references' systems. This indicates that the combination of the SOFC+GT system and heat integration SOEC system in this thesis is a promising step forwards towards the optimalisation of rSOC systems.

6. Conclusion

In the further advancement of the energy transition towards renewable energy sources, a significant role can be played by reversible solid oxide cell (rSOC) systems. In this thesis, three solid oxide electrolyser (SOEC) systems were designed and examined in order to redesign the solid oxide fuel cell and gas turbine (SOFC+GT) system designed by Malhotra, D. [16] into a reversible solid oxide cell and gas turbine (rSOC+GT) system.

One of the main challenges when designing an SOEC system is the heat requirement of the system. A significant amount of heat is required for the evaporation of water in an SOEC system. Furthermore, unlike a fuel cell, an electrolyser does not always operate exothermally and thus often requires heat to maintain its high operating temperature. Three SOEC systems, displaying different heat integration layouts, were designed and examined on their energy and exergy performance: The basis SOEC system, the heat integration SOEC system, and the oxygen-cooled SOEC system.

The first system, the basis SOEC system, reuses heat from the stack's hot outlet streams to heat up the stack's cold inlet streams. The basis SOEC system reaches energy and exergy efficiencies of 65.40% and 65.56% respectively. The second system, the heat integration SOEC system, evaporates water using heat exchangers instead of an electric heater and reaches energy and exergy efficiencies of 75.52% and 75.42% respectively. The third system, the oxygen-cooled SOEC system, requires a minimal number of alterations when combining the SOEC system with the SOFC+GT system and reaches energy and exergy efficiencies of 67.26% and 66.75% respectively. The results show that the highest energy and exergy efficiencies are obtained by the heat integration SOEC system. This is mainly due to the use of heat exchangers for the water evaporation and hydrogen and oxygen cooling. This results in no power requirement for the electric coolers and evaporation heater and decreased exergy destruction for evaporation compared to the basis SOEC system. Furthermore, the stack's thermo-neutral operating point and decreased oxygen recirculation mass flow rate result in a decreased power requirement and exergy destruction in the stack, the coolers, and the oxygen storage compressors compared to the oxygen-cooled SOEC system.

In order to examine how the efficiency of the heat integration SOEC system is affected by certain parameters, three parameters were altered to examine their effect on the energy efficiency of this system. The parameter analysis indicates that the energy efficiency of the heat integration SOEC system slightly increases to 75.64% with decreased stack operating temperature and to 75.81% with decreased cell operating voltage. This increase in efficiency is mainly caused by a change in the power requirements of the stack and superheater. The analysis also indicates that the heat loss in the system has a noteworthy effect on the energy efficiency of the heat integration SOEC system.

The heat integration SOEC system requires more alterations compared to the oxygen-cooled SOEC system but reaches a higher system efficiency. This poses a tradeoff between the complexity and the efficiency of the rSOC+GT system. However, since the difference in efficiencies between the two systems is almost ten percentage points, the heat integration SOEC system was selected for redesigning the SOFC+GT system into an rSOC+GT system. Analysis of this rSOC+GT system indicates that its round-trip energy efficiency, based on the lower heating value of hydrogen, reaches a value of 48.40%. These results show that a combination of the SOFC+GT system and heat integration SOEC system opens the door to new optimalisation possibilities for rSOC based energy storage systems.

7. Recommendations

From the three designed SOEC systems in this thesis, the heat integration SOEC system is recommended for coupling to the SOFC+GT system, because it reaches the highest energy efficiency. An advantage of this combination is that the rSOC+GT system reaches a higher round-trip energy efficiency compared to the referenced literature. However, a disadvantage is that coupling of the SOFC+GT system with the heat integration SOEC system requires more alterations compared to coupling with the oxygen-cooled SOEC system. Future research could examine whether a compromise between the complexity and the efficiency of the rSOC+GT system can be reached by either changing the SOEC system or the SOFC+GT system. For example, the ejector in the SOFC+GT system is designed for specific operating conditions, and therefore these conditions were also met in the oxygen-cooled SOEC system. In future research, the ejector could be replaced by a compressor to allow the oxygen electrode inlet stream of the SOEC system to have a different mass flow rate and temperature than the oxygen electrode inlet stream of the SOFC+GT system. This might result in an increased oxygen-cooled SOEC system's efficiency, while requiring less alterations when forming the rSOC+GT system. Another solution could be the use of a different stack cooling method. In the SOFC+GT system, an increased oxygen mass flow rate is used for cooling the stack, because this method results in a higher SOFC+GT system's efficiency than cooling with steam. However, in the SOEC system, the increased oxygen mass flow rate cooling method results in a lower SOEC system's efficiency. Future research could examine whether the use of another cooling method could be beneficial for the rSOC+GT system's round-trip energy efficiency.

Two other recommendations concern the modelling of the rSOC system. Firstly, the electrochemical model used in this thesis is a simplified representation of the complex electrochemical processes taking place inside an rSOC. The electrochemical model validation showed that the model resembled the experimental reference data, with a difference between the model and the experiment within the allowed 3% deviation. However, it was assumed that when changing the operating parameters of the rSOC, the electrochemical model would still resemble the actual performance of the rSOC. Since little experimental data on the performance of an rSOC using pure hydrogen and oxygen is available, future research could examine whether this assumption is valid, by either implementing a more detailed electrochemical model or conducting experiments on an rSOC. Secondly, the rSOC system in this thesis is evaluated for steady-state operation of the SOEC and SOFC+GT system. Future research may focus on modelling the transient behaviour of the rSOC stack when switching between the fuel cell and electrolyser mode, which might result in additional system requirements. For example, experiments on rSOC system design acknowledge the convenience of using electric heaters for regulating the stack temperature.

Another recommendation concerns the water and hydrogen recirculation in the SOEC system. In the SOEC systems designed in this thesis, water and hydrogen are recirculated at a low temperature, namely after the partial condensation. Some SOEC systems in the referenced literature recirculate the water and hydrogen at a medium temperature, before the partial condensation. One reference even recirculates the water and hydrogen at a high temperature, after membrane separation. Future research could examine whether recirculating the water and hydrogen at a different temperature results in a higher efficiency of the SOEC system.

Another research option is the use of a thermal energy storage (TES) system. In literature on rSOC systems, the excess heat that is released during SOFC mode is often stored in a TES system to cover the heat demand during SOEC mode. However, when implementing a TES system in the rSOC+GT system of this thesis, two challenges arise. Firstly, in the rSOC+GT system the excess SOFC heat is already utilized in a gas turbine system. Therefore, additional research altering the SOFC+GT system would be

required to evaluate the effects of adding a thermal energy storage system on the efficiency of the SOFC+GT system. Secondly, the heat integration SOEC system only requires heat addition for superheating the fuel electrode inlet stream. Additional research could examine whether the effect of lowering the stack's operating voltage, and thereby increasing the superheater power requirement, during electrolyser mode outweighs the decrease in fuel cell mode efficiency.

Other recommendations apply to the parameter analysis. In the parameter analysis, three parameters were altered to examine their effect on the energy efficiency of the SOEC system. For each parameter, three values were examined. To draw more general conclusions on the effects of the parameters on the SOEC system's efficiency, further research examining more values per parameter is required. Additionally, in order to accurately estimate the heat loss in the system, further research on the equipment specification and thermal insulation placement is advised.

References

1. Lemmon, E.W., M.L. Huber, and M.O. McLinden, *NIST Standard Reference Database 23 Version 9.0*, NIST, Editor. 2010.
2. European Parliament. *EU responses to climate change* 2022 17-06-2022 [cited 2023; Available from: https://www.europarl.europa.eu/news/en/headlines/society/20180703STO07129/eu-responses-to-climate-change.
3. Horowitz, A. *How We're Moving to Net-Zero by 2050*. 2021 2021 [cited 2023; Available from: https://www.energy.gov/articles/how-were-moving-net-zero-2050.
4. Eurostat, *Net electricity generation by type of fuel - monthly data*, Eurostat, Editor. 2023, Eurostat.
5. Luo, X., et al., *Overview of current development in electrical energy storage technologies and the application potential in power system operation.* Applied Energy, 2015. **137**: p. 511-536.
6. IEA, *World Energy Outlook 2022*. 2022, IEA: Paris License: CC BY 4.0 (report); CC BY NC SA 4.0 (Annex A).
7. Venkataraman, V., et al., *Reversible solid oxide systems for energy and chemical applications – Review & perspectives.* Journal of Energy Storage, 2019. **24**: p. 100782.
8. Wieliczko, M. and N. Stetson, *Hydrogen technologies for energy storage: A perspective.* MRS Energy & Sustainability, 2020. **7**: p. E41.
9. Larminie, J. and A. Dicks, *Fuel cell systems explained*. 2003, Wiley: Chichester.
10. AlZahrani, A.A. and I. Dincer, *Modeling and performance optimization of a solid oxide electrolysis system for hydrogen production.* Applied Energy, 2018. **225**: p. 471-485.
11. Wang, L., et al., *Reversible solid-oxide cell stack based power-to-x-to-power systems: Comparison of thermodynamic performance.* Applied Energy, 2020. **275**: p. 115330.
12. Salzgitter AG. *GrInHy2.0*. 2024 [cited 2024 January 1]; Available from: https://salcos.salzgitter-ag.com/en/grinhy-20.html.
13. Schwarze, K., et al., *Operational Results of an 150/30 kW RSOC System in an Industrial Environment.* Fuel Cells, 2019. **19**(4): p. 374-380.
14. REFLEX. *Project info*. 2024 [cited 2024 January 28]; Available from: https://www.reflex-energy.eu/project-info1.
15. Schouten, B., *Thermal efficiency improvement of closed hydrogen and oxygen fuelled combined cycle power plants with the application of solid oxide fuel cells using an exergy analysis method*. 2020, Delft University of Technology: Delft.
16. Malhotra, D., *Design of an H2 -O2 fired Solid Oxide Fuel Cell Gas Turbine Test Set Up*, in *Mechanical Engineering*. 2022, Delft University of Technology: Delft. p. 95.

17. Schmidt, O., et al., *Future cost and performance of water electrolysis: An expert elicitation study.* International Journal of Hydrogen Energy, 2017. **42**(52): p. 30470-30492.
18. Fan, L., Z. Tu, and S.H. Chan, *Recent development of hydrogen and fuel cell technologies: A review.* Energy Reports, 2021. **7**: p. 8421-8446.
19. Ni, M., M.K.H. Leung, and D.Y.C. Leung, *Parametric study of solid oxide steam electrolyzer for hydrogen production.* International Journal of Hydrogen Energy, 2007. **32**(13): p. 2305-2313.
20. Scott, K., *Electrochemical Methods for Hydrogen Production*. 2020, Croydon: Royal Society of Chemistry (RSC).
21. Stempien, J., Q. Sun, and S.H. Chan, *Solid Oxide Electrolyzer Cell Modeling: A Review.* Journal of Power Technologies, 2013. **93**: p. 216.
22. Bessler, W.G., *Multi-scale Modelling of Solid Oxide Fuel Cells*, in *Solid Oxide Fuel Cells: From Materials to System Modeling*, T.S. Zhao and M. Ni, Editors. 2013, The Royal Society of Chemistry. p. 0.
23. Bessler, W.G., S. Gewies, and M. Vogler, *A new framework for physically based modeling of solid oxide fuel cells.* Electrochimica Acta, 2007. **53**(4): p. 1782-1800.
24. Ni, M., M.K.H. Leung, and D.Y.C. Leung, *A modeling study on concentration overpotentials of a reversible solid oxide fuel cell.* Journal of Power Sources, 2006. **163**(1): p. 460-466.
25. Buttler, A., et al., *A detailed techno-economic analysis of heat integration in high temperature electrolysis for efficient hydrogen production.* International Journal of Hydrogen Energy, 2015. **40**(1): p. 38-50.
26. Petipas, F., A. Brisse, and C. Bouallou, *Benefits of external heat sources for high temperature electrolyser systems.* International Journal of Hydrogen Energy, 2014. **39**(11): p. 5505-5513.
27. O'Brien, J.E. *Thermodynamic Considerations for Thermal Water Splitting Processes and High Temperature Electrolysis*. in *ASME 2008 International Mechanical Engineering Congress and Exposition*. 2008. ASMEDC.
28. Jericha, H., *Efficient steam cycles with internal combustion of hydrogen and stoichiometric oxygen for turbines and piston engines.* International Journal of Hydrogen Energy, 1987. **12**(5): p. 345-354.
29. Jericha, H., et al., *Thermal Steam Power Plant Fired by Hydrogen and Oxygen in Stoichiometric Ratio, Using Fuel Cells and Gas Turbine Cycle Components*. Vol. 3. 2010.
30. Godula-Jopek, A. and D. Stolten, *Hydrogen Production : By Electrolysis*. 2015, Berlin, GERMANY: John Wiley & Sons, Incorporated.
31. Towler, G.P. and R.K. Sinnott, *Chemical engineering design : principles, practice and economics of plant and process design*. 2022, Butterworth-Heinemann is an imprint of Elsevier: Kidlington, Oxford.
32. Mohammadpour, M., E. Houshfar, and M. Ashjaee, *Sustainability analysis and optimization of innovative geothermal-driven energy storage system for green production of H2, NH3, and pure O2.* International Journal of Hydrogen Energy, 2022. **47**(62): p. 26156-26177.

33. Mohammadpour, M., E. Houshfar, and M. Ashjaee, *Performance evaluation and multi-objective optimization of an innovative solar-assisted multigeneration energy storage system for freshwater/O2/H2 generation.* Sustainable Energy Technologies and Assessments, 2022. **53**: p. 102755.
34. Restrepo, J.C., et al., *Techno-economical evaluation of renewable hydrogen production through concentrated solar energy.* Energy Conversion and Management, 2022. **258**: p. 115372.
35. Westover, T. and S. Hancock. *Thermal and Electrical Coupling to Electrolysis Plants*. in *Probabilistic Safety Assessment and Management, PSAM 2022*. 2022. International Association for Probablistic Safety Assessment and Management (IAPSAM).
36. Wang, F., et al., *Design and optimization of hydrogen production by solid oxide electrolyzer with marine engine waste heat recovery and ORC cycle.* Energy Conversion and Management, 2021. **229**: p. 113775.
37. Zhao, Y. and et al., *System level heat integration and efficiency analysis of hydrogen production process based on solid oxide electrolysis cells.* International Journal of Hydrogen Energy, 2021. **46**(77): p. 38163-38174.
38. Mastropasqua, L., et al., *Solar hydrogen production: Techno-economic analysis of a parabolic dish-supported high-temperature electrolysis system.* Applied Energy, 2020. **261**: p. 114392.
39. Yilmaz, F., M. Ozturk, and R. Selbas, *Development and performance analysis of a new solar tower and high temperature steam electrolyzer hybrid integrated plant.* International Journal of Hydrogen Energy, 2020. **45**(9): p. 5668-5686.
40. Raeissi Jelodar, H., G.R. Salehi, and R. Abedini, *The Energy and Exergy Analysis of Integrated Hydrogen Production System Using High Temperature Steam Electrolysis with Optimized Water Path (RESEARCH NOTE).* International Journal of Engineering, 2019. **32**(6): p. 893-900.
41. Schiller, G., et al., *Solar heat integrated solid oxide steam electrolysis for highly efficient hydrogen production.* Journal of Power Sources, 2019. **416**: p. 72-78.
42. Yuksel, Y.E., M. Ozturk, and I. Dincer, *Energetic and exergetic assessments of a novel solar power tower based multigeneration system with hydrogen production and liquefaction.* International Journal of Hydrogen Energy, 2019. **44**(26): p. 13071-13084.
43. Balta, M.T., O. Kizilkan, and F. Yılmaz, *Energy and exergy analyses of integrated hydrogen production system using high temperature steam electrolysis.* International Journal of Hydrogen Energy, 2016. **41**(19): p. 8032-8041.
44. Manage, M.N., et al., *A modelling approach to assessing the feasibility of the integration of power stations with steam electrolysers.* Chemical Engineering Research and Design, 2014. **92**(10): p. 1988-2005.
45. McKellar, M., et al., *Optimized Flow Sheet for a Reference Commercial-Scale Nuclear-Driven High-Temperature Electrolysis Hydrogen Production Plant.* 2023.
46. Sigurvinsson, J. and et al., *Can high temperature steam electrolysis function with geothermal heat?* International Journal of Hydrogen Energy, 2007. **32**(9): p. 1174-1182.

47. Ficili, M., et al., *Design and partial-load operation of a reversible Solid Oxide Cell system with molten salts thermal storage.* Journal of Physics: Conference Series, 2022. **2385**: p. 012022.
48. Perna, A., M. Minutillo, and E. Jannelli, *Designing and analyzing an electric energy storage system based on reversible solid oxide cells.* Energy Conversion and Management, 2018. **159**: p. 381-395.
49. Ni, M., M.K.H. Leung, and D.Y.C. Leung, *Energy and exergy analysis of hydrogen production by solid oxide steam electrolyzer plant.* International Journal of Hydrogen Energy, 2007. **32**(18): p. 4648-4660.
50. Hauch, A., et al., *Test and characterization of reversible solid oxide cells and stacks for innovative renewable energy storage.* Fuel Cells, 2021. **21**.
51. Choi, S. and J. Hong, *Versatile thermodynamic design of a solid oxide electrolysis cell system and its sensitivity to operating conditions.* Energy Conversion and Management, 2023. **298**: p. 117776.
52. Min, G., S. Choi, and J. Hong, *A review of solid oxide steam-electrolysis cell systems: Thermodynamics and thermal integration.* Applied Energy, 2022. **328**: p. 120145.
53. Saarinen, V., et al., *Design, manufacturing, and operation of movable 2 × 10 kW size rSOC system.* Fuel Cells, 2021. **21**(5): p. 477-487.
54. Sanz-Bermejo, J., et al., *Part load operation of a solid oxide electrolysis system for integration with renewable energy sources.* International Journal of Hydrogen Energy, 2015. **40**(26): p. 8291-8303.
55. Botta, G., et al., *Thermodynamic and Exergy Analysis of Reversible Solid Oxide Cell Systems.* ECS Transactions, 2015. **68**(1): p. 3265.
56. Peters, R. and et al., *Influence of operating parameters on overall system efficiencies using solid oxide electrolysis technology.* International Journal of Hydrogen Energy, 2015. **40**(22): p. 7103-7113.
57. Kupecki, J., et al., *Energy analysis of a 10 kW-class power-to-gas system based on a solid oxide electrolyzer (SOE).* Energy Conversion and Management, 2019. **199**: p. 111934.
58. AVL. *SOLID OXIDE ELECTROLYZES SYSTEM DEVELOPMENT*. 15. Symposium Energieinnovation 2018 15-02-2018 [cited 2023 14-02-2023]; Available from: https://www.tugraz.at/fileadmin/user_upload/Events/Eninnov2018/files/pr/Session_F4/PR_Schauperl.pdf.
59. FuelCell Energy. *Modular SOEC System for Efficient H2 Production at High Current Density*. 2020 DOE Hydrogen and Fuel Cells Program Review 2020 30-05-2020 [cited 2023 14-02-2023]; Available from: https://www.hydrogen.energy.gov/pdfs/review20/ta019_ghezel-ayagh_2020_p.pdf.
60. Peters, R., et al., *Long-Term Experience with a 5/15kW-Class Reversible Solid Oxide Cell System.* Journal of The Electrochemical Society, 2021. **168**(1): p. 014508.
61. Seader, J.D., E.J. Henley, and D.K. Roper, *Separation process principles : chemical and biochemical operations*. 3rd ed. ed. 2011, Hoboken, NJ: Wiley.

62. Petipas, F., A. Brisse, and C. Bouallou, *Model-based behaviour of a high temperature electrolyser system operated at various loads.* Journal of Power Sources, 2013. **239**: p. 584-595.
63. Zhang, X., et al., *Improved durability of SOEC stacks for high temperature electrolysis.* International Journal of Hydrogen Energy, 2013. **38**(1): p. 20-28.
64. The MathWorks, *MATLAB*. 2021.
65. Bell, I.H., et al., *Pure and Pseudo-pure Fluid Thermophysical Property Evaluation and the Open-Source Thermophysical Property Library CoolProp.* Industrial & Engineering Chemistry Research, 2014. **53**(6): p. 2498-2508.
66. Kazempoor, P. and R.J. Braun, *Model validation and performance analysis of regenerative solid oxide cells: Electrolytic operation.* International Journal of Hydrogen Energy, 2014. **39**(6): p. 2669-2684.
67. Chan, S.H., H.K. Ho, and Y. Tian, *Modelling of simple hybrid solid oxide fuel cell and gas turbine power plant.* Journal of Power Sources, 2002. **109**(1): p. 111-120.
68. Chan, S.H., K.A. Khor, and Z.T. Xia, *A complete polarization model of a solid oxide fuel cell and its sensitivity to the change of cell component thickness.* Journal of Power Sources, 2001. **93**(1): p. 130-140.
69. Moran, M., *Principles of engineering thermodynamics*. 8th ed. 2015, Hoboken, N.J: John Wiley & Sons.
70. Im-orb, K., et al., *Flowsheet-based model and exergy analysis of solid oxide electrolysis cells for clean hydrogen production.* Journal of Cleaner Production, 2018. **170**: p. 1-13.
71. Bakshi, B.R., T.G.P. Gutowski, and D.a.P. Sekulić, *Thermodynamics and the destruction of resources*. 2011, Cambridge University Press: New York.
72. Peters, R., et al., *Development and Testing of a 5kW-Class Reversible Solid Oxide Cell System.* ECS Transactions, 2019. **91**(1): p. 2495.
73. Mehrer Compression GmbH. *SINGLE- AND TWO STAGE, AIR-COOLED HIGH-PRESSURE COMPRESSORS*. 2023 [cited 2023 September 27]; Available from: https://www.mehrer.de/en/products/reciprocating-compressors/85-trx400.
74. Copeland LP. *Copeland Scroll Condensing Unit*. 2023 [cited 2023 September 27]; Available from: https://www.copeland.com/en-us/shop/1/climate-technologies/copeland-sku-ffap-040d-tfd-340.
75. Kruse, N., et al., *Experimental Investigation of Efficiency Maximization in Solid Oxide Electrolysis Systems by Internal Steam and Heat Recovery.* ECS Transactions, 2021. **103**(1): p. 555-560.
76. Li, G., et al., *Assessment of thermodynamic performance of a 20 kW high-temperature electrolysis system using advanced exergy analysis.* Fuel Cells, 2021. **21**(6): p. 550-565.
77. Aguiar, P., C.S. Adjiman, and N.P. Brandon, *Anode-supported intermediate-temperature direct internal reforming solid oxide fuel cell: II. Model-based dynamic performance and control.* Journal of Power Sources, 2005. **147**(1): p. 136-147.

78. Giap, V.-T., S. Kang, and K.Y. Ahn, *HIGH-EFFICIENT reversible solid oxide fuel cell coupled with waste steam for distributed electrical energy storage system.* Renewable Energy, 2019. **144**: p. 129-138.

Appendices

Appendix A – Stream data of the SOFC+GT system

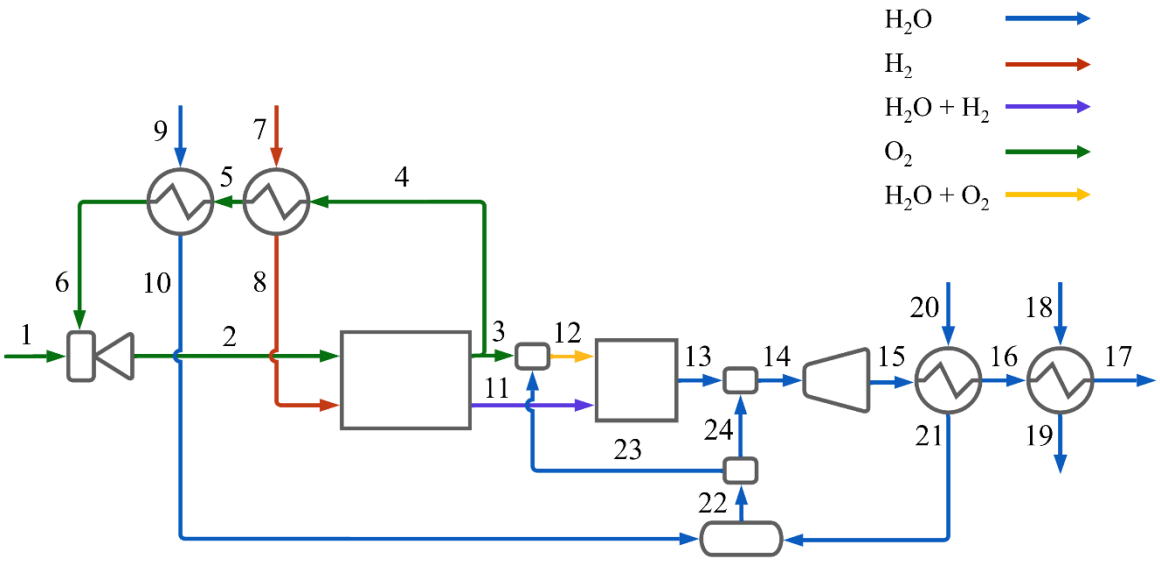

Figure 33 Layout of the SOFC+GT system, with numbered streams. Image adapted from [16].

Table 11 Stream data of the SOFC+GT system. Data from [16].
A dash indicates that the data is not given by Malhotra, D. [16].

Stream	Mass flow rate [kg/s]	Temperature [K]	Pressure [Pa]	Mole fraction [-]		
				H_2O	H_2	O_2
1	1.50E-4	288.15	600000	0	0	1
2	3.90E-3	923.15	100000	0	0	1
3	2.30E-5	1123.15	99000	0	0	1
4	3.76E-3	1123.15	99000	0	0	1
5	3.76E-3	-	-	0	0	1
6	3.76E-3	947.45	98000	0	0	1
7	1.90E-5	288.15	101000	0	1	0
8	1.90E-5	1073.15	100000	0	1	0
9	1.90E-4	288.15	101000	1	0	0
10	1.90E-4	923.15	100000	1	0	0
11	1.50E-4	1123.15	100000	0.85	0.15	0
12	1.80E-4	423.15	99000	0.93	0	0.07
13	3.30E-4	1236.95	98000	1	0	0
14	4.30E-4	1067.95	98000	1	0	0
15	4.30E-4	589.55	12000	1	0	0
16	4.30E-4	393.15	10000	1	0	0
17	4.30E-4	303.15	8000	1	0	0
18	2.50E-2	288.15	101000	1	0	0
19	2.50E-2	299.15	99000	1	0	0
20	6.40E-5	288.15	101000	1	0	0
21	6.40E-5	373.15	100000	1	0	0
22	2.50E-4	373.15	100000	1	0	0
23	1.60E-4	373.15	100000	1	0	0
24	2.90E-5	373.15	100000	1	0	0

Appendix B – Stream data of the basis SOEC system

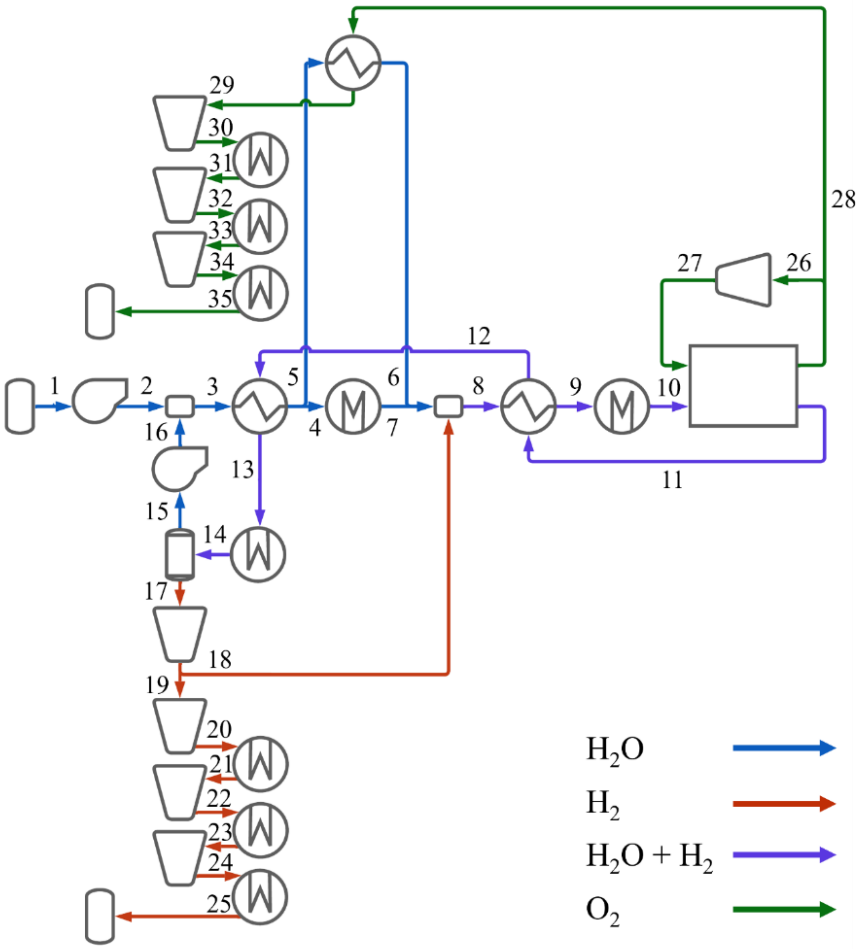

Figure 34 Layout of the basis SOEC system, with numbered streams.

Table 12 Stream data of the basis SOEC system.

Stream	Mass flow rate [kg/s]	Temperature [K]	Pressure [Pa]	Mole fraction [-]		
				H_2O	H_2	O_2
1	2.95E-4	298.15	101325	1	0	0
2	2.95E-4	298.15	103065	1	0	0
3	3.61E-4	298.15	103065	1	0	0
4	2.87E-4	372.00	102034	1	0	0
5	7.37E-5	372.00	102034	1	0	0
6	7.37E-5	380.04	101014	1	0	0
7	2.87E-4	380.04	101014	1	0	0
8	3.66E-4	374.01	101014	0.9	0.1	0
9	3.66E-4	906.30	100000	0.9	0.1	0
10	3.66E-4	1023.15	100000	0.9	0.1	0
11	1.09E-4	1023.15	98000	0.18	0.82	0
12	1.09E-4	388.84	97020	0.18	0.82	0
13	1.09E-4	377.69	96050	0.18	0.82	0
14	1.09E-4	298.15	96050	0.18	0.82	0
15	6.58E-5	298.15	96050	1	0	0
16	6.58E-5	298.15	103065	1	0	0
17	4.34E-5	298.15	96050	0.02	0.98	0

18	5.29E-6	304.36	101014	0.02	0.98	0
19	3.81E-5	304.36	101014	0.02	0.98	0
20	3.81E-5	575.35	555577	0.02	0.98	0
21	3.81E-5	387.00	550021	0.02	0.98	0
22	3.81E-5	729.70	3025117	0.02	0.98	0
23	3.81E-5	387.00	2994866	0.02	0.98	0
24	3.81E-5	731.47	16471762	0.02	0.98	0
25	3.81E-5	298.15	16307044	0.02	0.98	0
26	2.57E-5	1023.15	98000	0	0	1
27	2.57E-5	1023.15	100000	0	0	1
28	2.57E-5	1023.15	98000	0	0	1
29	2.57E-4	387.00	97020	0	0	1
30	2.57E-4	703.07	533610	0	0	1
31	2.57E-4	387.00	528274	0	0	1
32	2.57E-4	703.58	2905506	0	0	1
33	2.57E-4	387.00	2876451	0	0	1
34	2.57E-4	706.08	15820483	0	0	1
35	2.57E-4	298.15	15662278	0	0	1

Appendix C – Stream data of the heat integration SOEC system

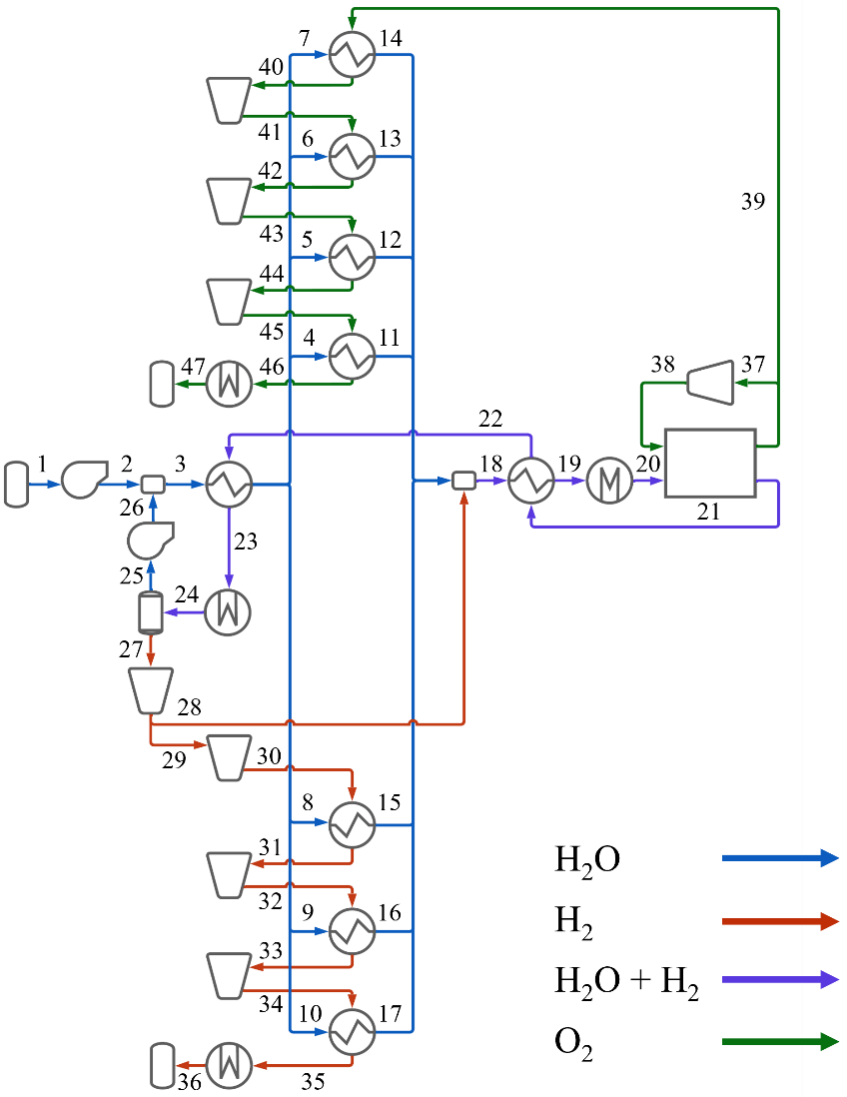

Figure 35 Layout of the heat integration SOEC system, with numbered streams.

Table 13 Stream data of the heat integration SOEC system.

Stream	Mass flow rate [kg/s]	Temperature [K]	Pressure [Pa]	Mole fraction [-]		
				H_2O	H_2	O_2
1	2.95E-4	298.15	101325	1	0	0
2	2.95E-4	298.15	103065	1	0	0
3	3.61E-4	298.15	103065	1	0	0
4	3.82E-5	372.00	102034	1	0	0
5	3.57E-5	372.00	102034	1	0	0
6	3.53E-5	372.00	102034	1	0	0
7	7.37E-5	372.00	102034	1	0	0
8	3.98E-5	372.00	102034	1	0	0
9	7.27E-5	372.00	102034	1	0	0
10	7.83E-5	372.00	102034	1	0	0
11	3.82E-5	380.04	101014	1	0	0
12	3.57E-5	380.04	101014	1	0	0
13	3.53E-5	380.04	101014	1	0	0

14	7.37E-5	380.04	101014	1	0	0
15	3.98E-5	380.04	101014	1	0	0
16	7.27E-5	380.04	101014	1	0	0
17	7.83E-5	380.04	101014	1	0	0
18	3.66E-4	374.01	101014	0.9	0.1	0
19	3.66E-4	906.30	100000	0.9	0.1	0
20	3.66E-4	1023.15	100000	0.9	0.1	0
21	1.09E-4	1023.15	98000	0.18	0.82	0
22	1.09E-4	388.84	97020	0.18	0.82	0
23	1.09E-4	377.69	96050	0.18	0.82	0
24	1.09E-4	298.15	96050	0.18	0.82	0
25	6.58E-5	298.15	96050	1	0	0
26	6.58E-5	298.15	103065	1	0	0
27	4.34E-5	298.15	96050	0.02	0.98	0
28	5.29E-6	304.36	101014	0.02	0.98	0
29	3.81E-5	304.36	101014	0.02	0.98	0
30	3.81E-5	575.35	555577	0.02	0.98	0
31	3.81E-5	387.00	550021	0.02	0.98	0
32	3.81E-5	729.70	3025117	0.02	0.98	0
33	3.81E-5	387.00	2994866	0.02	0.98	0
34	3.81E-5	731.47	16471762	0.02	0.98	0
35	3.81E-5	387.41	16307044	0.02	0.98	0
36	3.81E-5	298.15	16307044	0.02	0.98	0
37	2.57E-5	1023.15	98000	0	0	1
38	2.57E-5	1023.15	100000	0	0	1
39	2.57E-4	1023.15	98000	0	0	1
40	2.57E-4	387.00	97020	0	0	1
41	2.57E-4	703.07	533610	0	0	1
42	2.57E-4	387.00	528274	0	0	1
43	2.57E-4	703.58	2905506	0	0	1
44	2.57E-4	387.00	2876451	0	0	1
45	2.57E-4	706.08	15820483	0	0	1
46	2.57E-4	287.08	15662278	0	0	1
47	2.57E-4	298.15	15662278	0	0	1

Appendix D – Stream data of the oxygen-cooled SOEC system

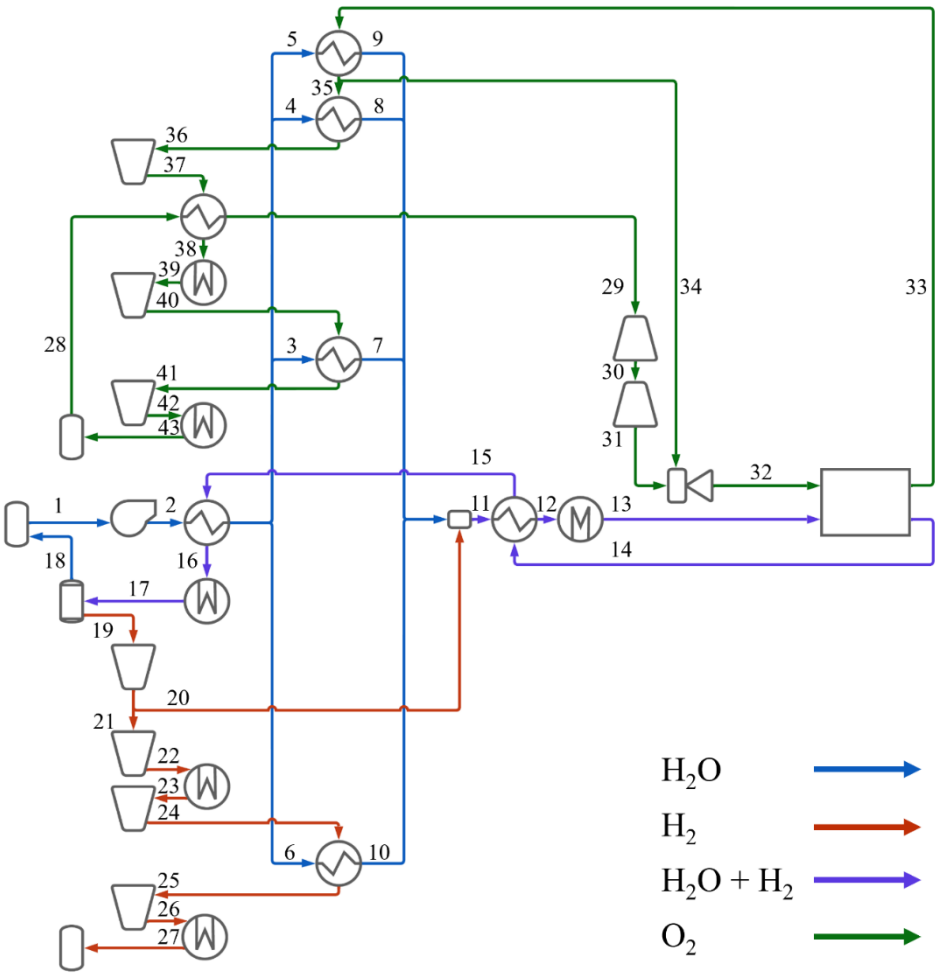

Figure 36 Layout of the oxygen-cooled SOEC system, with numbered streams.

Table 14 Stream data of the oxygen-cooled SOEC system.

Stream	Mass flow rate [kg/s]	Temperature [K]	Pressure [Pa]	Mole fraction [-]		
				H_2O	H_2	O_2
1	3.87E-4	298.15	101325	1	0	0
2	3.87E-4	298.15	103065	1	0	0
3	5.91E-5	373.32	102034	1	0	0
4	1.07E-4	373.32	102034	1	0	0
5	1.51E-4	373.32	102034	1	0	0
6	7.80E-5	373.32	102034	1	0	0
7	5.91E-5	380.04	101014	1	0	0
8	1.07E-4	380.04	101014	1	0	0
9	1.51E-4	380.04	101014	1	0	0
10	7.80E-5	380.04	101014	1	0	0
11	3.93E-4	374.01	101014	0.9	0.1	0
12	3.93E-4	913.27	100000	0.9	0.1	0
13	3.93E-4	923.15	100000	0.9	0.1	0
14	1.17E-4	1023.15	98000	0.18	0.82	0
15	1.17E-4	388.84	97020	0.18	0.82	0
16	1.17E-4	377.69	96050	0.18	0.82	0

17	1.17E-4	298.15	96050	0.18	0.82	0
18	7.06E-5	298.15	96050	1	0	0
19	4.65E-5	298.15	96050	0.02	0.98	0
20	5.68E-6	304.36	101014	0.02	0.98	0
21	4.09E-5	304.36	101014	0.02	0.98	0
22	4.09E-5	575.35	555577	0.02	0.98	0
23	4.09E-5	387.00	550021	0.02	0.98	0
24	4.09E-5	729.70	3025117	0.02	0.98	0
25	4.09E-5	387.00	2994866	0.02	0.98	0
26	4.09E-5	731.47	16474762	0.02	0.98	0
27	4.09E-5	298.15	16307044	0.02	0.98	0
28	1.50E-4	298.15	15505655	0	0	1
29	1.50E-4	525.00	15350598	0	0	1
30	1.50E-4	389.79	3039722	0	0	1
31	1.50E-4	288.12	601925	0	0	1
32	3.90E-3	923.15	100000	0	0	1
33	4.20E-3	1023.15	98000	0	0	1
34	3.80E-3	947.45	97020	0	0	1
35	4.26E-4	947.45	97020	0	0	1
36	4.26E-4	387.00	96050	0	0	1
37	4.26E-4	703.37	528274	0	0	1
38	4.26E-4	616.47	522991	0	0	1
39	4.26E-4	387.00	522991	0	0	1
40	4.26E-4	703.58	2876451	0	0	1
41	4.26E-4	387.00	2847687	0	0	1
42	4.26E-4	706.05	15662278	0	0	1
43	4.26E-4	298.15	15505656	0	0	1